



## Copyright Undertaking

This thesis is protected by copyright, with all rights reserved.

**By reading and using the thesis, the reader understands and agrees to the following terms:**

1. The reader will abide by the rules and legal ordinances governing copyright regarding the use of the thesis.
2. The reader will use the thesis for the purpose of research or private study only and not for distribution or further reproduction or any other purpose.
3. The reader agrees to indemnify and hold the University harmless from and against any loss, damage, cost, liability or expenses arising from copyright infringement or unauthorized usage.

### IMPORTANT

If you have reasons to believe that any materials in this thesis are deemed not suitable to be distributed in this form, or a copyright owner having difficulty with the material being included in our database, please contact [lbsys@polyu.edu.hk](mailto:lbsys@polyu.edu.hk) providing details. The Library will look into your claim and consider taking remedial action upon receipt of the written requests.

**ALKOXY- AND AMINO-BENZAMIDES AS  
INHIBITORS OF THE BACTERIAL CELL  
DIVISION PROTEIN FTSZ AND  
ANTIBACTERIAL AGENTS**

**LUI HOK KIU**

**M.Phil**

**The Hong Kong Polytechnic University**

**2014**

**The Hong Kong Polytechnic University**  
**Department of Applied Biology and Chemical Technology**

**Alkoxy- and Amino-benzamides as Inhibitors of the Bacterial Cell**  
**Division Protein FtsZ and Antibacterial Agents**

**Lui Hok Kiu**

**A Thesis Submitted in Partial Fulfillment of the**  
**Requirements for the Degree of Master of Philosophy**

**October 2013**

## **Certificate of Originality**

---

I hereby declare this thesis is my own work and that, to the best of my knowledge and belief, it reproduces no material previously published or written, nor material that has been accepted for the award of any other degree or diploma, except where due acknowledgement has been made in the text.

---

Lui Hok Kiu

September, 2013

## Abstract

---

Since their discovery in the 20<sup>th</sup> century, antibiotics have been prescribed for patients with bacterial infections. The first commercially available antibiotic was penicillin, which was discovered in 1928 by Alexander Fleming in St. Mary's Hospital, UK. Penicillin was effective to inhibit the growth of disease-causing microorganisms. However, in 1947, four years after the mass-production of penicillin, the first penicillin resistance case was identified. Since then, scientists have been looking for new targets to inhibit the bacterial growth. Among them, the bacterial cell division protein, filament temperature-sensitive Z (FtsZ), is a promising target for the development of new antibiotics.

FtsZ protein is an essential protein in bacterial cytoplasmic division. A GTPase active site is formed when two FtsZ monomers are joined together in head-to-tail manner. The presence of GTP induces the polymerization of FtsZ in the middle of the cell. FtsZ polymers act as a platform to recruit other cell division proteins in subsequent cytoplasmic division. The FtsZ homologue in eukaryotic cell is tubulin, which has similar three-dimensional structure and functions in prokaryotic cells. However, tubulin only shares a limited sequence identity with FtsZ. Therefore, scientists believe FtsZ inhibitor can perturb the normal functions of FtsZ without affecting tubulin in human.

3-Methoxybenzamide (**3-MBA**) has been shown to inhibit cell division in *Bacillus subtilis* 168. **PC190723**, a derivative of **3-MBA**, inhibits the growth of *Bacillus subtilis* 168 at 0.5  $\mu$ M. Although **PC190723** is by far the most effective FtsZ inhibitor, the oral bioavailability of **PC190723** in mice is only 57%. In this project, derivatives of

alkoxybenzamide and aminobenzamide were synthesized. Several of them can effectively inhibit the growth of *Bacillus subtilis* 168. Among them, **4-F332** inhibits the growth of *Bacillus subtilis* 168 and *Staphylococcus aureus* 29213 with MICs at 3.13  $\mu$ M and 12.5  $\mu$ M whereas **4-F361** does the same at 1.57  $\mu$ M and 3.13  $\mu$ M respectively. Both **4-F332** and **4-F361** inhibit the polymerization of *Staphylococcus aureus* FtsZ protein as demonstrated in light scattering assay. In GTPase activity assay, however, no significant inhibition was observed. Both **4-F332** and **4-F361** induce filamentation in *Bacillus subtilis* 168. The morphology of FtsZ polymers was observed by transmission electron microscope. Both **4-F332** and **4-F361** can reduce the length and thickness of *Staphylococcus aureus* FtsZ polymers. Cytotoxicity assay showed that **4-F361** has a selectivity ratio of 19, which indicates it has the potential to be developed into an antibiotic for clinical use.

## Acknowledgements

---

From the bottom of my heart, I hereby express my deep gratitude to my supervisor Professor K. Y. Wong for his enthusiastic supervision, unwavering support and valuable comments during my postgraduate study. In addition, I am grateful to him for his valuable comments on the draft of this thesis and teaching me to think critically about problems.

I would particularly like to thank Professor Y. C. Leung and Professor T. H. Chan for their invaluable advice. I would also like to thank Dr. F. Y. Chan for teaching me the basic laboratory techniques, Dr. N. Sun for his invaluable advice and patience throughout the course, Dr. K. F. Chan for helping in the synthesis of chemical compounds in this project, Dr. L. K. Wong for her assistance and expertise in the cytotoxicity experiments, and Dr. P. K. So for his assistance in mass spectrometry.

In addition, I am deeply indebted to my groupmates, Dr. W. L. Wong, Dr. Y.J Lu, Dr. W. H. Chung, Dr. Lawrence. Y.S. Lee, Dr. L. Y. So, Mr. Y. Wang, Mr. J. Yuan, Miss K. Y. Chow, Mr. M. H. So, Mr. Hugo Fung, Miss Enna Ha, Miss S. Y. Liu and my family for their encouragement and assistance throughout my study period.

I am also very grateful to all the technical staff members in the Department of Applied Biology and Chemical Technology of the Hong Kong Polytechnic University for their technical support and assistance.

Last but not the least, I would also like to acknowledge the Research Committee of the Hong Kong Polytechnic University for offering me a postgraduate studentship in 2011-2013.



# Table of contents

Certificate of Originality .....	ii
Abstract.....	iii
Acknowledgements .....	v
Table of contents .....	vii
List of Abbreviations .....	x
Chapter 1 Introduction.....	12
1.1 Bacterial infection and antibiotic resistance.....	12
1.2 Bacterial cell division and the role of FtsZ in cell division.....	15
1.3 FtsZ as a novel antibacterial target.....	23
1.4 FtsZ inhibitors .....	26
1.4.1 FtsZ inhibitors targeting at the GTP-binding site.....	26
1.4.2 FtsZ inhibitors targeting at the T7-loop.....	32
1.5 Drug discovery approaches .....	35
1.6 Aims and objectives .....	38
Chapter 2 Chemical synthesis of derivatives of 3-MBA .....	40
2.1 Introduction .....	40
2.2 Experimental.....	44
2.2.1 Materials .....	44
2.3 Instrumentation.....	45
2.4 Synthesis and characterization.....	46
2.4.1 Preparation of series 1 compounds.....	46

2.4.2 Preparation of series 2 compounds .....	49
2.4.3 Preparation of series 3 compounds .....	53
2.4.4 Preparation of series 4 compounds .....	55
2.4.5 Preparation of some other compounds .....	63
2.5 Results and discussion .....	66
2.6 Concluding remarks.....	67
Chapter 3 <i>In vivo</i> bioassays of 3-MBA derivatives .....	68
3.1 Introduction .....	68
3.2 Experimental.....	69
3.2.1 Materials .....	69
3.2.2 Instrumentation.....	70
3.2.3 Antibacterial susceptibility test .....	70
3.2.4 Visualization of bacterial morphology .....	71
3.2.5 Cytotoxicity test.....	72
3.3 Results and discussion .....	73
3.3.1 Antibacterial susceptibility .....	73
3.3.2 Effects on the morphology of <i>B.subtilis</i> cells.....	80
3.2.3 Cytotoxicity test.....	83
3.4 Concluding remarks.....	85
Chapter 4 <i>In vitro</i> biological studies of 3-MBA derivatives as FtsZ inhibitors .....	86
4.1 Introduction .....	86
4.2 Experimental section .....	87
4.2.1 Materials .....	87
4.2.2 Instrumentation.....	87
4.2.3 Preparation of <i>S.aureus</i> FtsZ protein.....	88

4.2.4 Light scattering assay .....	96
4.2.5 GTPase activity assay .....	97
4.2.6 Transmission electron microscopy (TEM) .....	98
4.3 Results and discussion .....	99
4.3.1 Light scattering assay .....	99
4.3.2 GTPase activity .....	103
4.3.3 Transmission electron microscopy (TEM).....	109
4.4 Concluding remarks.....	114
Chapter 5 Conclusions .....	115
Appendix I: High resolution mass spectra of compounds .....	118
Appendix II: <sup>1</sup> H NMR spectra of compounds .....	143
References .....	170

## List of Abbreviations

---

ATCC	American Type Culture Collection
NH <sub>3</sub>	Ammonia
CH <sub>3</sub> CN	Acetonitrile
<i>B.subtilis</i>	<i>Bacillus subtilis</i>
BSA	Bovine serum albumin
CaCl <sub>2</sub>	Calcium chloride
DMF	Dimethyl formamide
DMSO	Dimethyl sulfoxide
<i>E.coli</i>	<i>Escherichia coli</i>
FtsZ / <i>ftsZ</i>	Filamenting temperature sensitive Z
GDP	Guanosine diphosphate
GTP	Guanosine triphosphate
hrs	hours
IPTG	Isopropyl β-D-1-thiogalactopyranoside
LB medium	Luria-Bertani medium
MeOH	Methanol
MgCl <sub>2</sub>	Magnesium chloride
MOPS	4-morpholinepropanesulfonic acid
MIC	Minimum inhibitory concentration
MDRSA	Multi-drug resistant <i>Staphylococcus aureus</i>
MTS	3-(4,5-dimethylthiazol-2-yl)-5-(3-carboxy-methoxyphenyl)-2-(4-sulfophenyl)-2H-tetrazolium

MRSA	Methicillin-resistant <i>Staphylococcus aureus</i>
min	Minute(s)
OD <sub>x</sub>	Optical density at wavelength of x nm
K <sub>2</sub> CO <sub>3</sub>	Potassium carbonate
KCl	Potassium chloride
KOH	Potassium hydroxide
PBS	Phosphate-buffered saline
PDB	Protein Data Bank
PMSF	Phenazine methosulfate
PTA	Phosphotungstic acid
rpm	Revolution per min
<i>S.aureus</i>	<i>Staphylococcus aureus</i>
SDS	Sodium dodecyl sulphate
STD	Saturation transfer difference
THF	Tetrahydrofuran
SnCl <sub>2</sub>	Tin (II) chloride
TEM	Transmission electron microscopy
SOCl <sub>2</sub>	Thionyl chloride
3-MBA	3-Methoxybenzamide

# Chapter 1

## Introduction

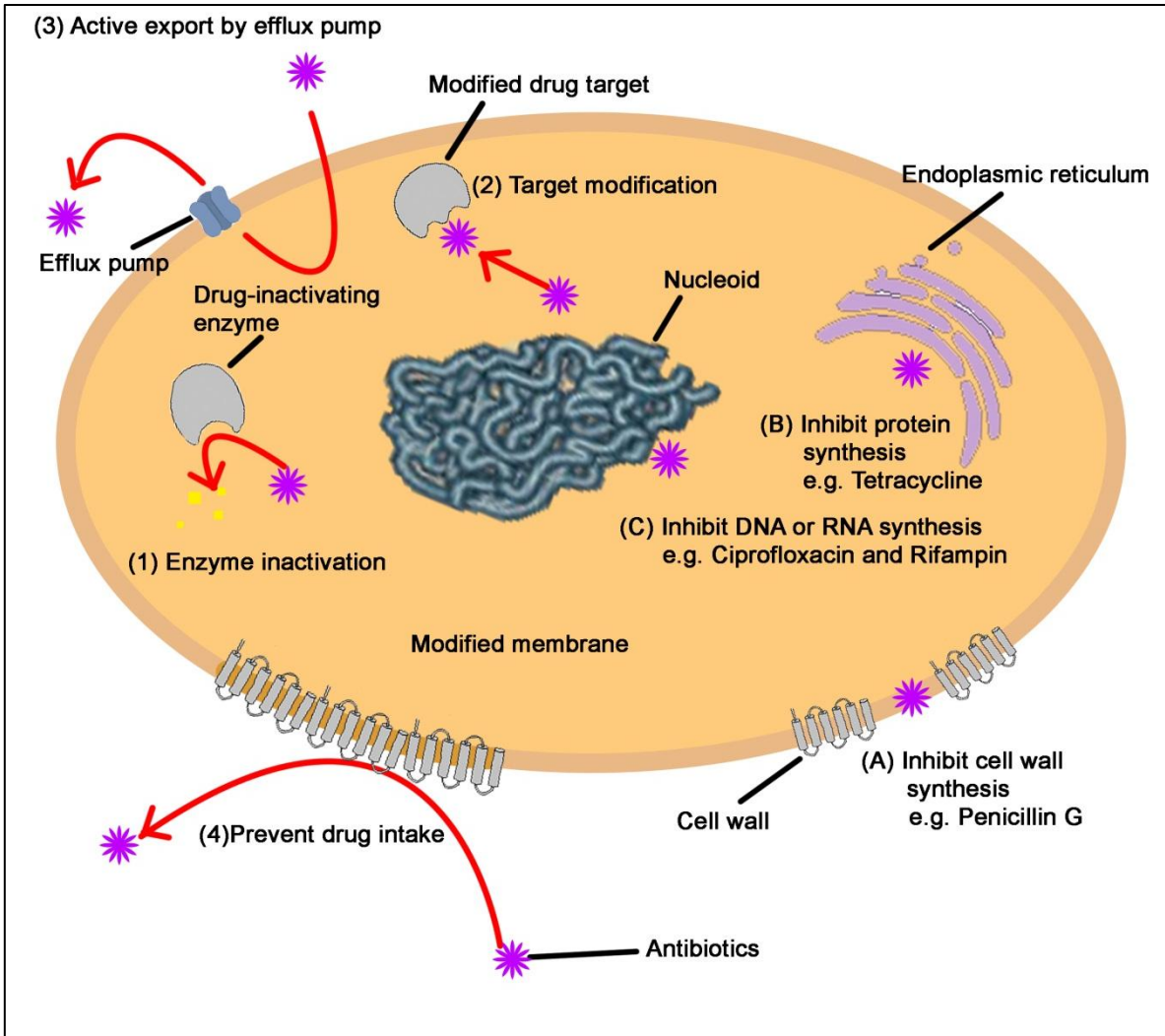
---

### 1.1 Bacterial infection and antibiotic resistance

Since the discovery and clinical use of penicillin, antibiotics have saved many lives from bacterial infections. In the late 1960s, the development of new antibiotics was slowed down because people believed bacterial infection was no longer a threat. Pharmaceutical industry therefore put less efforts and resources to develop new antibiotics [1]. However, the problem of drug resistance appeared and cases of antibiotic resistance were reported. According to the report of World Health Organization (WHO), there were 12 million cases of tuberculosis in 2011. Among them, over 630,000 cases showed multidrug-resistance [2]. Similar situation also happens in Hong Kong. According to the report published by Department of Health in 2012, 4.75% of notifiable infectious diseases were caused by community-associated methicillin-resistant *Staphylococcus aureus* (CA-MRSA) [3].

Bacteria have several means to inactivate the antibacterial activity of antibiotics. (Figure 1.1) The first mechanism is inactivation of antibiotics by hydrolytic enzymes. For example,  $\beta$ -lactamases can hydrolyze the  $\beta$ -lactam ring of penicillins and cephalosporins. As the four-membered  $\beta$ -lactam ring is chemically active for antibacterial activity, hydrolyzed  $\beta$ -lactam antibiotics cannot bind to penicillin-binding proteins (PBPs) on the cell membrane of bacterial cells [4]. The second mechanism is target modifications.

Several amino acids residues are mutated to alter the structure of the drug target. The binding affinity between the antibiotic and the drug target is reduced. As a result, the bacterial cell is protected from the action of antibiotics. The third mechanism is active export of antibiotics. Efflux pump is a trans-membrane protein in cell membranes. The antibiotic molecules are actively exported so that the therapeutic concentration cannot be attained in bacterial cytoplasm [5]. The fourth mechanism is prevention of antibiotics to access the target sites. The mutated porins in the outer membrane can prevent the antibiotics from entering the cells. For example, *P.aeruginos* can resist  $\beta$ -lactams and aminoglycosides by changing its porin structure. In the development of new antibiotics, only linezolid and daptomycin are the novel antibacterial agents launched in the past 30 years [1]. Most new approved antibiotics are analogues of existing antibiotics, which were resisted by certain groups of bacteria. Bacteria can resist the antibacterial action of new antibiotics by applying similar resistance mechanisms. Therefore, there is a desperate need to develop a novel antibacterial agent based on new mechanism of action.



**Figure 1.1** Mechanisms of antibiotic resistance and antibacterial actions by antibiotics



## 1.2 Bacterial cell division and the role of FtsZ in cell division

FtsZ stands for filamentous temperature sensitive Z [6]. It is an essential protein responsible for cytoplasmic division in bacteria. Bacterial cell division is an essential process in the life cycle of bacteria. It is responsible to increase the number of cells for the survival of species. Bacterial cell division is a highly coordinated process which involves nucleoid and cytoplasmic division. In nucleoid division, the nucleoid replicates itself and moves to the two poles of the cell. Cytoplasmic division takes place after nucleoid division. A protofilament called Z-ring is formed in the middle of the cell by polymerization of FtsZ monomers, which were evenly distributed in the cytoplasm before cytoplasmic division takes place. Z-ring recruits subsequent division proteins and reduces the perimeter of the Z-ring until two separate bacterial cells are formed (Figure 1.1).

The homologue of FtsZ in animal cell is tubulin, the protein that makes up microtubules. Tubulin has similar tertiary structure as FtsZ though only share limited sequence identity [7]. Tubulin has sequence motif (A/G)GGTG(S/A) for GTPase activity. A similar glycine-rich sequence motif GGGTGTG can also be found in FtsZ [8]. Mutating this sequence motif of FtsZ can reduce the GTPase activity of FtsZ significantly [9]. Scientists believe FtsZ and tubulin may evolve from the same ancestor [7]. FtsZ is composed of two domains. They are connected by a central H7-helix (Figure 1.2). The N-terminal domain side contains nucleotide binding site while the C-terminal domain side contains the catalytic T7-loop [10]. FtsZ monomers polymerize into a protofilament in head-to-tail manner in the presence of GTP. A GTP-hydrolysis site is formed when the N-terminal side of one FtsZ monomer binds with the C-terminal side of another FtsZ

monomer. GTP hydrolysis will take place and GDP will be formed in the polymer. High concentration of GDP would induce depolymerization of FtsZ polymer. Another GTP molecule will enter the GTP-hydrolysis site to replace GDP and the same process repeats until cytoplasmic division is finished. The FtsZ polymer is dynamic in nature and the length of the polymer is determined by the relative rate of depolymerization and polymerization (Figure 1.3) [7]. It is estimated that about 15,000 FtsZ monomers are evenly distributed in the cytoplasm of one *E.coli* cell. The intracellular concentration of FtsZ in cytoplasm is approximately 10.9  $\mu\text{M}$  in the log phase of *E.coli* cell, which is well above the critical concentration for FtsZ proteins to polymerize [11]. However, the Z-ring only forms during the cytoplasmic division and appears in the middle of the cell. It is believed the Min system and nucleoid occlusion are responsible for controlling Z-ring formation in the middle of the cell [12].

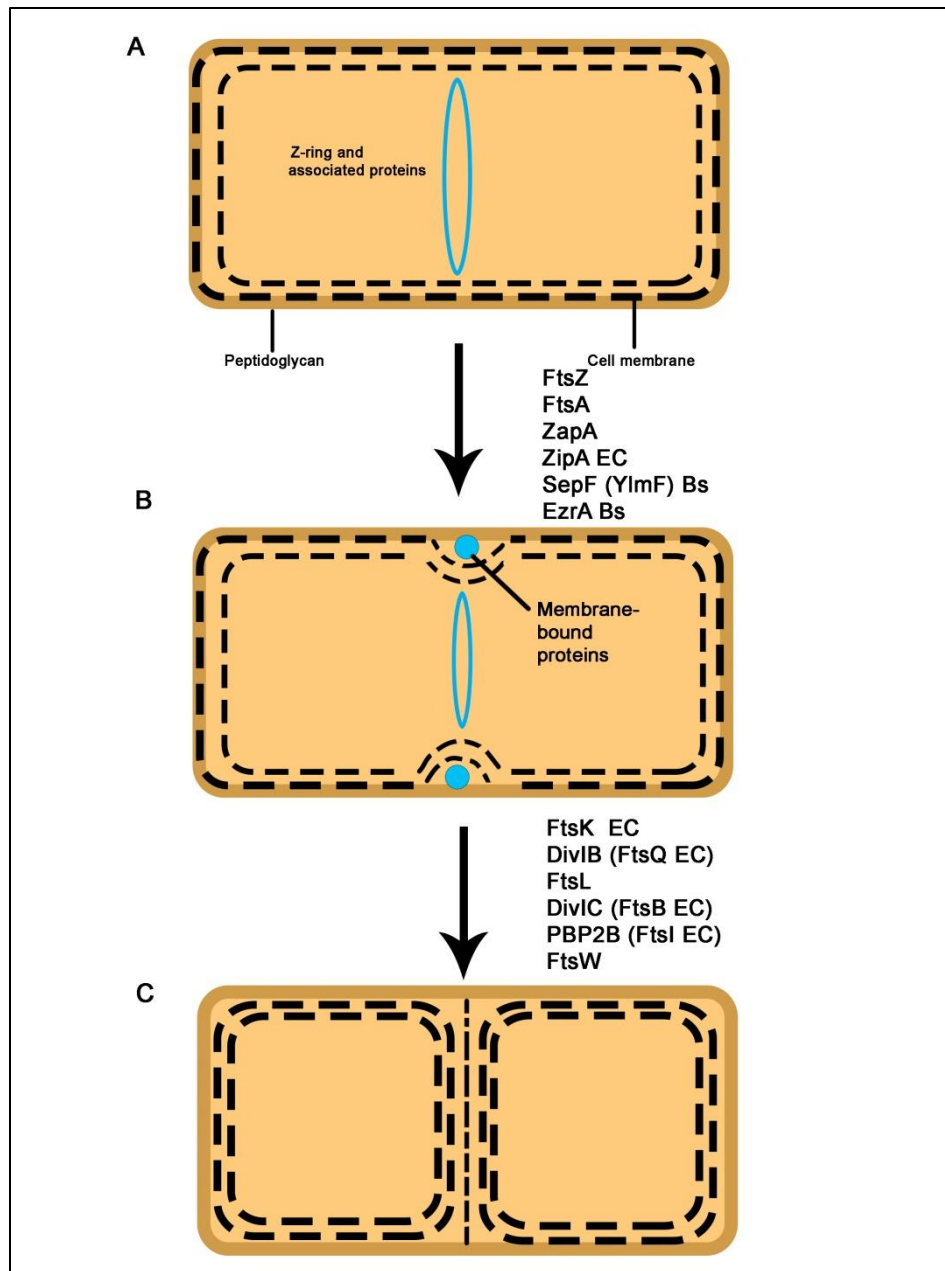
The Min system is dynamic in nature [13]. It ensures the polymerization of FtsZ only takes place in the middle of the cell by inhibiting cell division at the polar zone. MinC, MinD and MinE protein form the Min system in bacterial cell. MinC is a division inhibitor, which is responsible to inhibit cell division to take place. MinD provides a surface for MinC to bind. MinD contains an ATP binding domain and possesses ATPase activity, which is essential for its function because only MinD-ATP can attach on the cell membrane. MinE is present as a ring at the edge of the MinD polar zone. It is responsible to induce the ATPase activity of MinD, causing release of MinD from the cell membrane [14].

In the cell division of *E.coli*, MinD oscillates between poles with a periodicity in the order of ~40 seconds at 20°C [13]. MinD forms a polar zone on the cell membrane and

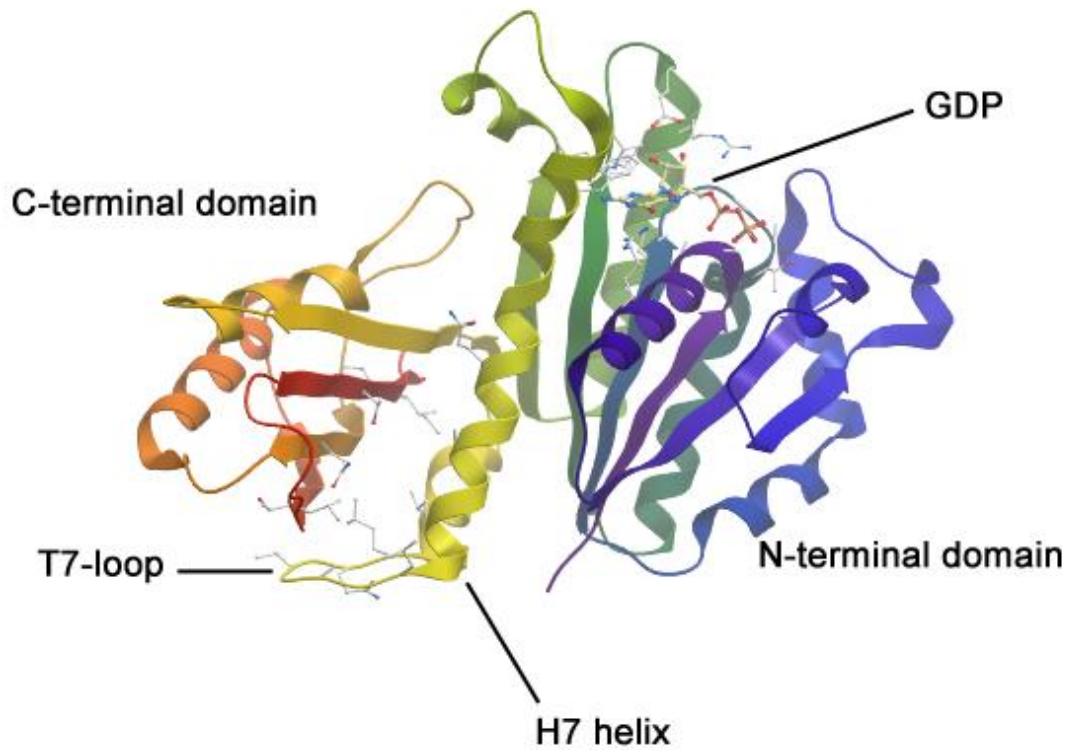
extends toward middle of the cell. As the polar zone continues to grow toward the opposite pole, MinE induces ATPase activity of MinD, causing release of MinD from the cell membrane. MinD-ADP in the cytoplasm will move to the opposite pole and undergoes nucleotide exchange, forming MinD-ATP again and forms a new polar zone at the other end. The cycle is then repeated throughout cell division (Figure 1.4).

If cytoplasmic division takes place in the vicinity of the nucleoid, the nucleoid will be bisected by the septum. Therefore, cytoplasmic division can only be initiated after nucleoid segregation. Nucleoid occlusion is a mechanism which is responsible to prevent cytoplasmic division to take place before nucleoid segregation [15]. The exact mechanism of nucleoid occlusion is still not clear. In the most recent proposed mechanism, a dimer form of DNA binding protein in *E.coli*, SlmA, is believed to be the active FtsZ antagonist [16]. Prior to the nucleoid segregation, a dimer of SlmA proteins was activated by binding to 24 SlmA-binding sequences (SBSs). The SlmA-SBS complexes enhance the GTPase activity of FtsZ. As a result, the FtsZ polymers disassemble because of high concentration of GDP within polymers [16].

When two nucleoids start to segregate, a nucleoid-free zone is formed between replicating nucleoids. Therefore, the Z ring starts to form in the middle of the cell. A complete Z ring will be formed after the two nucleoids segregate to the opposite poles (Figure 1.5).

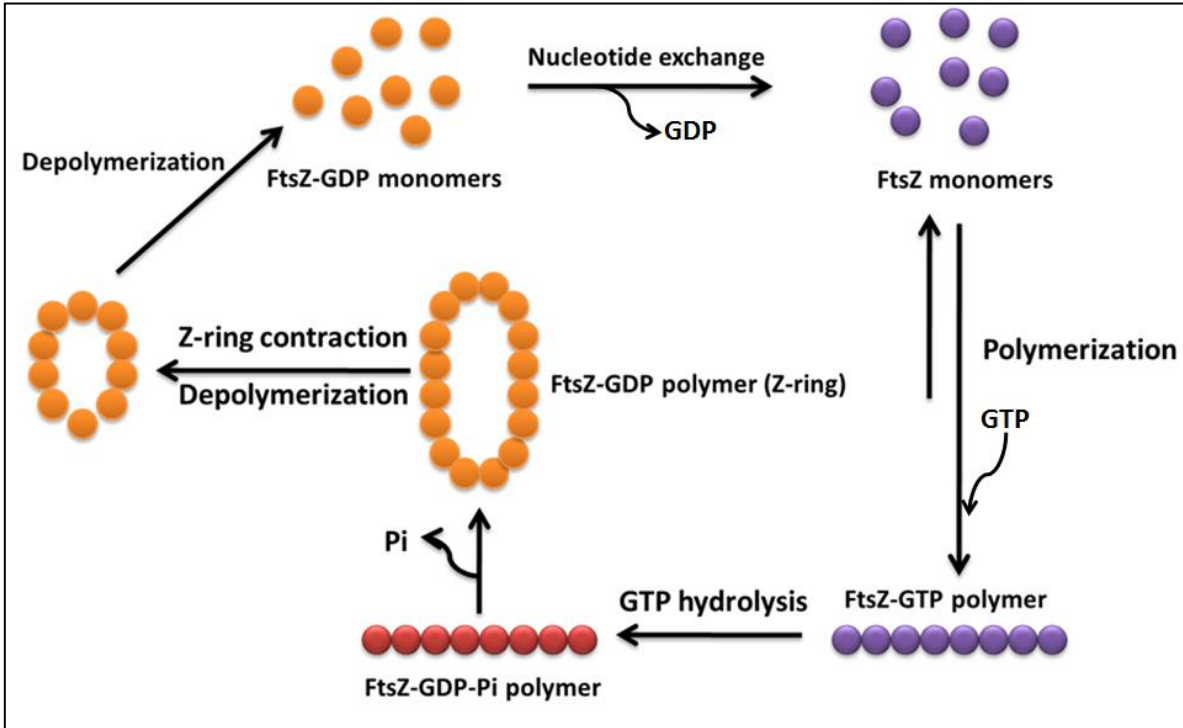


**Figure 1.1** Cytokinesis of bacterial cell and associated proteins. **A:** Z-ring is formed in the middle of the cell. **B:** Membrane-bound proteins are recruited, resulting in invagination of cell membrane and cell wall to form a division septum. **C:** Cell division is completed and two daughter cells are formed. (Adapted from [17])

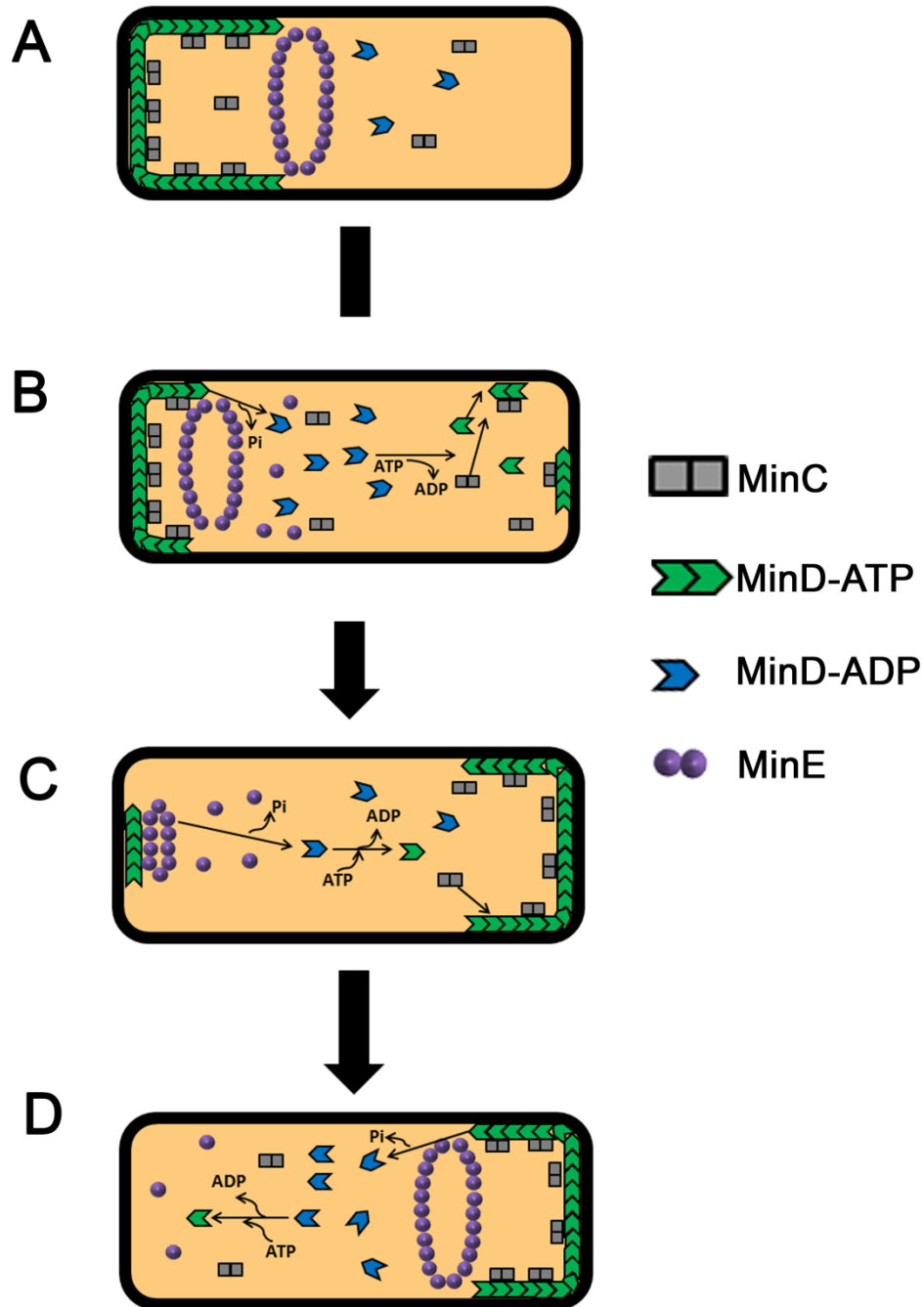


**Figure 1.2** The molecular structure of *S. aureus* FtsZ with GDP (PDB code: 3VOB)

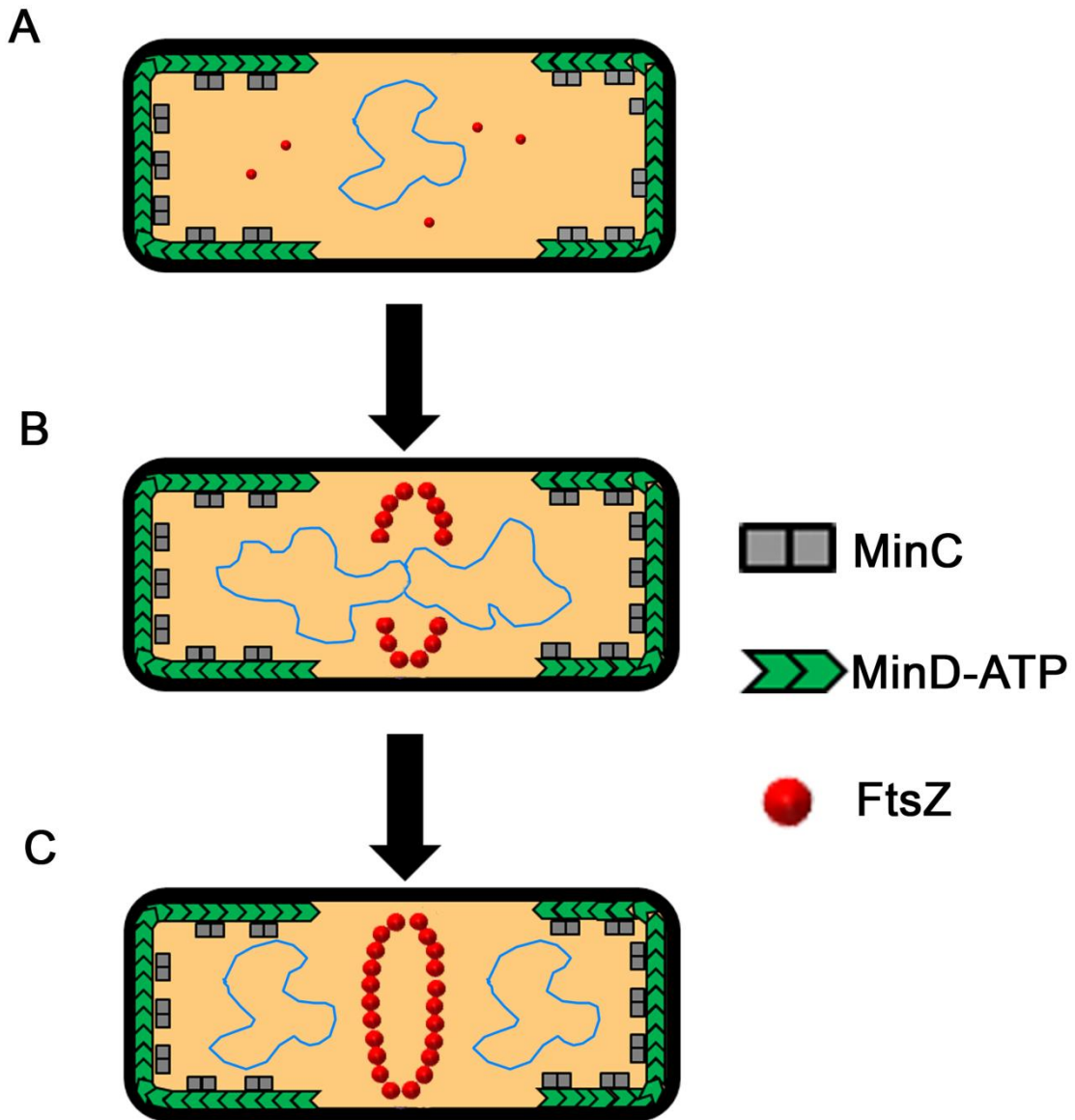
(Prepared by ICM Molsoft LCC)



**Figure 1.3** Schematic diagram of Z-ring formation [7, 9]



**Figure 1.4:** (A) Oscillation of the Min proteins in *E.coli*. MinD-ATP attached to the cell membrane and recruits MinC; (B) MinE induces dissociation of MinC from the cell membrane and stimulates MinD-ATPase, causing release of the MinD proteins from the cell membrane; (C) MinD-ADP undergoes nucleotide exchange to regenerate MinD-ATP in cytoplasm and attaches the cell membrane on the opposite pole; (D) A new polar zone is formed because of increasing concentration of MinD-ATP at the pole (Adapted from [18]).



**Figure 1.5:** (A) Spatial regulation of cell division by nucleoid occlusion and the Min system in a *E.coli* cell prior nucleoid replication; (B) FtsZ polymerizes in the middle of the cell because of formation of nucleoid-free zone between replicating nucleoids; (C) Z ring is formed in the middle of the cell after two nucleoids segregated to the opposite poles. (C)



### 1.3 FtsZ as a novel antibacterial target

Antibiotics should kill or inhibit the growth of bacteria with low side-effect on human. The targets of antibiotics on bacteria are usually absent in or structurally different from those in human. Antibiotics may inhibit cell wall synthesis, protein synthesis, folate coenzyme biosynthesis, DNA replication and repair in bacteria [5]. Although more than 47 new antibiotics were approved by US Food and Drug Administration in the past 30 years, only linezolid and daptomycin are antibacterial agents with new chemotype scaffolds [1]. According to the report of The Infectious Diseases Society of America (IDSA) in 2013, only one new system antibiotic was approved by FDA since 2010 [19]. As bacteria can resist new antibiotics if they have similar chemical structures as existing antibiotics, there is a pressing need to develop new drugs targeting on unexploited target.

Cytoplasmic division is a crucial process in bacteria. FtsZ plays a key role in bacterial cytoplasmic division and is commonly found in gram-positive and gram-negative bacteria with few exceptions [7, 17]. High resolution protein X-ray crystallography provides detailed structural information of FtsZ. Also, different *in vitro* assays also available to characterize FtsZ protein. As FtsZ is highly conserved in bacteria [20], FtsZ becomes an attractive novel antibacterial target.

The GTP-binding site on N-terminal region and the T7-loop on C-terminal region of FtsZ protein are important for Z-ring formation. An unknown mechanism is regulating the rate of polymerization-depolymerization of Z-ring during cytoplasmic division. FtsZ inhibitors targeting on these two regions can perturb either the polymerization or GTPase

activity of FtsZ protein, or both. A filamentous cell would be observed if a septum cannot form properly during cytoplasmic division [21].

Although more than 80% of the FtsZ sequence is different from that of tubulin [22], FtsZ and tubulin have a high degree of structural similarity [21]. Both FtsZ and tubulin have two domains in their structures. From the sequence alignment between FtsZ and tubulin, it is expected that their N-terminal domains should have very similar structure because of substantial sequence identity [21, 23]. On the other hand, the amino acid sequence of C-terminal domains between FtsZ and tubulin are less conserved. However, as revealed from the three-dimensional structures of FtsZ and tubulin, the structures of N-terminal domains and the C-terminal domains of FtsZ and tubulin are very similar, suggesting that FtsZ and tubulin performing similar functions *in vivo*.

Both FtsZ and tubulin have similar three-dimensional structures, but that does not mean tubulin inhibitors always target on FtsZ as well. The mechanisms of forming FtsZ and tubulin protofilaments are different. Two tubulin subunits ( $\alpha$  and  $\beta$ ) are longitudinally associated in tubulin polymerization, whereas FtsZ subunits are identical in FtsZ polymerization [21]. The polymerization mechanism in tubulin is also different from that of FtsZ. In tubulin polymerization, GTP binds to the exchangeable site (E-site) of  $\beta$ -tubulin and being hydrolyzed within polymer. Unlike nucleotide exchange in FtsZ polymer, the resulting GDP does not exchange in tubulin polymer. The GDP at the E-site can only be released when the tubulin subunits are released in depolymerization. Finally, a new GTP binds to tubulin subunits again and undergoes another round of polymerization [24]. Because of small sequence identity and distinct polymerization mechanisms between FtsZ

and tubulin, it is possible to develop antibacterial agents that are specific to FtsZ with few adverse effects [21].

## 1.4 FtsZ inhibitors

### 1.4.1 FtsZ inhibitors targeting at the GTP-binding site

The GTP-binding site of FtsZ is located on the N-terminal domain and is conserved among distantly-related bacterial species [25]. Most FtsZ inhibitors perturb the function of FtsZ by binding to the GTP-binding site of the protein. Berberine is a natural compound that inhibits the growth of *B.subtilis* (ATCC 6633) with MIC of 100 µg/mL. *In silico* molecular docking showed that berberine binds to in the GTP binding pocket. In hemolytic assay on human cells, berberine did not induce hemolysis in human erythrocytes up to 2 mg/mL [26]. 8-bromoguanosine 5'-triphosphate (BrGTP), is a semi-synthetic FtsZ inhibitor. Previous studies showed that the bromine or hydroxyl group at the C8 position on BrGTP does not affect tubulin assembly. BrGTP inhibits both polymerization and GTPase activity of FtsZ. GTP can displace BrGTP from FtsZ as demonstrated in competition assay [27]. This proves BrGTP has the same binding site as GTP in FtsZ. PC58538 is a synthetic FtsZ inhibitor. It inhibits both the GTPase activity and polymerization of *B. subtilis* FtsZ *in vitro*. It has inhibitory effect on the growth of *B.subtilis* 168 with MIC of 128 ug/mL. Selective amino acid substitutions around the edge of the GTP-binding pocket can prevent the binding of PC58538 to FtsZ *in vivo*. This indicates PC58538 bind to the GTP-binding site of FtsZ protein [28]. Viriditoxin was identified as a FtsZ inhibitor by screening more than 100,000 extracts of microbial fermentation broths and plants. Viriditoxin was found to inhibit a broad range of clinically-relevant pathogens, such as vancomycin-resistant *Enterococci* and methicillin-resistant *S.aureus*. It blocks the polymerization of FtsZ and

inhibits GTPase activity of FtsZ with an IC<sub>50</sub> of 8.2 µg/mL and 7.0 µg/mL respectively [29]. *In silico* molecular docking showed that viriditoxin binds to the GTP-binding site [30]. However, viriditoxin is highly toxic and chemically unstable. Previous study showed that viriditoxin has both myotoxic and hemorrhagic activities which prevent further development of viriditoxin in clinical use [31, 32]. Curcumin is a natural polyphenolic compound extracted from the rhizomes of *Curcuma longa* which is known to have various biological activities such as anti-proliferation of cancer cells, antimicrobial activity, wound healing ability and tubulin polymerization perturbation. Curcumin induces cell filamentation of *B. subtilis* 168. The average cell length of *B. subtilis* 168 increased by 6 folds in the presence of 50 µM curcumin. Interestingly, curcumin increases the GTPase activity of FtsZ but inhibits the assembly of FtsZ [33]. Molecular docking indicated that curcumin binds preferentially to the GTP-binding site [34]. Curcumin showed 35% toxicity to normal fibroblast cells NIH3T3 at a concentration of 40 µM as demonstrated in cytotoxicity assay [35]. Amikacin is a second-line drug used for the treatment of resistant *Mycobacterium* infections. It is believed that Amikacin induces misreading during protein synthesis. However, the exact mechanisms and their antimicrobial activities are still not well understood. Christophe Possoz et al investigated the *E. coli* elongation in the presence of sublethal concentration of Amikacin. They found that Amikacin can perturb the assembly of the Z-ring at low concentration [36]. Molecular docking suggested that Amikacin likely binds to the GTP-binding site of FtsZ protein [30]. Amikacin has the potential to develop into a specific FtsZ inhibitor because of its low cytotoxicity to mammalian cells [37]. UCM05, UCM44 and UCM53 were identified as FtsZ inhibitors by virtual screening. Among them, UCM53 has lowest MIC value of 13 µM against *B. subtilis*

168. UCM05 or UCM44 inhibit the GTPase activity and polymerization of FtsZ as demonstrated in GTPase activity assay and sedimentation assay respectively. The binding site is believed to be the GTP-binding site of FtsZ as GTP can displace these compounds in competition assay. Among these three compounds, UCM53 has lowest cytotoxicity to animal cells as demonstrated in cytotoxicity assay [38]. A list of the FtsZ inhibitors targeting at the GTP-binding site is given in Table 1.1.

**Table 1.1 A list of FtsZ inhibitors targeting at the GTP-binding site**

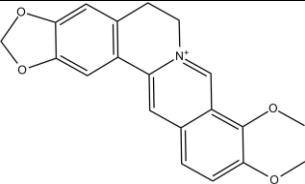
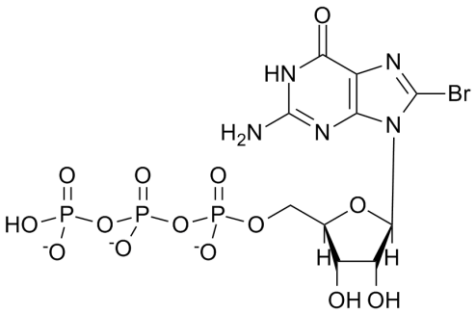
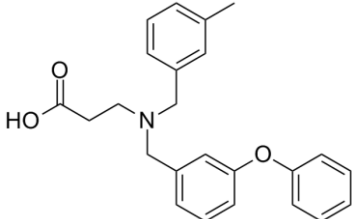
Compound	Structure	Binding site (Detection method) and antibacterial activity	Cytotoxicity
Berberine		GTP-binding site (Docking) <i>B. subtilis</i> 168 (MIC=100 ug/mL)	Non-toxic up to 2 mg/mL (Erythrocytes)
BrGTP		GTP-binding site (Experimental) Unknown antibacterial activity	No result
PC58538		GTP-binding site (Experimental) <i>B. subtilis</i> 168 (MIC=128 ug/mL)	No result

Table 1.1 continue

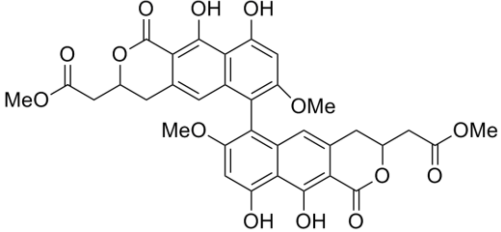
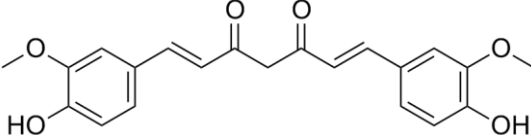
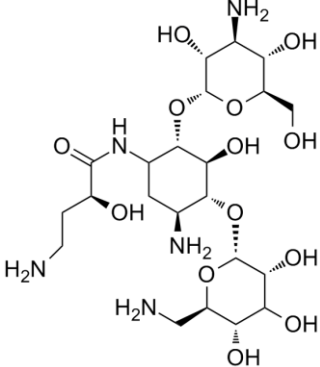
Compound	Structure	Binding site (Detection method) and antibacterial activity	Cytotoxicity
Viriditoxin		GTP-binding site (Docking) <i>S.aureus</i> CL9080 (MSSA) (MIC=4 ug/mL)	LD <sub>50</sub> =5 ug/g (Mice)
Curcumin		GTP-binding site (Docking) <i>B.subtilis</i> (MIC=17 μM)	(35% cell death at 40 μM) (NIH3T3)
Amikacin		GTP-binding site (Docking) <i>P.aeruginosa</i> (MIC= 16 ug/mL)	Low cytotoxicity



Table 1.1 continue

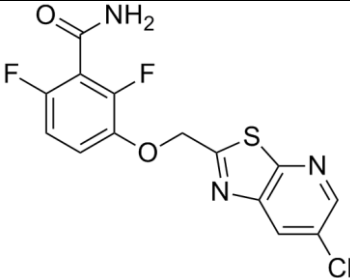
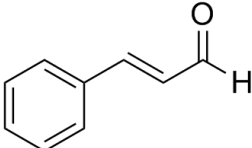
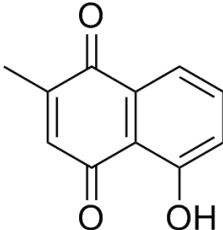
Compound	Structure	Binding site (Detection method) and antibacterial activity	Cytotoxicity
UCM05		GTP-binding site (Docking) <i>B.subtilis</i> 168 (MIC=100 μM)	LD <sub>50</sub> =30 ± 9 μM (HUVEC)
UCM44		GTP-binding site (Docking) <i>B.subtilis</i> 168 (MIC=25 μM)	LD <sub>50</sub> =44 ± 4 μM (HUVEC)
UCM53		GTP-binding site (Docking) <i>B.subtilis</i> 168 (MIC=13 μM)	LD <sub>50</sub> =50 ± 1 μM (HUVEC)

#### 1.4.2 FtsZ inhibitors targeting at the T7-loop

**PC190723** is by far the most successful FtsZ inhibitor reported. It is a derivative of 3-methoxybenzamide (**3-MBA**). 3-MBA inhibits the growth of *B.subtilis* 168 with a MIC of 4000 µg/mL [39], but **PC190723** inhibits the growth of *B.subtilis* as well as all strains of *Staphylococci* with MIC in the range of 0.5-1.0 µg/mL, including the methicillin-resistant *S.aureus* (MRSA) and the multi-drug-resistant *S.aureus* (MDRSA) [40]. **PC190723** inhibits the GTPase activity of FtsZ *in vitro* in a dose-dependent manner but promotes polymerization of FtsZ as evidenced by light scattering experiment. **PC190723** does not have inhibitory effects on some Gram-positive and Gram-negative bacteria such as *S.pneumoniae* and *E.coli*. Mice infected with a lethal dose of *S.aureus* were cured by intravenous administration of **PC190723** [40]. Molecular model suggested that **PC190723** would bind to the T7-loop of the protein which was later proved by the crystal structure of *S.aureus* FtsZ with **PC190723** [40, 41]. **PC190723** is a promising FtsZ inhibitor and it has become a good lead compound for further modification. Trans-cinnamaldehyde is a natural FtsZ inhibitor extracted from *Cinnamomum cassia*. It has been used to treat gastritis and bacterial infections in traditional Chinese medicine. Cinnamaldehyde inhibits the growth of *E.coli*, *B.subtilis* and MRSA with MICs of 1000 µg/mL, 500 µg/mL and 250 µg/mL respectively. Cinnamaldehyde also inhibits the GTPase activity of FtsZ *in vitro* [42]. Polymerization of FtsZ was inhibited *in vivo* and *in vitro* by cinnamaldehyde as demonstrated by the reduction of light scattering and loss of Z-ring formation in the bacterial cells under confocal microscopy. No hemolytic activity toward human eukaryotic cells was observed up to 2000 µg/mL. This indicates that cinnamaldehyde can inhibit the

growth of bacteria without affecting the normal activity of human cells. The binding site of cinnamaldehyde to FtsZ involves the T7-loop pocket, similar to Sula which is a natural FtsZ inhibitor found in bacterial cells [42]. Plumbagin is secondary metabolite in *Nepenthes insignis* [43]. It inhibits the growth of *B.subtilis* 168 and *M.smegmatis* with MICs of 29  $\mu$ M and 31  $\mu$ M respectively. However, no discernible effect on *E.coli* was observed. The GTPase activity of *B.subtilis* FtsZ was inhibited to 58% in the presence of 24  $\mu$ M plumbagin. Plumbagin was found to inhibit the formation of the Z-ring in *B.subtilis* 168. Also, the number of Z-ring per micrometer of the cell length was reduced in the presence of plumbagin. Molecular docking suggested that plumbagin binds to the C-terminal region of *B.subtilis* FtsZ. Selected amino acids mutations in the C-terminal domain of FtsZ confirmed that plumbagin binds to the T7-loop as demonstrated by the reduced binding affinity between plumbagin and mutated *B.subtilis* FtsZ [44]. Plumbagin is highly toxic to human skin cells. Indeed, plumbagin has been known as a mutagen [45]. The IC<sub>50</sub> of cytotoxicity to keratinocytes was found to be 18  $\mu$ M, which is close to its MIC value in *B.subtilis* 168. Due to its high cytotoxicity, plumbagin does not appear a good hit compound for further drug development. A list of FtsZ inhibitors targeting at the T7-loop with their structures is given in Table 1.2.

**Table 1.2 A list of FtsZ inhibitors targeting at the T7-loop**

Compound	Structure	Binding site (Detection method) and antibacterial activity	Cytotoxicity
PC190723		<p>T7-loop (Crystal structure, PDB ID: 3VOB) <i>B. subtilis</i> 168 (MIC=0.5-1.0 ug/mL)</p>	<p>Non-toxic up to 30 mg/kg (Mice)</p>
Trans-cinnamaldehyde		<p>T7-loop <i>E. coli</i> (MIC=1000 ug/mL) <i>B. subtilis</i> 168 (MIC=500 ug/mL) MRSA (MIC=250 ug/mL)</p>	<p>Non-toxic up to 2000 ug/mL (Human red blood cells)</p>
Plumbagin		<p>C-terminal domain (Experimental) <i>B. subtilis</i> 168 (MIC=29 μM) <i>M. smegmatis</i> (MIC=31 μM)</p>	<p>IC<sub>50</sub>=18 μM (Keratinocytes)</p>

## 1.5 Drug discovery approaches

All the drugs presently available in the market interact with less than 500 molecular targets [46, 47]. Those drugs were discovered from different sources by different approaches. In fact, 80% of drugs available in the market were natural products or inspired by a natural compound [48]. All the drugs need to be clinically tested to ensure they are active and safe for human use before going for sale in the market. In the initial stage of a drug discovery process, hit compounds are identified first. A hit compound is a primary compound which has non-promiscuous binding to a drug target [47]. It can be identified from natural extracts, combinatorial chemistry or *in silico* virtual screening. Natural products from plants, microbes and animals provide a great diversity of chemical compounds. Natural products usually retained relatively low partition coefficient (log P) values compared with synthetic drugs. It means the natural products can be absorbed easily by the human and become an important source of chemicals for drug discovery [48]. Combinatorial chemistry is another source to provide chemical compounds for drug discovery. Combinatorial chemistry provides thousands to millions of compounds in a single process [49]. The academia and pharmaceutical companies were not interested in combinatorial chemistry at first because of low product purity and overloaded molecular complexity. However, the problem can be solved by focusing on synthesizing smaller and drug-like compounds [47]. *In silico* virtual screening becomes a trend in current drug discovery. With the advent in computational power and biotechnology, protein crystals of potential drug targets are readily available. The binding poses as well as the affinity of drug candidates to the drug target can be predicted virtually by docking program. Drug

candidates with good docking scores will be synthesized and assayed *in vivo* and *in vitro*. *In silico* virtual screening can reduce laboratory works as well as the cost in primary stage of drug discovery. Although inhibitors of the protein kinase CDK2 and Plk1 were discovered successfully by virtual screening [50], the results are varied among different docking programs. Many studies have shown that the performance of most docking programs is largely dependent on the target and it is impossible to predict which program is suitable for a given target [51]. As a result, *in silico* docking program can be a tool to predict how the drug binds to the drug target, but it does not always give accurate results in drug discovery.

High-Throughput Screening (HTS) and Fragment-Based Drug Discovery (FBDD) have been implemented to identify a hit compound from a large number of drug candidates. HTS identifies hit compounds by screening hundreds to millions of compounds that either inhibit or activate the target to give an assay signal above a defined threshold value [52]. Chemicals screened by HTS usually obey Lipinski's rule of five which means a drug-like chemicals should have not more than 5 hydrogen bond donors, not more than 10 hydrogen bond acceptors, the molecular weight should be smaller than 500 Da and the calculated partition coefficient (CLogP) value should be smaller than 5 [53]. However, the number of chemical compounds fulfilled these requirements is very large. Moreover, the compounds identified from HTS are not always suitable for further drug development [47]. The low hit rate of HTS discourages pharmaceutical companies and academia in drug discovery. On the other hand, FBDD has become a trend in recent drug discovery. Small molecules are described as fragments because they are part of the final product obtained by joining or merging a number of small molecules together through chemical synthesis. Recently, FBDD draws the attention of many drug screening groups. FBDD focuses on screening

small molecules with weak binding affinity to the drug target. Compounds screened in FBDD follow the rule of three in which the molecular weight of compounds should be smaller than 300, the value of Clog P should be smaller than or equal to 3 and the number of hydrogen bond donors and acceptors should not be more than 3 [54]. The number of compounds fulfilled these requirement is much smaller than those screened in HTS. It would be more efficient to identify hit compound in FBDD. Although small molecules have very weak binding affinity to the drug target, the ligand efficiency is higher compared with large molecules screened in HTS. As a result, FBDD has become a promising drug discovery approach in the 21<sup>st</sup> century.

## 1.6 Aims and objectives

3-Methoxybenzamide (**3-MBA**) is known as an inhibitor of ADP-ribosyltransferase (ADPRT), which is a bacterial toxin catalyzing the ADP-riboxylation of GTP-binding proteins in mammalian cells [55]. It has been reported that ADP-riboxylation is important in cell differentiation in *Streptomyces* and sporulation in *Bacillus subtilis* [56, 57]. Scientists have isolated a mutant of *B.subtilis* which can resist to the lethal effect of **3-MBA** by mutating the *ftsZ* gene of *B.subtilis*, indicating that **3-MBA** can perturb the normal function of FtsZ in *B.subtilis* [39].

Later on, it was demonstrated that **3-MBA** is a weak FtsZ inhibitor which shows inhibitory effect on the growth of *B.subtilis* [39]. This discovery has led to the identification of the most potent FtsZ inhibitor so far, **PC190723**, which inhibits the growth of *B.subtilis* and various *Staphylococci* including MRSA in the range of 0.5-1.0 µg/mL without appreciable cytotoxicity [40]. **3-MBA** is a good starting point to develop potent FtsZ inhibitors because of its low molecular weight and high ligand efficiency although it has only weak on-target antibacterial activity against *B.subtilis* (MIC: 4000 µg/mL) [39, 58, 59]. Moreover, it can pass through the barrier of bacterial cell easily [60]. Czaplewski et al found that certain 3-alkoxybenzamide derivatives show higher antibacterial activity than **3-MBA** [58]. Based on these studies, 3-alkoxybenzamide and 3-aminobenzamide derivatives were chosen as lead compounds to develop potent derivatives FtsZ inhibitors in this project.

In this thesis, the synthesis of some alkoxybenzamide and aminobenzamide derivatives will be described in chapter 2. The antibacterial properties, influence on



bacterial cell morphology and cytotoxicity of the synthesized compounds will be described in chapter 3. The *in vitro* assays of these compounds with the FtsZ protein will be reported in chapter 4.

## Chapter 2

### Chemical synthesis of derivatives of 3-MBA

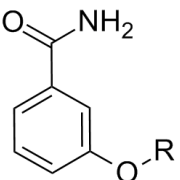
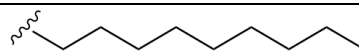
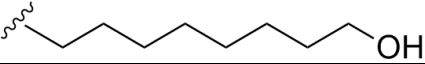
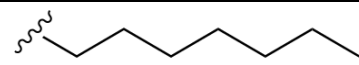
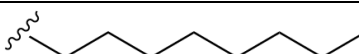
---

#### 2.1 Introduction

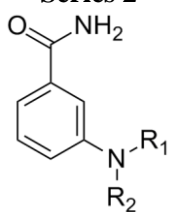
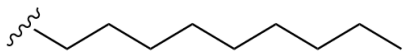
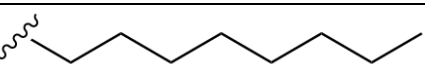
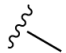
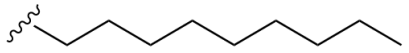
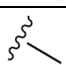
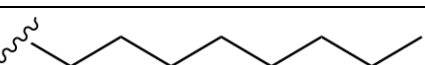
A total of 4 series of alkoxy- and amino- derivatives of **3-MBA** have been synthesized. The chemical structures of these derivatives are given in Table 2.1-2.4.

Series 1 are 3-alkoxybenzamides (Table 2.1) with alkoxy groups of different aliphatic chain length. Series 2 are 3-aminobenzamides (Table 2.2) containing amino groups with different substituents. Series 3 are fluorinated derivatives of 3-alkoxy-benzene, 3-alkoxy-benzoic acid and 3-alkoxybenzamide (Table 2.3). Series 4 are 2,6-difluoro-3-aminobenzamide derivatives (Table 2.4) containing amino groups with different substituents. The detailed synthesis of these 4 series are given in the following section.

**Table 2.1 Chemical structures of series 1**

<p style="text-align: center;"><b>Series 1</b></p> 	
Compound	R
<b>1-F302</b>	
<b>1-F304</b>	
<b>1-F313</b>	
<b>1-F320</b>	

**Table 2.2 Chemical structures of series 2**

<p style="text-align: center;"><b>Series 2</b></p> 		
Compound	R <sub>1</sub>	R <sub>2</sub>
<b>2-F411</b>	H	
<b>2-F412</b>	H	
<b>2-F413</b>		
<b>2-F414</b>		

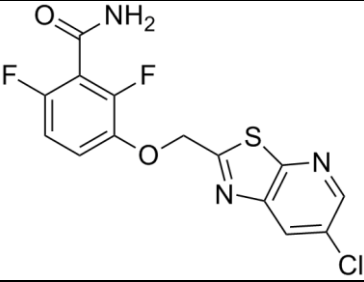
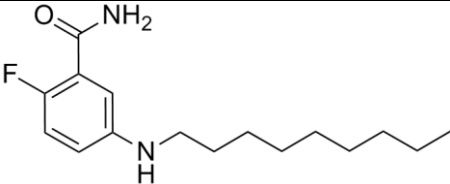
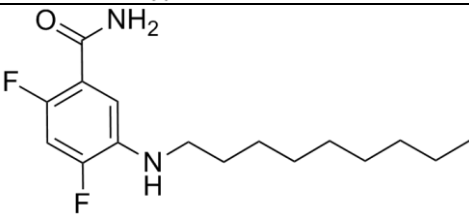
**Table 2.3 Chemical structures of series 3**

Series 3		
Compound	R <sub>1</sub>	R <sub>2</sub>
<b>3-F324</b>	H	
<b>3-F325</b>		
<b>3-F326</b>		

**Table 2.4 Chemical structures of series 4**

Series 4			
Compound	R <sub>1</sub>	R <sub>2</sub>	R <sub>3</sub>
<b>4-F332</b>	H	H	
<b>4-F333</b>	H	H	
<b>4-F334</b>	H	H	
<b>4-F350</b>	H	H	
<b>4-F361</b>	H		
<b>4-F369</b>	H	H	
<b>4-F370</b>	H	H	
<b>4-F371</b>	Br	H	
<b>4-F391</b>	H	H	
<b>4-F409</b>	H		
<b>4-F410</b>	H		

**Table 2.5 Chemical structures of other compounds**

Compound	
<b>F327</b> <b>(PC190723)</b>	
<b>F342</b>	
<b>F345</b>	

## 2.2 Experimental

### 2.2.1 Materials

3-Aminobenzamide, 1-bromononane, 1-bromooctane, dimethyl sulfate, 2-fluoro-5-aminobenzamide, 2,4-difluoro-5-aminobenzamide, 2,6-difluoro-3-nitrobenzoic acid, 1-bromodecane, 1-bromo-4-butoxybutane, geranyl bromide, (Z)-1-bromonon-2-ene, 1-bromoheptane, methyl iodide, bromoethane, 1,4-dibromobutane, 1,5-dibromobutane, 3,4-difluorobenzyl bromide, 2,4-difluorobenzyl bromide, 2,6-difluorobenzyl bromide, nonanoyl chloride, 3-butoxybenzaldehyde, 3-(pentyloxy)benzaldehyde, 3-(sec-butoxy)benzaldehyde, 3-((4-(trifluoromethyl)benzyl)oxy)benzaldehyde, hept-1-yne, oct-1-yne, non-1-yne, 1-chloro-4-ethynylbenzene, 1-fluoro-4-ethynylbenzene, dec-1-yne, 1-methoxy-4-ethynylbenzene and 1-(pro-2-yn-1-yloxy)hexane were obtained from Sigma-Aldrich.  $\text{Cu}(\text{PPh}_3)_3\text{Br}$  catalyst was prepared according to the literature [61]. All chemicals and solvents were reagent grade and were used without further purification unless otherwise stated. The thin-layer chromatography (TLC) plates were obtained from Merck. (Silica Gel 60F<sub>254</sub>, 0.25-mm thickness) and they were visualized under short (254-nm) and long (365-nm) UV light or potassium permanganate stain followed by heating. Chromatographic purifications were carried out using MN silica gel 60 (230 – 400 mesh).

### 2.3 Instrumentation

<sup>1</sup>H NMR spectra were recorded with a Bruker 400 MHz DPX-400 NMR spectrometer. All NMR measurements were carried out at room temperature and the chemical shifts are reported as parts per million (ppm) in unit relative to the <sup>1</sup>H residual resonance of CDCl<sub>3</sub> (7.28 ppm in the <sup>1</sup>H spectra). Mass spectra were recorded with a Finnigan MAT 95S mass spectrometer. The purity of tested compounds were determined by HPLC with an Agilent series 1100 chromatograph equipped with an Agilent Prep-Sil Scalar column (4.6 mm x 250 mm, 5-μm) and UV detection at 265 nm (reference at 450 nm). The compounds were eluted with hexane /ethyl acetate (60:40) at a flow rate of 1.0 mL/min. All tested compounds were shown to be >95% pure according to HPLC.

## 2.4 Synthesis and characterization

### 2.4.1 Preparation of series 1 compounds

The synthesis of **1-F300**, **1-F301**, **1-F302**, **1-F304**, **1-F313** and **1-F320** have been described in a previous publication [58]. The synthetic pathway of these compounds is given in Scheme 2.1.

**(Methyl 3-(nonyloxy)benzoate (1-F300):**  $^1\text{H}$  NMR (400 MHz, CHLOROFORM-*d*) ppm 0.91 (t,  $J=6.60$  Hz, 3 H) 1.25 - 1.41 (m, 10 H) 1.44 - 1.54 (m, 2 H) 1.76 - 1.86 (m, 2 H) 3.93 (s, 3 H) 4.01 (t,  $J=6.60$  Hz, 2 H) 7.11 (dd,  $J=8.31, 2.45$  Hz, 1 H) 7.34 (t,  $J=8.07$  Hz, 1 H) 7.57 (s, 1 H) 7.63 (d,  $J=7.34$  Hz, 1 H); ESI-MS  $m/z$ : 279.2  $[\text{M}+\text{H}]^+$ , 301.2  $[\text{M}+\text{Na}]^+$

**3-(Nonyloxy)benzoic acid (1-F301):**  $^1\text{H}$  NMR (400 MHz, CHLOROFORM-*d*) ppm 0.92 (t,  $J=6.85$  Hz, 3 H) 1.25 - 1.56 (m, 12 H) 1.83 (quin,  $J=6.97$  Hz, 2 H) 4.04 (t,  $J=6.60$  Hz, 2 H) 7.18 (dd,  $J=8.07, 2.20$  Hz, 1 H) 7.40 (t,  $J=7.82$  Hz, 1 H) 7.65 (s, 1 H) 7.74 (d,  $J=7.83$  Hz, 1 H); ESI-MS  $m/z$ : 265.2  $[\text{M}+\text{H}]^+$ , 287.2  $[\text{M}+\text{Na}]^+$

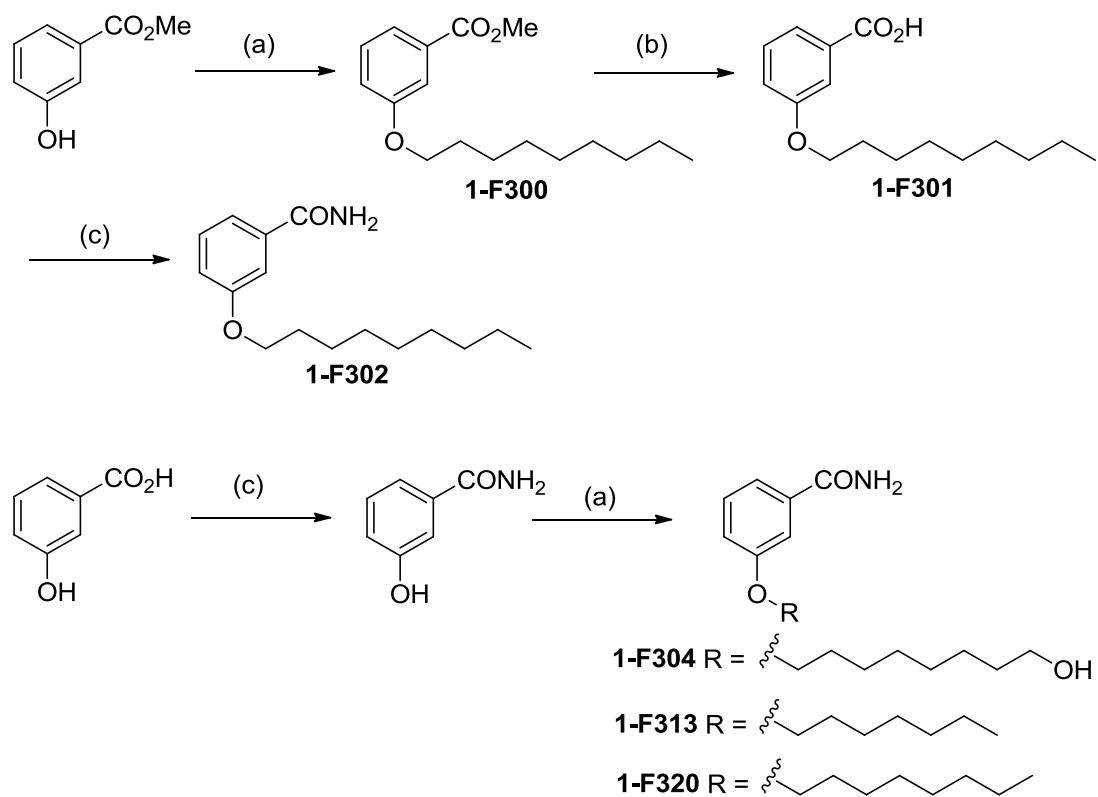
**3-(Nonyloxy)benzamide (1-F302):**  $^1\text{H}$  NMR (400 MHz, CHLOROFORM-*d*) ppm 0.90 (t,  $J=6.60$  Hz, 3 H) 1.22 - 1.52 (m, 12 H) 1.72 - 1.86 (m, 2 H) 4.00 (t,  $J=6.60$  Hz, 2 H) 6.26 (br. s., 2 H) 7.00 - 7.14 (m, 1 H) 7.31 - 7.47 (m, 3 H); ESI-MS  $m/z$ : 264.2  $[\text{M}+\text{H}]^+$ , 287.2  $[\text{M}+\text{Na}]^+$



**3-((8-hydroxyoctyl)oxy)benzamide (1-F304):**  $^1\text{H}$  NMR (400 MHz, CHLOROFORM-*d*) ppm 1.34 - 1.63 (m, 10 H) 1.73 - 1.88 (m, 2 H) 3.66 (t,  $J=6.60$  Hz, 2 H) 4.02 (t,  $J=6.36$  Hz, 2 H) 5.79 - 6.29 (m, 2 H) 7.07 (dt,  $J=6.85, 2.45$  Hz, 1 H) 7.26 - 7.45 (m, 3 H); ESI-MS  $m/z$ : 266.2  $[\text{M}+\text{H}]^+$ , 289.2  $[\text{M}+\text{Na}]^+$

**3-(Heptyloxy)benzamide (1-F313):**  $^1\text{H}$  NMR (400 MHz, CHLOROFORM-*d*) ppm 0.92 (t,  $J=6.60$  Hz, 3 H) 1.25 - 1.52 (m, 8 H) 1.76 - 1.88 (m, 2 H) 4.02 (t,  $J=6.36$  Hz, 2 H) 5.87 - 6.27 (m, 2 H) 7.02 - 7.15 (m, 1 H) 7.27 - 7.45 (m, 3 H); ESI-MS  $m/z$ : 236.2  $[\text{M}+\text{H}]^+$ , 259.1  $[\text{M}+\text{Na}]^+$

**3-(Octyloxy)benzamide (1-F320):**  $^1\text{H}$  NMR (400 MHz, CHLOROFORM-*d*) ppm 0.91 (t,  $J=6.60$  Hz, 3 H) 1.23 - 1.54 (m, 9 H) 1.74 - 1.88 (m, 2 H) 4.01 (t,  $J=6.60$  Hz, 2 H) 6.19 (br. s., 2 H) 7.02 - 7.13 (m, 1 H) 7.25 - 7.49 (m, 3 H); ESI-MS  $m/z$ : 250.2  $[\text{M}+\text{H}]^+$ , 273.2  $[\text{M}+\text{Na}]^+$



**Scheme 2.1.** (a) Various alkyl bromide,  $\text{K}_2\text{CO}_3$ , DMF, reflux, 4 hrs; (b) KOH, MeOH, reflux, 14 hrs; (c)  $\text{SOCl}_2$ , PhMe, reflux, 3 hrs, then aq.  $\text{NH}_3$  solution, THF, r.t., 3 hrs.

## 2.4.2 Preparation of series 2 compounds

The synthesis of **2-F411**, **2-F412**, **2-F413** and **2-F414** are shown in Scheme 2.2. Treatment of 3-aminobenzamide with 1-bromononane or 1-bromooctane in acetonitrile under basic condition at refluxing temperature furnished **2-F411** and **2-F412** respectively. These two compounds were further alkylated to tertiary amine using dimethyl sulphate under basic condition to afford **2-F413** and **2-F414**. The detailed experimental procedure is described as follows:

**3-(Nonylamino)benzamide (2-F411):** To a well stirred solution of 3-aminobenzamide (0.20 g, 1.4 mmol) and 1-bromononane (0.32 g, 1.5 mmol) in acetonitrile (20 mL) was added  $K_2CO_3$  (0.23 g, 1.6 mmol). The reaction mixture was heated to reflux for 4 hrs. After the complete disappearance of starting material as indicated by TLC, the reaction mixture was subjected to pass through a short pad of silica gel. The filtrate obtained was evaporated under reduced pressure and subjected to flash column chromatography using silica gel. The titled compound (0.15 g) was obtained in 39% yield:  $^1H$  NMR (400 MHz, CHLOROFORM-*d*) ppm 0.85 - 0.96 (m, 3 H), 1.19 - 1.45 (m, 12 H), 1.63 (quin,  $J=7.21$  Hz, 2 H), 3.15 (t,  $J=7.09$  Hz, 2 H), 5.86 - 6.25 (m, 2 H), 6.75 (dd,  $J=7.58, 2.20$  Hz, 1 H), 7.03 (d,  $J=7.34$  Hz, 1 H), 7.11 (t,  $J=1.96$  Hz, 1 H), 7.23 (t,  $J=7.83$  Hz, 1 H); ESI-MS  $m/z$ : 263  $[M+H]^+$ , 285  $[M+Na]^+$ .

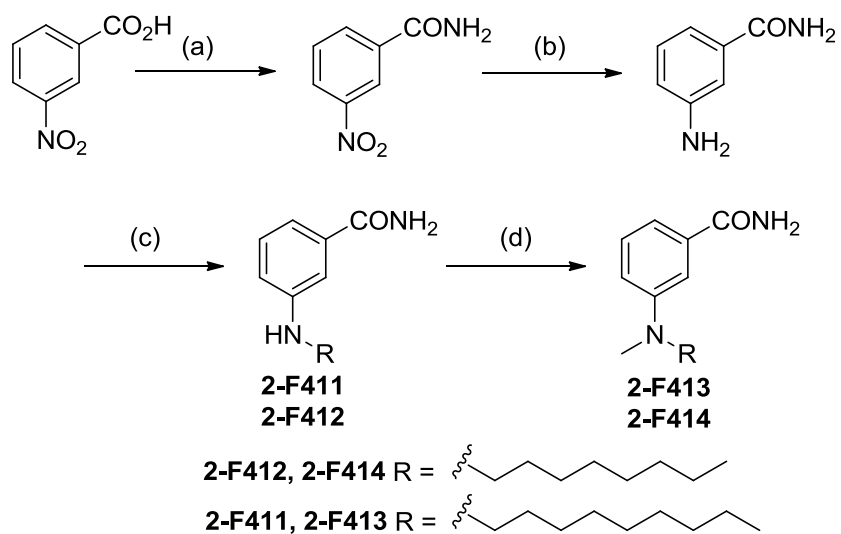
**3-(Octylamino)benzamide (2-F412):** To a well stirred solution of 3-aminobenzamide (0.20 g, 1.4 mmol) and 1-bromooctane (0.29 g, 1.5 mmol) in acetonitrile (20 mL) was added  $K_2CO_3$  (0.23 g, 1.6 mmol). The reaction mixture was heated to reflux for 4 hrs. After

the complete disappearance of starting material as indicated by TLC, the reaction mixture was subjected to pass through a short pad of silica gel. The filtrate obtained was evaporated under reduced pressure and subjected to flash column chromatography using silica gel. The titled compound (0.18 g) was obtained in 47% yield:  $^1\text{H}$  NMR (400 MHz, CHLOROFORM-*d*) ppm 0.91 (t,  $J=6.85$  Hz, 3 H), 1.22 - 1.46 (m, 10 H), 1.64 (quin,  $J=7.21$  Hz, 2 H), 3.15 (t,  $J=7.09$  Hz, 2 H), 5.88 - 6.25 (m, 2 H), 6.75 (dd,  $J=7.58, 2.20$  Hz, 1 H), 7.00 - 7.06 (m, 1 H), 7.09 - 7.14 (m, 1 H), 7.23 (t,  $J=7.83$  Hz, 1 H); ESI-MS  $m/z$ : 249  $[\text{M}+\text{H}]^+$ , 271  $[\text{M}+\text{Na}]^+$ .

**3-(Methyl(nonyl)amino)benzamide (2-F413):** To a well stirred solution of 3-(nonylamino)benzamide (0.09 g, 0.3 mmol) and dimethyl sulfate (0.06 g, 0.5 mmol) in acetonitrile (10 mL) was added  $\text{K}_2\text{CO}_3$  (0.06 g, 0.4 mmol). The reaction mixture was heated to reflux for 12 hrs. After the complete disappearance of starting material as indicated by TLC, the reaction mixture was diluted with ethyl acetate (20 mL) and subjected to pass through a short pad of silica gel. The filtrate obtained was evaporated under reduced pressure and subjected to flash column chromatography using silica gel. The titled compound (0.04 g) was obtained in 42% yield:  $^1\text{H}$  NMR (400 MHz, CHLOROFORM-*d*) ppm 0.82 - 0.96 (m, 3 H), 1.20 - 1.39 (m, 12 H), 1.51 - 1.66 (m, 2 H), 2.98 (s, 3 H), 3.30 - 3.41 (m, 2 H), 5.88 - 6.22 (m, 2 H), 6.84 (dd,  $J=8.31, 2.45$  Hz, 1 H), 6.99 (d,  $J=7.34$  Hz, 1 H), 7.21 (s, 1 H), 7.24 - 7.30 (m, 1 H); ESI-MS  $m/z$ : 277  $[\text{M}+\text{H}]^+$ , 299  $[\text{M}+\text{Na}]^+$ .

**3-(Methyl(octyl)amino)benzamide (2-F414):** To a well stirred solution of 3-(octylamino)benzamide (0.08 g, 0.3 mmol) and dimethyl sulfate (0.05 g, 0.4 mmol) in acetonitrile (10 mL) was added  $\text{K}_2\text{CO}_3$  (0.06 g, 0.4 mmol). The reaction mixture was heated

to reflux for 12 hrs. After the complete disappearance of starting material as indicated by TLC, the reaction mixture was diluted with ethyl acetate (20 mL) and subjected to pass through a short pad of silica gel. The filtrate obtained was evaporated under reduced pressure and subjected to flash column chromatography using silica gel. The titled compound (0.04 g) was obtained in 47% yield:  $^1\text{H}$  NMR (400 MHz, CHLOROFORM-*d*) ppm 0.84 - 0.96 (m, 3 H), 1.20 - 1.40 (m, 10 H), 1.53 - 1.66 (m, 2 H), 2.98 (s, 3 H), 3.30 - 3.45 (m, 2 H), 5.84 - 6.28 (m, 2 H), 6.84 (dd,  $J=8.31, 2.45$  Hz, 1 H), 6.99 (d,  $J=7.82$  Hz, 1 H), 7.16 - 7.23 (m, 1 H), 7.24 - 7.31 (m, 1 H); ESI-MS  $m/z$ : 263  $[\text{M}+\text{H}]^+$ , 285  $[\text{M}+\text{Na}]^+$ .



**Scheme 2.2.** (a)  $\text{SOCl}_2$ , reflux, 2 hr, then aq.  $\text{NH}_3$  solution,  $0^\circ\text{C}$ , 2 hr; (b)  $\text{SnCl}_2$ , conc.  $\text{HCl}$ , r.t., 12 hrs; (c) 1-bromononane or 1-bromooctane,  $\text{K}_2\text{CO}_3$ ,  $\text{CH}_3\text{CN}$ , reflux, 4 hrs; (d)  $\text{Me}_2\text{SO}_4$ ,  $\text{K}_2\text{CO}_3$ ,  $\text{CH}_3\text{CN}$ , reflux, 12 hrs.

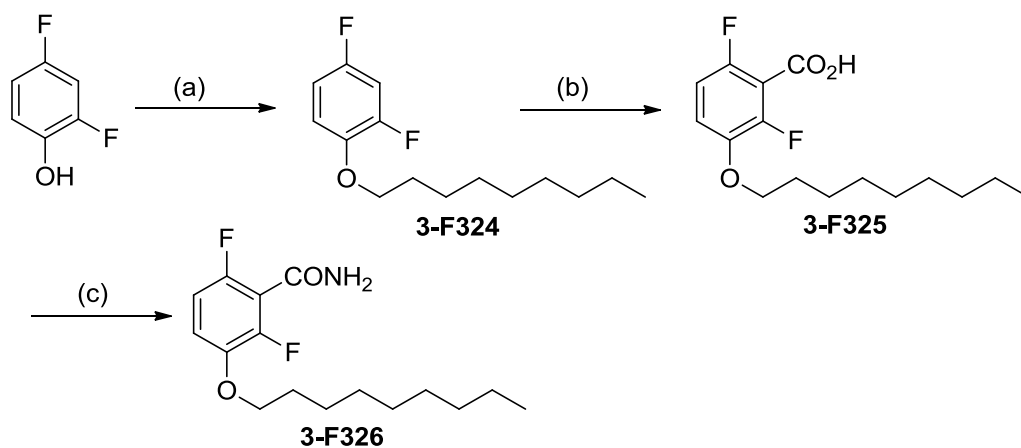
### 2.4.3 Preparation of series 3 compounds

The synthesis of **3-F324**, **3-F325** and **3-F326** have been described in a previous publication [58]. The synthetic pathway of these compounds is shown in Scheme 2.3.

**2,4-Difluoro-1-(nonyloxy)benzene (3-F324):**  $^1\text{H}$  NMR (400 MHz, CHLOROFORM-*d*) ppm 0.91 (t,  $J=6.60$  Hz, 3 H) 1.24 - 1.54 (m, 12 H) 1.82 (quin,  $J=7.09$  Hz, 2 H) 4.01 (t,  $J=6.60$  Hz, 2 H) 6.68 - 6.83 (m, 1 H) 6.83 - 6.96 (m, 2 H); ESI-MS  $m/z$ : 256.3  $[\text{M}+\text{H}]^+$ , 279.3  $[\text{M}+\text{Na}]^+$ .

**2,6-Difluoro-3-(nonyloxy)benzoic acid (3-F325):**  $^1\text{H}$  NMR (400 MHz, CHLOROFORM-*d*) ppm 0.90 (t,  $J=6.60$  Hz, 3 H) 1.30 (br. s., 10 H) 1.48 (quin,  $J=7.09$  Hz, 2 H) 1.82 (quin,  $J=6.97$  Hz, 2 H) 4.03 (t,  $J=6.60$  Hz, 2 H) 6.86 - 6.95 (m, 1 H) 7.10 (td,  $J=9.05$ , 4.89 Hz, 1 H); ESI-MS  $m/z$ : 301.2  $[\text{M}+\text{H}]^+$ , 323.2  $[\text{M}+\text{Na}]^+$ .

**2,6-Difluoro-3-(nonyloxy)benzamide (3-F326):**  $^1\text{H}$  NMR (400 MHz, CHLOROFORM-*d*) ppm 0.87 (t,  $J=6.60$  Hz, 3 H) 1.17 - 1.37 (m, 10 H) 1.39 - 1.50 (m, 2 H) 1.68 - 1.85 (m, 2 H) 3.96 (t,  $J=6.36$  Hz, 2 H) 6.38 (br. s., 1 H) 6.73 - 6.86 (m, 1 H) 6.91 - 6.99 (m, 1 H) 7.13 (br. s., 1 H); ESI-MS  $m/z$ : 300.2  $[\text{M}+\text{H}]^+$ , 322.2  $[\text{M}-\text{H}+\text{Na}]^+$ , 323.2  $[\text{M}+\text{Na}]^+$ .



**Scheme 2.3.** (a) 1-bromononane,  $\text{K}_2\text{CO}_3$ , DMF, reflux, 12 hrs; (b) *n*-BuLi, THF,  $-78^\circ\text{C}$ , then  $\text{CO}_2$  gas; (c)  $\text{SOCl}_2$ , reflux, 2 hrs, then aq.  $\text{NH}_3$  solution,  $0^\circ\text{C}$ , 2 hrs.



#### 2.4.4 Preparation of series 4 compounds

The synthesis of **4-F332**, **4-F333**, **4-F334**, **4-F350**, **4-F361**, **4-F369**, **4-F370**, **4-F371**, **4-F391**, **4-F409** and **4-F410** are shown in Scheme 2.4. 2,6-Difluoro-3-aminobenzamide was prepared in two steps from commercially available 2,6-difluoro-3-nitrobenzoic acid in high yield. Firstly, treatment of 2,6-difluoro-3-nitrobenzoic acid with thionyl chloride followed by aqueous ammonia solution furnished 2,6-difluoro-3-nitrobenzamide, which was further reduced to 2,6-difluoro-3-aminobenzamide using tin (II) chloride in conc. hydrochloric acid. Treatment of 2,6-difluoro-3-aminobenzamide with various alkyl halides, such as 1-bromononane, 1-bromooctane, 1-bromodecane, 1-bromo-4-butoxybutane, geranyl bromide, trans-1-bromonon-2-ene and 1-bromoheptane, in acetonitrile under basic condition for 4 hours gave **4-F332**, **4-F333**, **4-F334**, **4-F350**, **4-F369**, **4-F370**, **4-F391** respectively. Bromination of **4-F332** furnished **4-F371**. Further alkylation of **4-F332** and **4-F333** using dimethyl sulphate or bromoethane afforded **4-F409**, **4-F410** and **4-F361**. The detailed experimental procedure is described as follows:

**2,6-Difluoro-3-aminobenzamide:** A well stirred mixture of 2,6-difluoro-3-nitrobenzoic acid (44 g, 216 mmol) and thionyl chloride (100 mL) was heated to reflux for 2 hrs. Excess thionyl chloride was removed by evaporation to afford 2,6-difluoro-3-nitrobenzoic acid chloride, which was used in the next step without further purification. To a well stirred aqueous 30% ammonia solution (300 mL) at 0°C was added 2,6-difluoro-3-nitrobenzoic acid chloride dropwise. After the addition, the precipitate formed was collected by filtration to afford 2,6-difluoro-3-nitrobenzamide (40 g, 91%), which was used in the next step without further purification. To a well stirred solution of tin (II) chloride (80 g, 421 mmol)

in conc. HCL (200 mL) at 0°C was added 2,6-difluoro-3-nitrobenzamide in portions. After the addition, the reaction mixture was stirred at room temperature for 12 hrs. The reaction was quenched by adding to the reaction mixture excess potassium hydroxide solution until the pH was > 12 at 0°C. The aqueous solution was extracted with ethyl acetate (200 mL x 4). The combined organic layers were dried over MgSO<sub>4</sub>, filtered and evaporated to dryness to give 2,6-difluoro-3-aminobenzamide (18 g, 53%). <sup>1</sup>H NMR (400 MHz, acetone) ppm 4.67 (br. s., 2 H) 6.73 - 6.81 (m, 1 H) 6.87 (td, *J*=9.29, 5.38 Hz, 1 H) 6.98 - 7.23 (m, 1 H) 7.36 (br. s., 1 H); ESI-MS *m/z*: 173 [M+H]<sup>+</sup>, 195 [M+Na]<sup>+</sup>.

**2,6-Difluoro-3-(nonylamino)benzamide (4-F332):** To a well stirred solution of 2,6-difluoro-3-aminobenzamide (0.74 g, 4.3 mmol) and 1-bromononane (1.20 g, 5.8 mmol) in acetonitrile (50 mL) was added K<sub>2</sub>CO<sub>3</sub> (1.20 g, 8.7 mmol) and catalytic amount of NaI (0.08 g). The reaction mixture was heated to reflux for 4 hrs. After the complete disappearance of starting material as indicated by TLC, the reaction mixture was subjected to pass through a short pad of silica gel. The filtrate obtained was evaporated under reduced pressure and subjected to flash column chromatography using silica gel. The titled compound (0.49 g) was obtained in 38% yield: <sup>1</sup>H NMR (400 MHz, CHLOROFORM-*d*) ppm 0.90 (t, *J*=6.85 Hz, 3 H), 1.20 - 1.46 (m, 12 H), 1.56 - 1.73 (m, 3 H), 3.12 (t, *J*=7.09 Hz, 2 H), 5.94 - 6.27 (m, 2 H), 6.69 (td, *J*=9.29, 5.38 Hz, 1 H), 6.84 (td, *J*=9.29, 1.47 Hz, 1 H); ESI-MS *m/z*: 299 [M+H]<sup>+</sup>, 322 [M+Na]<sup>+</sup>.

**2,6-Difluoro-3-(octylamino)benzamide (4-F333):** To a well stirred solution of 2,6-difluoro-3-aminobenzamide (0.40 g, 2.3 mmol) and 1-bromooctane (0.45 g, 2.3 mmol) in acetonitrile (20 mL) was added K<sub>2</sub>CO<sub>3</sub> (0.40 g, 2.9 mmol) and catalytic amount of NaI

(0.04 g). The reaction mixture was heated to reflux for 4 hrs. After the complete disappearance of starting material as indicated by TLC, the reaction mixture was subjected to pass through a short pad of silica gel. The filtrate obtained was evaporated under reduced pressure and subjected to flash column chromatography using silica gel. The titled compound (0.26 g) was obtained in 39% yield:  $^1\text{H}$  NMR (400 MHz, CHLOROFORM-*d*) ppm 0.90 (t,  $J=6.60$  Hz, 3 H), 1.17 - 1.49 (m, 11 H), 1.64 (quin,  $J=7.09$  Hz, 2 H), 3.04 - 3.20 (m, 2 H), 6.09 (br. s., 1 H), 6.36 (br. s., 1 H), 6.68 (td,  $J=9.05, 5.38$  Hz, 1 H), 6.85 (m,  $J=9.29, 9.29$  Hz, 1 H); ESI-MS  $m/z$ : 282  $[\text{M}+\text{H}]^+$ , 307  $[\text{M}+\text{Na}]^+$ .

**3-(Decylamino)-2,6-difluorobenzamide (4-F334):** To a well stirred solution of 2,6-difluoro-3-aminobenzamide (0.40 g, 2.3 mmol) and 1-bromodecane (0.56 g, 2.5 mmol) in acetonitrile (20 mL) was added  $\text{K}_2\text{CO}_3$  (0.40 g, 2.9 mmol) and catalytic amount of NaI (0.04 g). The reaction mixture was heated to reflux for 4 hr. After the complete disappearance of starting material as indicated by TLC, the reaction mixture was subjected to pass through a short pad of silica gel. The filtrate obtained was evaporated under reduced pressure and subjected to flash column chromatography using silica gel. The titled compound (0.27 g) was obtained in 37% yield:  $^1\text{H}$  NMR (400 MHz, CHLOROFORM-*d*) ppm 0.90 (t,  $J=6.36$  Hz, 3 H), 1.20 - 1.51 (m, 11 H), 1.64 (quin,  $J=7.21$  Hz, 2 H), 2.21 (s, 1 H), 2.28 - 2.36 (m, 1 H), 2.99 - 3.23 (m, 3 H), 3.81 (d,  $J=2.93$  Hz, 1 H), 6.10 (br. s., 1 H), 6.29 (br. s., 1 H), 6.68 (td,  $J=9.17, 5.14$  Hz, 1 H), 6.76 - 6.90 (m, 1 H); ESI-MS  $m/z$ : 312  $[\text{M}+\text{H}]^+$ , 335  $[\text{M}+\text{Na}]^+$ .

**3-((4-Butoxybutyl)amino)-2,6-difluorobenzamide (4-F350):** To a well stirred solution of 2,6-difluoro-3-aminobenzamide (0.17 g, 1.0 mmol) and 1-bromo-4-butoxybutane (0.21 g, 1.0 mmol) in acetonitrile (20 mL) was added  $K_2CO_3$  (0.15 g, 1.1 mmol). The reaction mixture was heated to reflux for 4 hr. After the complete disappearance of starting material as indicated by TLC, the reaction mixture was subjected to pass through a short pad of silica gel. The filtrate obtained was evaporated under reduced pressure and subjected to flash column chromatography using silica gel. The titled compound (0.05 g) was obtained in 17% yield:  $^1H$  NMR (400 MHz, CHLOROFORM-*d*) ppm 0.93 (t,  $J=7.34$  Hz, 3 H), 1.38 (dq,  $J=14.98, 7.23$  Hz, 2 H), 1.50 - 1.62 (m, 2 H), 1.64 - 1.84 (m, 4 H), 3.05 - 3.22 (m, 2 H), 3.31 - 3.53 (m, 4 H), 3.95 (br. s., 1 H), 5.88 - 6.41 (m, 2 H), 6.68 (td,  $J=9.29, 5.38$  Hz, 1 H), 6.77 - 6.89 (m, 1 H); ESI-MS  $m/z$ : 301  $[M+H]^+$ .

**2,6-Difluoro-3-(methyl(nonyl)amino)benzamide (4-F361):** To a well stirred solution of 2,6-difluoro-3-(nonylamino)benzamide (0.15 g, 0.5 mmol) and dimethyl sulphate (0.15 g, 1.2 mmol) in acetone (20 mL) was added  $K_2CO_3$  (0.15 g, 1.1 mmol). The reaction mixture was heated to reflux for 14 hrs. After the complete disappearance of starting material as indicated by TLC, the reaction mixture was subjected to pass through a short pad of silica gel. The filtrate obtained was evaporated under reduced pressure and subjected to flash column chromatography using silica gel. The titled compound (0.03 g) was obtained in 19% yield:  $^1H$  NMR (400 MHz, CHLOROFORM-*d*) ppm 0.89 (t,  $J=6.60$  Hz, 3 H), 1.27 (br. s., 12 H), 1.53 (br. s., 2 H), 2.75 - 2.83 (m, 3 H), 3.00 - 3.08 (m, 2 H), 6.05 (br. s., 1 H), 6.39 (br. s., 1 H), 6.82 - 6.89 (m, 1 H), 6.95 (td,  $J=9.05, 5.87$  Hz, 1 H); ESI-MS  $m/z$ : 313  $[M+H]^+$ .

**(E)-3-((3,7-Dimethylocta-2,6-dien-1-yl)amino)-2,6-difluorobenzamide (4-F369):** To a well stirred solution of 2,6-difluoro-3-aminobenzamide (0.34 g, 2.0 mmol) and geranyl bromide (0.42 g, 2.0 mmol) in acetonitrile (20 mL) was added  $K_2CO_3$  (0.29 g, 2.1 mmol). The reaction mixture was heated to reflux for 4 hrs. After the complete disappearance of starting material as indicated by TLC, the reaction mixture was subjected to pass through a short pad of silica gel. The filtrate obtained was evaporated under reduced pressure and subjected to flash column chromatography using silica gel. The titled compound (0.29 g) was obtained in 48% yield:  $^1H$  NMR (400 MHz, CHLOROFORM-*d*) ppm 1.51 - 1.91 (m, 10 H), 1.96 - 2.19 (m, 4 H), 3.66 - 3.77 (m, 2 H), 3.83 (br. s., 1 H), 5.02 - 5.19 (m, 1 H), 5.30 (t,  $J=6.11$  Hz, 1 H), 6.11 (br. s., 1 H), 6.48 (br. s., 1 H), 6.68 (td,  $J=9.05, 5.38$  Hz, 1 H), 6.83 (td,  $J=9.29, 1.47$  Hz, 1 H); ESI-MS  $m/z$ : 309  $[M+H]^+$ .

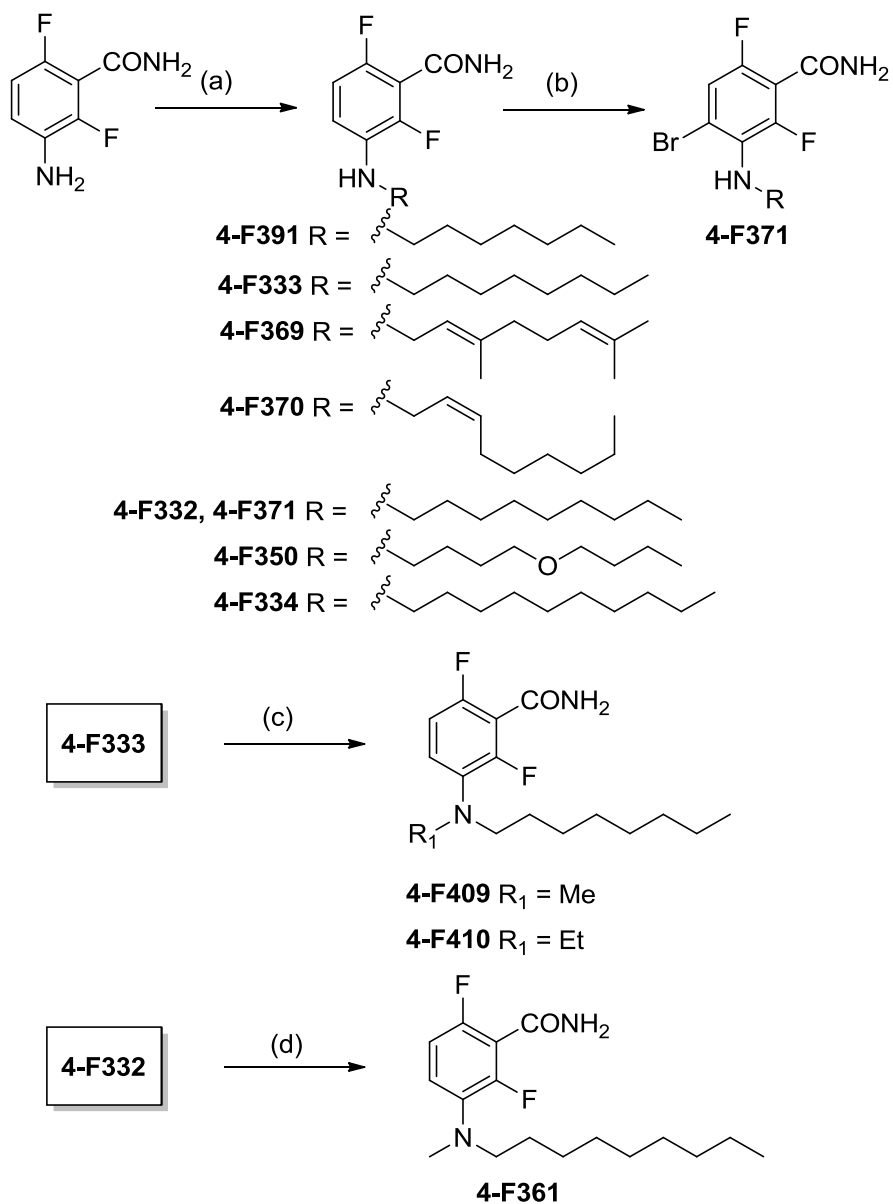
**(Z)-2,6-Difluoro-3-(non-2-en-1-ylamino)benzamide (4-F370):** To a well stirred solution of 2,6-difluoro-3-aminobenzamide (0.17 g, 1.0 mmol) and (Z)-1-bromonon-2-ene (0.21 g, 1.0 mmol) in acetonitrile (20 mL) was added  $K_2CO_3$  (0.15 g, 1.1 mmol). The reaction mixture was heated to reflux for 4 hrs. After the complete disappearance of starting material as indicated by TLC, the reaction mixture was subjected to pass through a short pad of silica gel. The filtrate obtained was evaporated under reduced pressure and subjected to flash column chromatography using silica gel. The titled compound (0.13 g) was obtained in 44% yield:  $^1H$  NMR (400 MHz, CHLOROFORM-*d*) ppm 0.90 (t,  $J=6.85$  Hz, 3 H), 1.19 - 1.46 (m, 6 H), 2.06 (q,  $J=7.17$  Hz, 2 H), 2.25 - 2.54 (m, 2 H), 3.07 - 3.25 (m, 2 H), 3.73 - 4.00 (m, 1 H), 5.24 - 5.47 (m, 1 H), 5.51 - 5.63 (m, 1 H), 6.08 (br. s., 1 H), 6.18 - 6.35 (m, 1 H), 6.70 (td,  $J=9.29, 5.38$  Hz, 1 H), 6.84 (td,  $J=9.29, 1.47$  Hz, 1 H); ESI-MS  $m/z$ : 297  $[M+H]^+$  319  $[M+Na]^+$ .

**4-Bromo-2,6-difluoro-3-(nonylamino)benzamide (4-F371):** To a well stirred solution of 2,6-difluoro-3-(nonylamino)benzamide (0.3 g, 1.0 mmol) in dichloromethane (20 mL) at room temperature was added excess bromine (1 mL) and stirred for 12 hrs. After the complete disappearance of starting material as indicated by TLC, the reaction mixture was poured into a separating funnel containing saturated sodium thiosulfate solution (30 mL) and extracted with ethyl acetate (20 mL x 3). The combined organic layers was dried over MgSO<sub>4</sub>, filtered and evaporated to give a crude product which was further subjected to purification by flash column chromatography to afford the titled compound (0.28 g, 74%).  
<sup>1</sup>H NMR (400 MHz, CHLOROFORM-*d*) ppm 0.79 - 0.97 (m, 3 H), 1.18 - 1.45 (m, 12 H), 1.56 (quin, *J*=7.09 Hz, 2 H), 3.28 (t, *J*=6.11 Hz, 2 H), 3.74 (br. s., 1 H), 6.19 (br. s., 1 H), 6.76 (br. s., 1 H), 7.11 (dd, *J*=8.80, 1.96 Hz, 1 H); ESI-MS *m/z*: 377 [M+H]<sup>+</sup>, 399 [M+Na]<sup>+</sup>.

**2,6-Difluoro-3-(heptylamino)benzamide (4-F391):** To a well stirred solution of 2,6-difluoro-3-aminobenzamide (0.70 g, 4.1 mmol) and 1-bromoheptane (0.80 g, 4.4 mmol) in acetonitrile (50 mL) was added K<sub>2</sub>CO<sub>3</sub> (0.60 g, 4.4 mmol) and catalytic amount of NaI (0.08 g). The reaction mixture was heated to reflux for 4 hrs. After the complete disappearance of starting material as indicated by TLC, the reaction mixture was subjected to pass through a short pad of silica gel. The filtrate obtained was evaporated under reduced pressure and subjected to flash column chromatography using silica gel. The titled compound (0.40 g) was obtained in 36% yield: <sup>1</sup>H NMR (400 MHz, CHLOROFORM-*d*) ppm 0.82 - 0.97 (m, 3 H), 1.22 - 1.46 (m, 8 H), 1.65 (quin, *J*=7.09 Hz, 2 H), 3.12 (t, *J*=7.09 Hz, 2 H), 5.92 - 6.27 (m, 2 H), 6.69 (td, *J*=9.29, 5.38 Hz, 1 H), 6.85 (m, *J*=9.29, 9.29, 1.96 Hz, 1 H); ESI-MS *m/z*: 271 [M+H]<sup>+</sup>, 293 [M+Na]<sup>+</sup>.

**2,6-Difluoro-3-(methyl(octyl)amino)benzamide (4-F409):** To a well stirred solution of 2,6-difluoro-3-(octylamino)benzamide (0.12 g, 0.4 mmol) and methyl iodide (0.30 g, 2.1 mmol) in acetonitrile (10 mL) was added  $K_2CO_3$  (0.30 g, 2.1 mmol). The reaction mixture was heated to reflux for 14 hrs. After the complete disappearance of starting material as indicated by TLC, the reaction mixture was subjected to pass through a short pad of silica gel. The filtrate obtained was evaporated under reduced pressure and subjected to flash column chromatography using silica gel. The titled compound (0.03 g) was obtained in 24% yield:  $^1H$  NMR (400 MHz, CHLOROFORM-*d*) ppm 0.89 (t,  $J=6.85$  Hz, 3 H), 1.28 (d,  $J=2.93$  Hz, 10 H), 1.52 (d,  $J=6.85$  Hz, 2 H), 2.79 (s, 3 H), 2.99 - 3.09 (m, 2 H), 6.11 (br. s., 1 H), 6.63 (br. s., 1 H), 6.81 - 6.88 (m, 1 H), 6.95 (td,  $J=9.17, 5.62$  Hz, 1 H); ESI-MS  $m/z$ : 299  $[M+H]^+$ , 321  $[M+Na]^+$ .

**3-(Ethyl(octyl)amino)-2,6-difluorobenzamide (4-F410):** To a well stirred solution of 2,6-difluoro-3-(octylamino)benzamide (0.12 g, 0.4 mmol) and bromoethane (0.30 g, 2.7 mmol) in acetonitrile (10 mL) was added  $K_2CO_3$  (0.30 g, 2.1 mmol). The reaction mixture was heated to reflux for 14 hrs. After the complete disappearance of starting material as indicated by TLC, the reaction was subjected to pass through a short pad of silica gel. The filtrate obtained was evaporated under reduced pressure and subjected to flash column chromatography using silica gel. The titled compound (0.04 g) was obtained in 30% yield:  $^1H$  NMR (400 MHz, CHLOROFORM-*d*) ppm 0.85 (m,  $J=6.60, 6.60$  Hz, 3 H), 1.02 (t,  $J=7.09$  Hz, 3 H), 1.24 (br. s., 10 H), 1.43 (br. s., 2 H), 2.96 - 3.07 (m, 2 H), 3.12 (q,  $J=7.01$  Hz, 2 H), 6.20 (br. s., 1 H), 6.75 - 7.02 (m, 3 H); ESI-MS  $m/z$ : 313  $[M+H]^+$ , 335  $[M+Na]^+$ .



**Scheme 2.4.** (a) various alkyl bromides,  $K_2CO_3$ ,  $CH_3CN$ , reflux, 4 hrs; (b)  $Br_2$ , DCM, r.t., 12 hr; (c) methyl iodide or bromoethane,  $K_2CO_3$ ,  $CH_3CN$  reflux, 14 hrs; (d)  $Me_2SO_4$ ,  $K_2CO_3$ ,  $CH_3CN$ , reflux, 12 hrs.



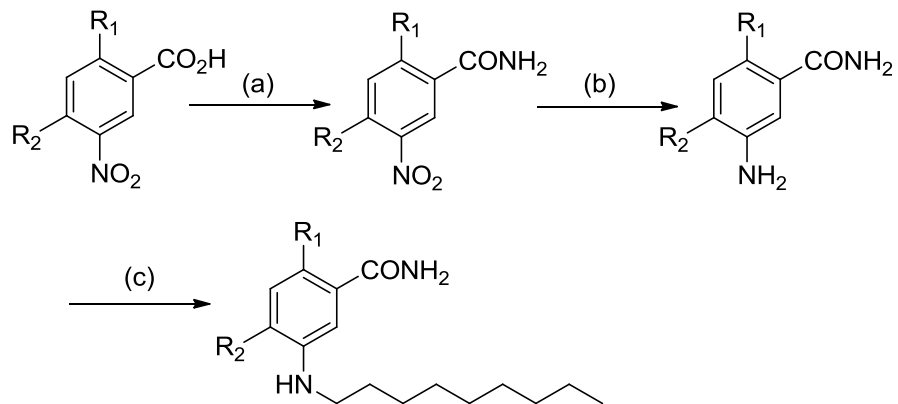
#### 2.4.5 Preparation of some other compounds

**F327** is **PC190723**, which is a reported potent FtsZ inhibitor. The synthesis of compound **F342** and **F345** followed the procedures described in a previous publication [62].

**2-Fluoro-5-(nonylamino)benzamide (F342)**: To a well stirred solution of 2-fluoro-5-aminobenzamide (0.20 g, 1.3 mmol) and 1-bromononane (0.30 g, 1.4 mmol) in acetonitrile (20 mL) was added  $K_2CO_3$  (0.25 g, 1.8 mmol). The reaction mixture was heated to reflux for 4 hrs. After the complete disappearance of starting material as indicated by TLC, the reaction mixture was subjected to pass through a short pad of silica gel. The filtrate obtained was evaporated under reduced pressure and subjected to flash column chromatography using silica gel. The titled compound (0.11 g) was obtained in 30% yield:  $^1H$  NMR (400 MHz, CHLOROFORM-*d*) ppm 0.89 (t,  $J=6.60$  Hz, 3 H), 1.21 - 1.49 (m, 12 H), 1.61 (quin,  $J=7.09$  Hz, 2 H), 3.11 (t,  $J=7.09$  Hz, 2 H), 3.70 (br. s., 1 H), 6.28 (br. s., 1 H), 6.59 - 6.84 (m, 2 H), 6.95 (dd,  $J=11.74, 8.80$  Hz, 1 H), 7.17 - 7.38 (m, 1 H); ESI-MS  $m/z$ : 281  $[M+H]^+$ , 303  $[M+Na]^+$ .

**2,4-Difluoro-5-(nonylamino)benzamide (F345)**: To a well stirred solution of 2,4-difluoro-5-aminobenzamide (0.20 g, 1.1 mmol) and 1-bromononane (0.28 g, 1.4 mmol) in acetonitrile (20 mL) was added  $K_2CO_3$  (0.23 g, 1.7 mmol). The reaction mixture was heated to reflux for 4 hrs. After the complete disappearance of starting material as indicated by TLC, the reaction mixture was subjected to pass through a short pad of silica gel. The obtained filtrate was evaporated under reduced pressure and subjected to flash column chromatography using silica gel. The titled compound (0.09 g) was obtained in 26% yield:

$^1\text{H}$  NMR (400 MHz, CHLOROFORM-*d*) ppm 0.79 - 0.96 (m, 3 H), 1.17 - 1.46 (m, 12 H), 1.54 - 1.71 (m, 2 H), 3.09 - 3.50 (m, 2 H), 3.79 (br. s., 1 H), 6.68 (d,  $J=9.29$  Hz, 1 H), 6.76 - 6.88 (m, 1 H), 7.33 - 7.59 (m, 1 H); ESI-MS  $m/z$ : 299  $[\text{M}+\text{H}]^+$ , 321  $[\text{M}+\text{Na}]^+$ .



**F342**  $R_1 = F, R_2 = H$

**F345**  $R_1 = R_2 = F$

**Scheme 2.5.** (a)  $\text{SOCl}_2$ , reflux, 2 hr, then aq.  $\text{NH}_3$  solution,  $0^\circ\text{C}$ , 2 hrs; (b)  $\text{SnCl}_2$ , conc.  $\text{HCl}$ , r.t., 12 hrs; (c) 1-bromononane,  $\text{K}_2\text{CO}_3$ ,  $\text{CH}_3\text{CN}$ , reflux, 4 hrs.

## 2.5 Results and discussion

Compounds in series 1 are 3-alkoxybenzamide derivatives (Table 2.1), except **1-F304**, which was prepared to investigate the effect of hydroxyl group on the change of antibacterial activity. The compounds in series 1 were synthesized to verify the results in a previous report which stated that the potency of alkoxybenzamide increases 1000 to 8000 folds comparing with **3-MBA** [58]. Compounds in series 2 are 3-(alkylamino)benzamide derivatives (Table 2.2). This series of compounds are structural analog of compounds in series 1. The alkoxy groups in series 1 are replaced with the amino groups in series 2. As the compounds in series 2 have relatively smaller ClogP values than those in series 1, it is expected that they are more readily taken up by bacteria than the compounds in series 1. **3-F326** in series 3 has been reported to have antibacterial activity [58]. Derivatives of **3-F326** were synthesized to replace the amide group to investigate the role of amide group in antibacterial activity (Table 2.3). The ClogP values of **3-F324**, **3-F325** and **3-F326** are 5.55, 5.11 and 4.46 respectively. A previous publication showed that fluorine substitutions at carbon 2 and 6 on the phenyl ring of **3-MBA** reduces the MIC value by 8 folds [58]. Therefore, a series compounds of 2,6-difluoro substituted 3-aminobenzamide were synthesized (Series 4) (Table 2.4).. A previous study have shown that the number and the position of fluorine atom on the phenyl ring of alkoxybenzamide play a key role on antibacterial activity [58]. In order to investigate whether it is also valid in aminobenzamide, **F342** and **F345** were synthesized to investigate the effect on antibacterial activity by changing the number and the position of fluorine atoms on the phenyl ring of 3-(nonylamino)benzamide (Table 2.5).

## 2.6 Concluding remarks

A total of 4 series of derivatives of **3-MBA** containing alkoxy-, amino- and fluorine substituents have been synthesized. The bioassays with bacteria and influence on FtsZ protein of these compounds will be reported in the following chapters.

## Chapter 3

### *In vivo* bioassays of 3-MBA derivatives

#### 3.1 Introduction

In this project, selected chemical compounds will be subjected to microbial susceptibility test in order to find out whether they can inhibit the growth of bacteria. Compounds which do not inhibit the growth of bacteria will be eliminated. This preliminary screening ensures that the compounds can go through the barrier of the bacterial cell wall and perturb the normal metabolism of bacteria. As the number of chemical compounds to be tested is usually enormous, preliminary screening can reduce the number of compounds to be tested for *in vitro* assays. Moreover, a chemical compound which is active *in vitro* does not mean it can penetrate the barrier of a bacterial cell. As a result, a microbial susceptibility test is usually implemented in the beginning of drug screening.

Chemical compounds with positive results in microbial susceptibility test will be further studied to see whether they target at cytoplasmic division proteins. The growth of bacteria in the presence of sub-lethal concentrations of compound will be monitored under light microscopy. Filamentous cells will be observed if a compound is targeting the cytoplasmic division protein of bacteria.

In this chapter, *in vivo* bioassays were also conducted to test the cytotoxicity of compounds on animal cells in addition to the ability of these compounds to inhibit the growth of *B.subtilis* 168, *S.aureus* 29213 and *E.coli*.

## **3.2 Experimental**

### **3.2.1 Materials**

#### **(A) Bacterial strains and cell lines**

The bacterial strains used in microbial susceptibility test were *E.coli*, *S.aureus* 29213 and *B.subtilis* 168. *E.coli* and *S.aureus* 29213 were obtained from our laboratory collection. *B.subtilis* 168 was purchased from American Type Culture Collection (USA). The mammalian cell lines L929 (mouse fibroblast cells), LCC6 (a wild type breast cancer cell line), LCC6MDR (Pgp-overexpressed breast cancer cell line) were stocks in our department.

#### **(B) Media**

Nutrient Agar, tryptone and yeast extract were purchased from Oxoid Limited (Nepean, Ontario, Canada). Luria-Bertani (LB) medium was prepared from 2 g tryptone, 1 g yeast extract, and 2 g sodium chloride in 200 ml deionized water and sterilized. Müller-Hinton broth (MHB), cation-adjusted Müller-Hinton broth (CA-MHB) and trypticase soy broth (TSB) for microbial susceptibility test were purchased from Becton, Dickinson and Company (New Jersey, USA).

### 3.2.2 Instrumentation

A microplate reader (Bio-Rad Laboratories Model 680) was used to measure bacterial growth and cytotoxicity. An Olympus FSX100<sup>®</sup> Bio Imaging Navigator Microscope was used to observe the morphology of *B.subtilis* cell.

### 3.2.3 Antibacterial susceptibility test

The minimum inhibitory concentrations (MICs) of chemical compounds were determined using microbroth dilution method according to the National Committee for Clinical Laboratory Standards (CLSI) guidelines [63]. Compounds were dissolved in DMSO and diluted in a serial two-fold manner. A single colony of bacterial strain on a TSB agar plate was inoculated in 5 mL MHB or CA-MHB. The bacterial cells were incubated at 37°C until the optimal density (OD<sub>600</sub>) of the growing cells reached 1.0. The cells were then diluted to a final concentration of approximately  $5 \times 10^5$  CFU/mL in MHB or CA-MHB containing two fold dilutions of compounds in a sterile 96-well microtiter plate (Iwaki, Japan). Ampicillin and **PC190723** were used as positive controls. After 18 hours of incubation at 37°C, the OD<sub>600</sub> values were measured by a microplate absorbance reader to calculate the percentage inhibition of bacterial growth with respect to control. The compound is defined to be active if the MIC value is equal to or greater than 90%, which means that the compound causes more than 90% inhibition of bacterial growth.



### 3.2.4 Visualization of bacterial morphology

A single colony of *B.subtilis* 168 was grown in 10 mL LB medium at 37°C for 14 hours. An overnight culture was then diluted to an OD<sub>600</sub> of 0.01 by the same medium containing different sub-lethal concentrations of tested compounds and grew at 37°C. After 4 hours of incubation, the cells were pelleted and resuspended in 100 µL PBS buffer containing 0.25% agarose. 10 µL suspension was then placed on the microscopic slide which was pretreated with 0.1% (w/v) poly-L-lysine. The morphology of bacterial cells was observed under a phase-contrast microscope at 40X magnification. The images were captured by the software of Olympus FSX100<sup>®</sup> Bio Imaging Navigator. The length of the bacterial cells was measured by the software ImageJ (National Institutes of Health, USA).

### 3.2.5 Cytotoxicity test

The cell lines used in cytotoxicity test were stocks in our department. In this assay, a mouse fibroblast cell line (L929), a wild type breast cancer cell line (LCC6) and a Pgp-overexpressed breast cancer cell line (LCC6MDR) were mixed with compounds of various concentrations and made up to a final volume of 100  $\mu$ L in 96-well plates. The cells were then incubated at 37°C for 3 days. The half-maximal inhibitions ( $IC_{50}$ ) of the compounds were determined using the CellTiter 96 AQueous One Solution cell Proliferation Assay (Promega). 3-(4,5-Dimethylthiazol-2-yl)-5-(3-carboxy-methoxyphenyl)-2-(4-sulfophenyl)-2H-tetrazolium (2 mg/mL ,MTS, Promega) and phenzaine methosulfate (0.92 mg/mL PMS, Sigma-Aldrich) were mixed in a ratio of 20:1. The MTS/PMS mixture (10  $\mu$ L) was added into each well, and the plate was incubated at 37°C for 2 hours. The absorbance at 490 nm was then measured with a microplate absorbance reader (Bio-Rad). The  $IC_{50}$  values were calculated from the dose-response curves using GraphPad (Prism 4.0). The selective index of each compound was calculated from the ratio between the toxicity level of L929 and the MIC value of *S.aureus* 29213. A compound is defined as a potential antibiotic if the selective index is greater than 10.

### 3.3 Results and discussion

#### 3.3.1 Antibacterial susceptibility

In this section, the antibacterial activities of the **3-MBA** and amino-benzamide derivatives are reported. The chemical structures of the compounds and their MIC values are given in Tables 3.1 to 3.5

Czaplweski et al found that 3-alkoxybenzamides are more potent to inhibit bacterial growth than **3-MBA** [58]. As a result, some 3-alkoxybenzamides and 3-aminobenzamides were synthesized to investigate their antibacterial activities (Table 3.1). Compounds **1-F302**, **1-F313** and **1-F320** were reported to have higher antibacterial activity than **3-MBA** [58]. However, **1-F313** and **1-F320** did not show high antibacterial activity in our microbial susceptibility test. Only **1-F302** and **1-F320** inhibit the growth of *B.subtilis* 168 with MIC values of 3  $\mu$ M and 50  $\mu$ M respectively. Derivative **1-F304** is structurally similar to **1-F302** except the nonyl chain is replaced by a hydroxyoctyl chain. However, no antibacterial activity was observed in **1-F304**. The results showed that the presence of an appropriate alkyl chain in 3-alkoxybenzamide is essential for the antibacterial activity. In order to improve the antibacterial activities of **1-F302** and **1-F320**, structural analogues of **1-F302** and **1-F320** were synthesized to further investigate their antibacterial activities (Series 2) (Table 3.2).

The partition coefficient (logP) is related to the hydrophobicity of chemical compounds. The calculated logP (ClogP) value is important in predicting the transport of drugs in animals [64]. **2-F411** is structurally similar to **1-F302** and their MIC values against

*B.subtilis* 168 are also similar. In order to compare their hydrophobicity, the ClogP values of **1-F302** and **2-F411** were found to be 4.14 and 3.76 respectively using the software ChemBioDraw Ultra (CambridgeSoft). The ClogP values indicated that **2-F411** is more water soluble than **1-F302**. As a result, **2-F411** is believed to have better bioavailability in animals, and further modifications were carried out to improve the antibacterial activity of **2-F411**.

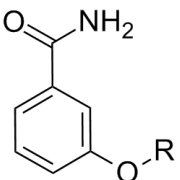
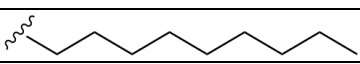
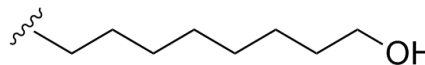
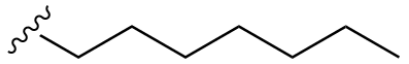
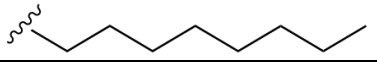
Czaplewski et al. found that a fluorine substituted 3-alkoxybenzamide is 10,000 times more potent than **3-MBA** [58]. **3-F326** (2,6-difluoro-3-nonyloxybenzamide), was found to inhibit the growth of *B.subtilis* 168 and *S.aureus* 29213 with MIC values of 0.25  $\mu$ M and 6.25  $\mu$ M respectively in our microbial susceptibility test (Table 3.3). Fluorinated 3-aminobenzamide derivatives were also synthesized to explore their antibacterial activities (Table 3.4). **4-F332** was found to inhibit the growth of *B.subtilis* 168 and *S.aureus* 29213 with MIC values of 3  $\mu$ M and 12.5  $\mu$ M respectively. The ClogP values of **3-F326** and **4-F332** are 4.46 and 4.08 respectively. Although **4-F332** was not as potent as **3-F326**, it is believed to have better bioavailability than **3-F326** as a result of its smaller ClogP value. The effect on antibacterial activity by changing the number and the position of fluorine atoms on compound **4-F332** were also investigated. Two analogues of **4-F332**, **F342** and **F345** were synthesized (Table 3.5). **F342** has only one fluorine substituent while **F345** has two fluorine substituents on the phenyl ring of aminobenzamide. **F342** and **F345** have weaker potency against the growth of *B.subtilis* 168 compared to **4-F332**. No inhibitory effect on the growth of *S.aureus* 29213 was observed by **F342** and **F345**. The antibacterial activity test showed that the position and the number of fluorine atoms on the ring of aminobenzamide play a key role in antibacterial activity.

From the results of **F342** and **F345**, the two fluorine atoms should be retained at carbon 2 and 6 on the phenyl ring of benzamide. Also, the relatively smaller ClogP values of series 2 compounds encourage us to synthesize derivatives of 2,6-difluoro-3-aminobenzamide (Series 4).

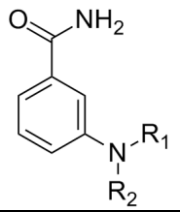
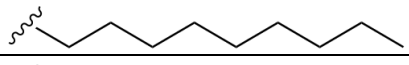
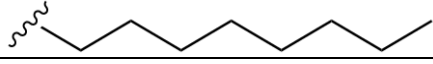

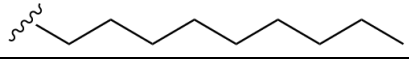
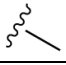
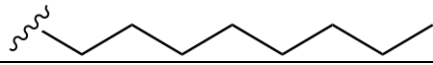
The effect of aliphatic chain length on the amino group of series 4 compounds was therefore investigated (Table 3.4). Among them, **4-F332** is still the most potent antibacterial compound. The MICs values of **4-F332**, **4-F333**, **4-F334**, **4-F350**, **4-F369**, **4-F370** and **4-F391** showed that the optimal chain length is a nonyl alkyl chain. Both branched and unsaturated aliphatic chains reduced the antibacterial activities.

**4-F361** contains both a nonyl alkyl chain and a methyl group in the amino group. **4-F361** inhibited the growth of *B.subtilis* 168 and *S.aureus* 29213 with MIC values of 2  $\mu$ M and 3  $\mu$ M respectively, and is the most potent FtsZ inhibitors that we discovered so far. The ClogP value of **4-F361** is 4.87 which suggested that it has poorer bioavailability than **4-F332**. However, the MIC value of **4-F361** against *S.aureus* 29213 is 4 folds lower than that of **4-F332**. Further experiments should be conducted to study the pharmacokinetics of **4-F332** and **4-F361** to identify which compound has more drug-like properties.

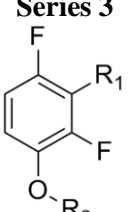
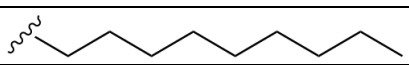
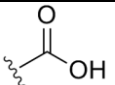
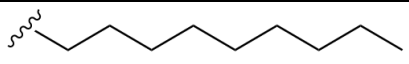
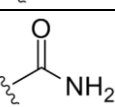
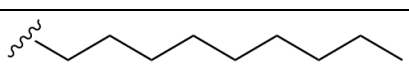
**Table 3.1 Antibacterial activities of series 1**

Series 1				
				
MIC (μM)				
Compound	R	<i>B.subtilis</i> 168	<i>E.coli</i>	<i>S.aureus</i> 29213
<b>1-F302</b>		3	>100	>100
<b>1-F304</b>		>100	>100	>100
<b>1-F313</b>		>100	>100	>100
<b>1-F320</b>		50	>100	12.5

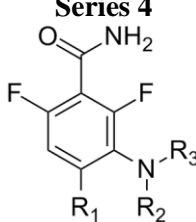
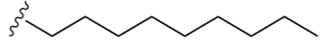
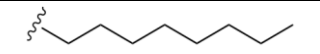
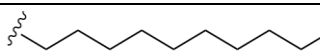
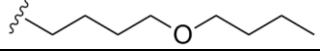

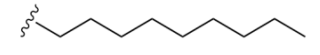
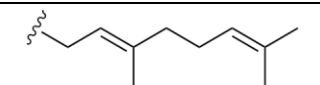
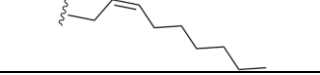
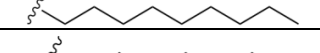


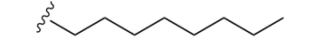
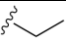
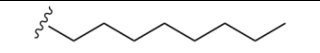
**Table 3.2 Antibacterial activities of series 2**

Series 2					
					
MIC (μM)					
Compound	R <sub>1</sub>	R <sub>2</sub>	<i>B.subtilis</i> 168	<i>E.coli</i>	<i>S.aureus</i> 29213
<b>2-F411</b>	H		6	>100	>100
<b>2-F412</b>	H		25	>100	>100
<b>2-F413</b>			>100	>100	>100
<b>2-F414</b>			>100	>100	>100

**Table 3.3 Antibacterial activities of series 3**

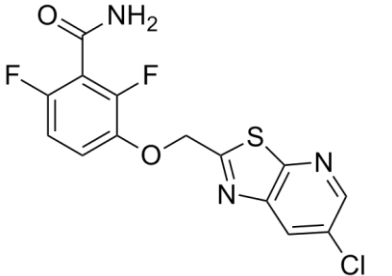
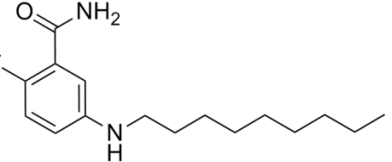
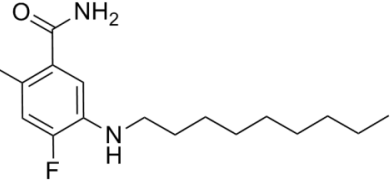
<div style="text-align: center;"> <b>Series 3</b>              MIC (<math>\mu\text{M}</math>)         </div>					
Compound	R <sub>1</sub>	R <sub>2</sub>	<i>B.subtilis</i> 168	<i>E.coli</i>	<i>S.aureus</i> 29213
<b>3-F324</b>	H		>100	>100	>100
<b>3-F325</b>			>100	>100	>100
<b>3-F326</b>			0.3	>100	6.0

**Table 3.4 Antibacterial activities of series 4**

<div style="text-align: center;"> <b>Series 4</b>   </div>						
MIC ( $\mu$ M)						
Compound	R <sub>1</sub>	R <sub>2</sub>	R <sub>3</sub>	<i>B.subtilis</i> 168	<i>E.coli</i>	<i>S.aureus</i> 29213
<b>4-F332</b>	H	H		3	>100	12.5
<b>4-F333</b>	H	H		6	>100	50
<b>4-F334</b>	H	H		>100	>100	>100
<b>4-F350</b>	H	H		>100	>100	>100
<b>4-F361</b>	H			2	>100	3
<b>4-F369</b>	H	H		50	>100	>100
<b>4-F370</b>	H	H		6	>100	25
<b>4-F371</b>	Br	H		6	>100	>100
<b>4-F391</b>	H	H		50	>100	50
<b>4-F409</b>	H			25	>100	12.5
<b>4-F410</b>	H			25	>100	50



**Table 3.5 Antibacterial activities of other derivatives**

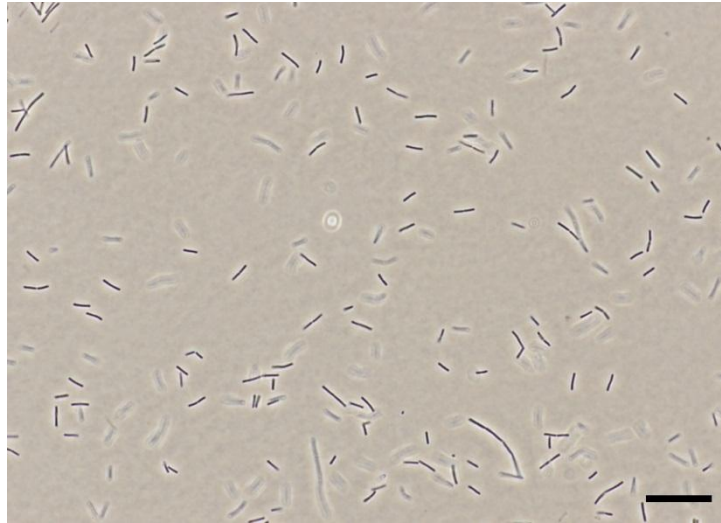
Compound	Structures	MIC ( $\mu\text{M}$ )		
		<i>B.subtilis</i> 168	<i>E.coli</i>	<i>S.aureus</i> 29213
<b>F327</b> <b>(PC190723)</b>		0.5	>2	0.5
<b>F342</b>		25	>100	>100
<b>F345</b>		100	>100	>100

### 3.3.2 Effects on the morphology of *B.subtilis* cells

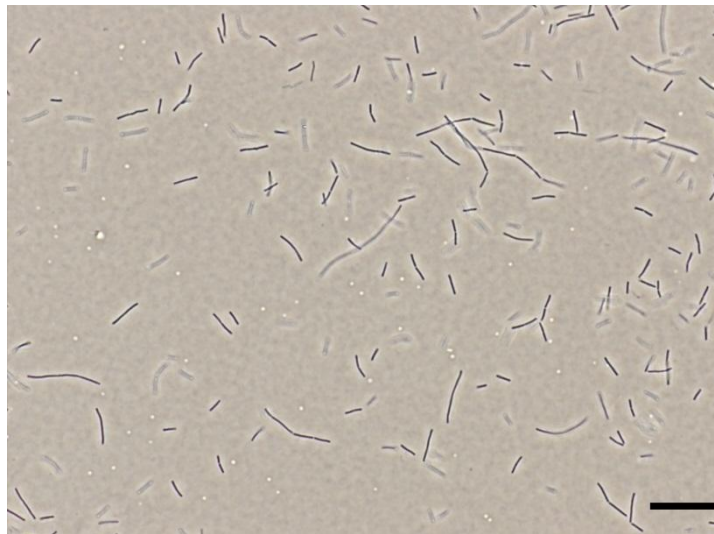
The two most potent compounds, **4-F332** and **4-F361**, were tested for their effects on the cell morphology of *B.subtilis* 168 strain (Figure 3.1 and 3.2). The log-phase culture of *B.subtilis* was tested with the two compounds with a final concentration of 0.5X MIC. A 1% DMSO solution was used as the control. The results indicated that both compounds had the ability to induce filamentation on *B.subtilis* cells. The average cell length of untreated *B.subtilis* was  $3.5 \pm 0.7 \mu\text{m}$ . **4-F332** induced a 3X lengthening in the cell size of *B.subtilis*. **4-F332** extended the average cell length of *B.subtilis* from  $3.5 \pm 0.7 \mu\text{m}$  to  $11.7 \pm 4.5 \mu\text{m}$ . On the other hand, **4-F361** induced a 6X lengthening of cell size in *B.subtilis*, from  $3.5 \pm 0.7 \mu\text{m}$  to  $21.1 \pm 1.8 \mu\text{m}$ . In the absence of compound, the length of the *B.subtilis* 168 cells were found to be within 0 to 4  $\mu\text{m}$  (75%) and 4-8  $\mu\text{m}$  (25%) respectively. When the *B.subtilis* 168 cells were treated with **4-F332** (1.6  $\mu\text{M}$ ), all the cells were found to be longer than 8  $\mu\text{m}$ . On the other hand, when the *B.subtilis* 168 cells were treated with **4-F361** (0.8  $\mu\text{M}$ ), 33% cells were found to be within 4-8  $\mu\text{m}$  and 67% cells were found to be greater 8  $\mu\text{m}$ .

**4-F332** and **4-F361** were found to cause filamentation of *B.subtilis* 168 cells at sub-lethal concentrations. The results showed that both compounds may inhibit bacterial proliferation by blocking cytoplasmic division.

**A**

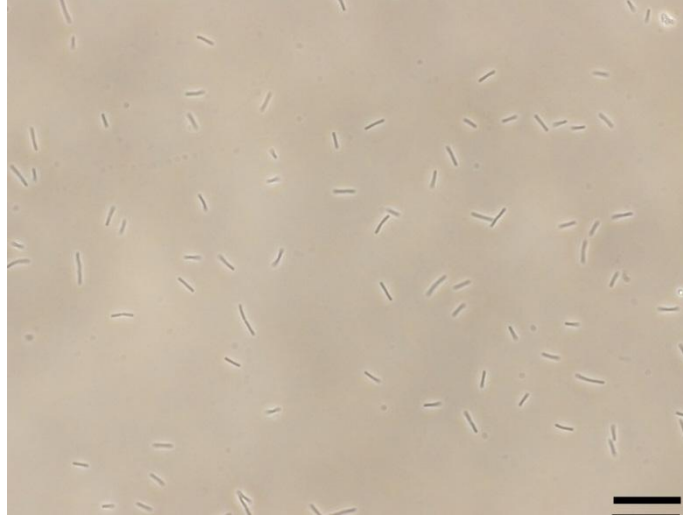


**B**

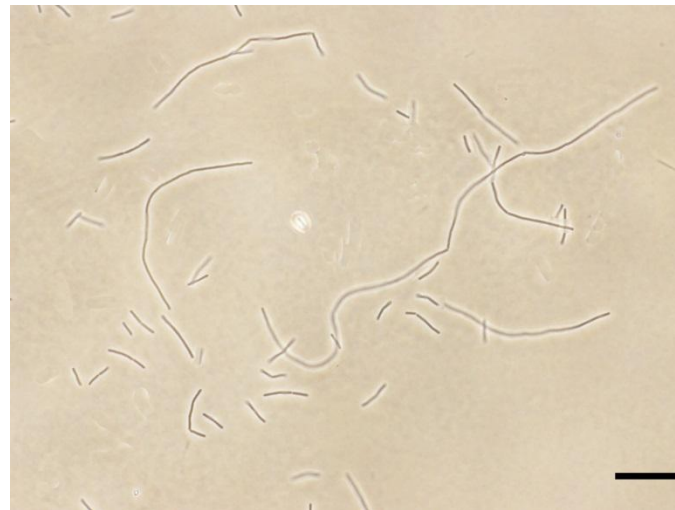


**Figure 3.1** Effects of compound **4-F332**. Cells of *B.subtilis* 168 were grown for 4 hours in the absence (A) or presence of half of MIC of 4-F332 (B). The scale bar is 20  $\mu\text{m}$ . The experiment was repeated 3 times.

**A**



**B**



**Figure 3.2** Effects of compound **4-F361**. Cells of *B.subtilis* 168 were grown for 4 hours in the absence (A) or presence of half of MIC of 4-F361 (B). The scale bar is 20  $\mu\text{m}$ . The experiment was repeated 3 times.

### 3.2.3 Cytotoxicity test

The toxicity of **4-F332** and **4-F361** were tested on three mammalian cell lines. The results are shown in Table 3.6. **4-F332** and **4-F361** inhibited a normal cell line, L929, with  $IC_{50}$  of 100  $\mu$ M and 60  $\mu$ M respectively. Although the results showed that **4-F332** is less toxic to L929 when comparing with **4-F361**. The MIC of **4-F332** is 4 folds higher than that of **4-F361**. Based on the results in cytotoxicity test, the selectivity indices of **4-F332** and **4-F361** were calculated to be 8 and 20 respectively. As a result, **4-F361** is a potential antibacterial agent as its selectivity index is greater than 10.

**Table 3.6 Cytotoxicity results of 4-F332 and 4-F361**

Compound	<i>S.aureus</i> 29213 (MIC, $\mu$ M)	LCC6 (IC <sub>50</sub> , $\mu$ M)	LCC6MDR (IC <sub>50</sub> , $\mu$ M)	L929 (IC <sub>50</sub> , $\mu$ M)	Selectivity index (L929:MIC)
<b>4-F332</b>	12.5	78	100	100	8
<b>4-F361</b>	3	60	52	60	20

LCC6: Wild type breast cancer line;

LCC6MDR: Pgp-overexpressed breast cancer cell line;

L929: mouse fibroblast cell line

### 3.4 Concluding remarks

The presence of a nonyl alkyl chain and a methyl group on the amino group of **4-F361** allow the compound to exhibit strong antibacterial activity and induce filamentation of *B.subtilis* 168. The position and number of fluorine substituents are important for potent antibacterial activity. Cell elongation was observed under normal light microscope when *B.subtilis* 168 cells was incubated with sub-lethal concentrations of **4-F361**, suggesting that the compound may perturb the normal functions of cytoplasmic division proteins.

In general, aminobenzamides have relatively smaller ClogP values than alkoxybenzamide, indicating that aminobenzamide derivatives are likely to possess better bioavailability. Furthermore, cytotoxicity assay showed that **4-F361** kills *S.aureus* 29213 with a favourable selectivity index of 20.

## Chapter 4

### *In vitro* biological studies of 3-MBA derivatives as FtsZ inhibitors

---

#### 4.1 Introduction

Chemical compounds with positive results in the microbial susceptibility test were further studied to investigate their interactions with FtsZ protein. GTPase activity assay and light scattering assay are commonly used to study the effects of compounds on enzymatic activity and polymerization of FtsZ. Transmission electron microscopy (TEM) allows us to observe the effect of compounds on the morphology of FtsZ protofilament.

In this chapter, the expression of recombinant *S.aureus* FtsZ is discussed. The effects of **4-F332** and **4-F361** on the GTPase activity, polymerization and the changes of morphology of FtsZ protofilaments are reported.



## **4.2 Experimental section**

### **4.2.1 Materials**

Sodium dodecyl sulphate, glycerol, glycine, tris(hydroxymethyl)aminomethane, guanosine triphosphate (GTP) and bovine serum albumin (BSA) were purchased from Sigma-Aldrich. Acrylamide solution, coomassie blue and Bradford's reagent were purchased from Bio-Rad. The CytoPhos<sup>TM</sup> phosphate assay Biochem Kit<sup>TM</sup> was purchased from Cytoskeleton, Inc. Glow-discharged Formvar carbon-coated copper grids were purchased from SPI Supplies / Structure Probe, Inc.

### **4.2.2 Instrumentation**

A microplate reader (Bio-Rad Laboratories Model 680) was used to measure the change in GTPase assays. A transmission electron microscope (JEOL Model JEM-2011) was used to observe the morphology of FtsZ protein. A fluorescence spectrometer (Pelkin-Elmer Model LS50) was used to measure the light scattering signal in FtsZ polymerization.

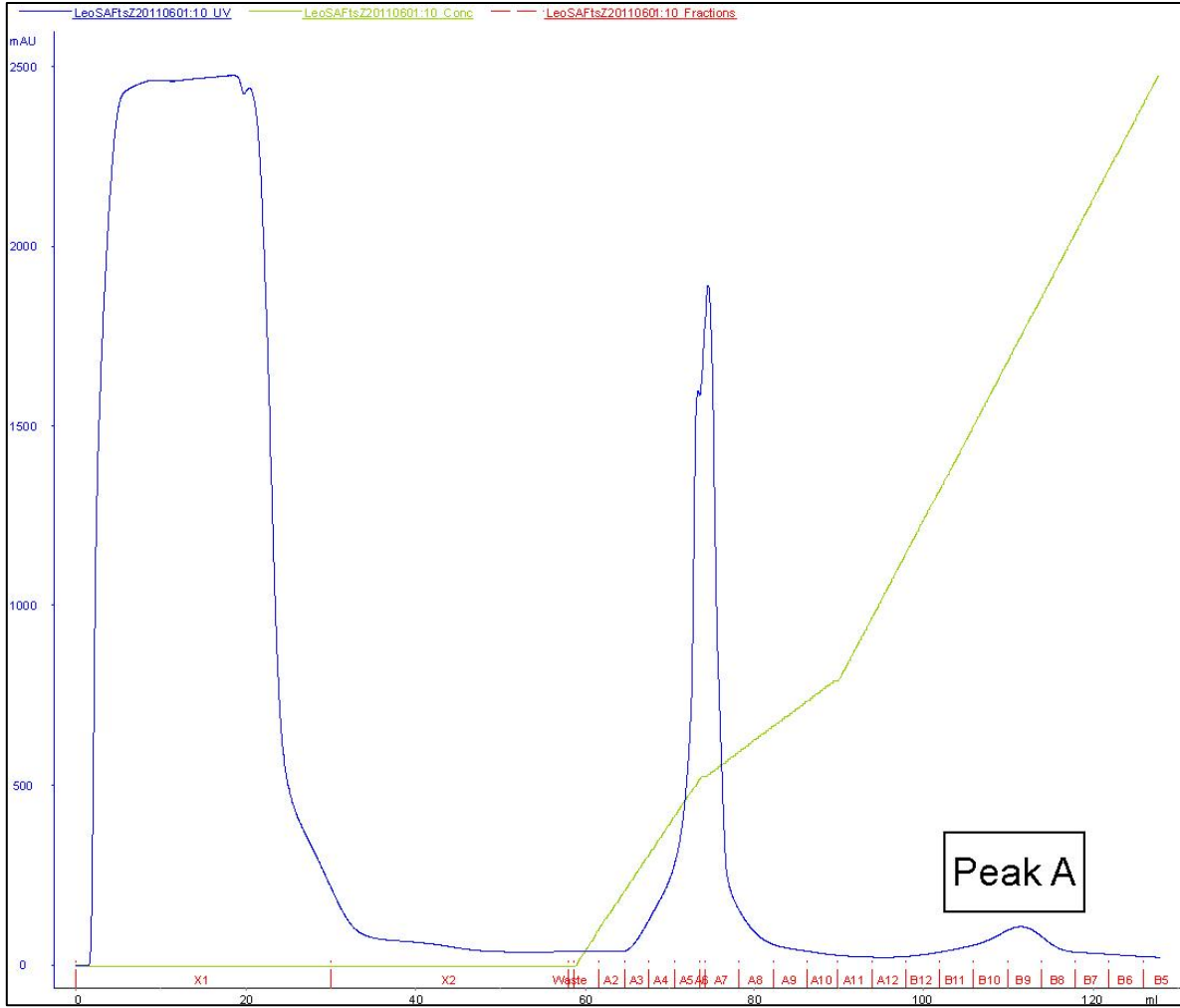
### 4.2.3 Preparation of *S.aureus* FtsZ protein

#### 4.2.3.1 Expression and purification of FtsZ protein

*E.coli* BL21 cells carrying *S.aureus ftsZ* gene were obtained from a stock in our laboratory. The *E.coli* strain from the stock was amplified in 5 mL LB medium in the presence of 100 µg/mL ampicillin at 37°C for 14-16 hours. The bacterial culture (2 mL) from overnight culture was transferred to 200 mL of 2 X TY medium containing 100 µg/mL ampicillin and allowed to grow at 37°C until the optical absorbance (OD<sub>600</sub>) reached 0.8. Protein expression was induced by the addition of 0.4 mM isopropyl-β-D-1-thiogalactopyranoside (IPTG) for another 4 hours. The bacterial cells were collected by centrifugation at 9000 rpm at 4°C for 20 minutes. Cell pellets were then resuspended in 20 mL starting buffer (0.02M sodium phosphate, 0.5M sodium chloride, pH 7.4). The cells were homogenized by sonication operated at 50% amplitude with 30 seconds pulse-on and 30 seconds pulse-off for 5 cycles. The insoluble cell debris was removed by centrifugation at 13,000 rpm at 4°C for 1.5 hours. The supernatant was collected and filtered by sterile 0.22 µm filter.

The FtsZ protein in supernatant was purified by Fast Protein Liquid Chromatography (FPLC). A 5 mL HiTrap chelating column activated by nickel (II) sulphate solution was used in FPLC in order to capture His-tagged *S.aureus* FtsZ proteins. The activated column was then equilibrated by starting buffer. The soluble protein solution containing His-tagged protein was passed through the column with starting buffer. The His-tagged protein (Peak A) was then eluted with elution buffer (0.02M sodium phosphate, 0.5

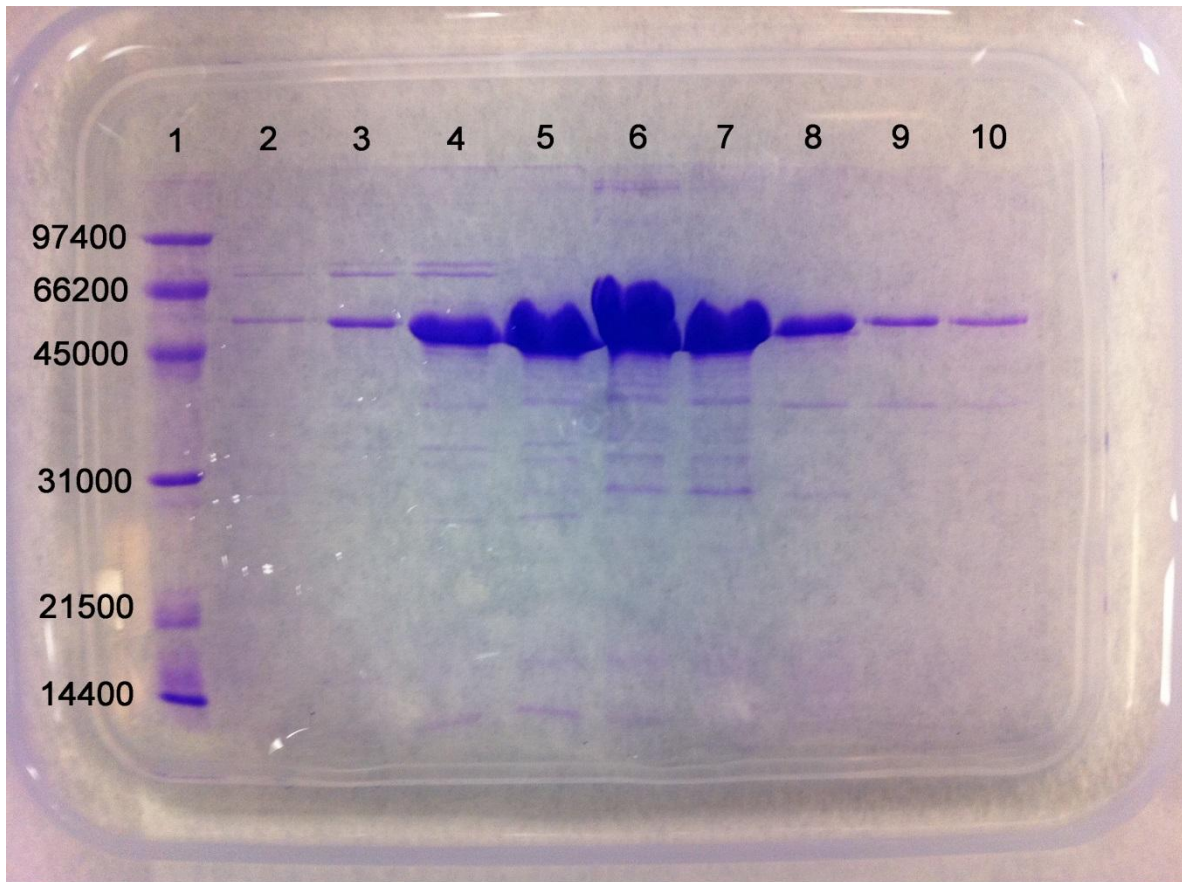
M sodium chloride, 0.5 M imidazole, pH 7.4). The chromatogram is shown in Figure 4.1. The fractions were collected and analyzed by SDS-PAGE, followed by dialysis against 50 mM MOPS buffer and stored at -80°C.



**Figure 4.1** The FPLC chromatogram of *S.aureus* FtsZ

#### **4.2.3.2 Sodium dodecyl sulphate-polyacrylamide gel electrophoresis (SDS-Page)**

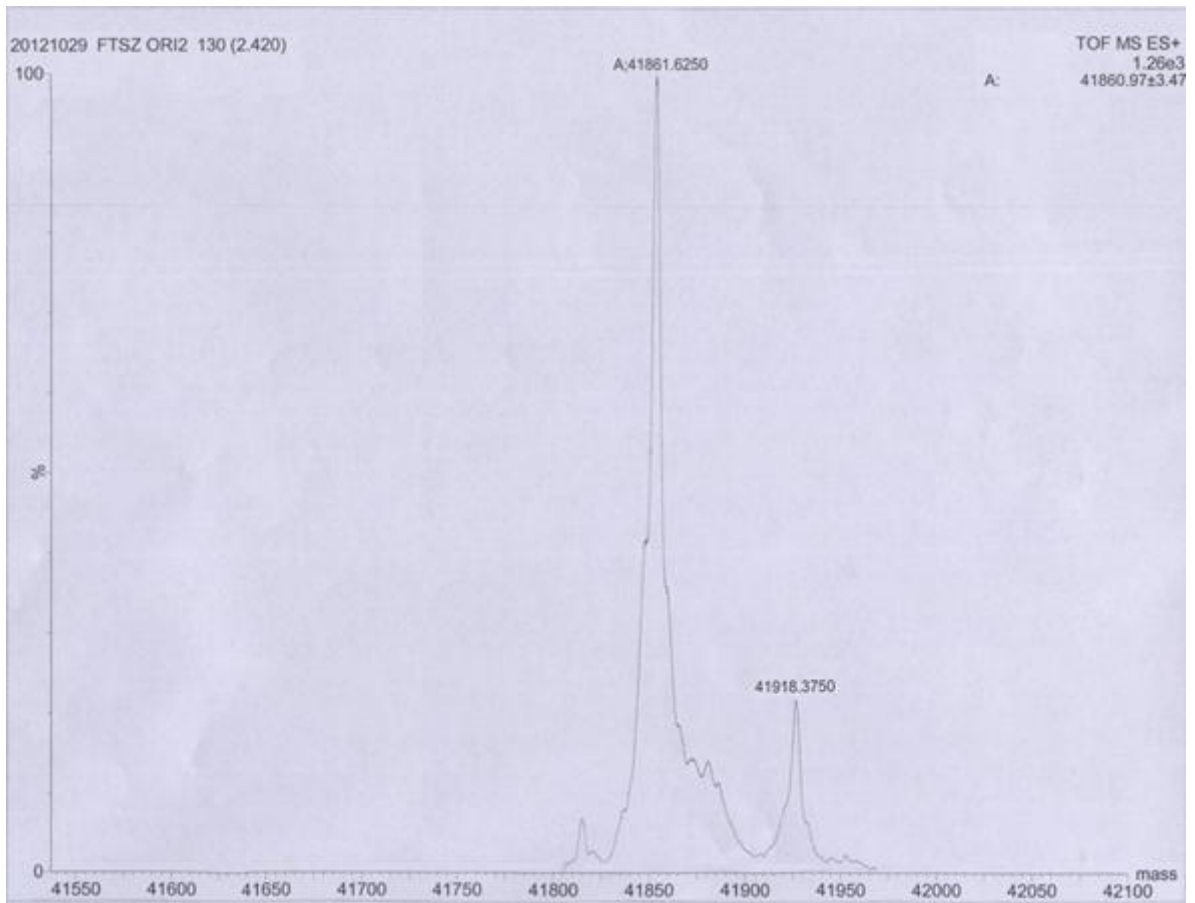
Protein fractions collected from FPLC were analyzed by 12% SDS-Page in a Mini-PROTEAN III dual slab cell (Bio-Rad). 10  $\mu$ L of protein fraction was mixed with 10  $\mu$ L of 2X protein gel loading buffer (4% SDS, 20% Glycerol, 0.12 M Tris pH 6.8 and 10%  $\beta$ -mercaptoethanol) and heated at 100°C for 10 minutes. The SDS-Page gel was prepared by 5% stacking gel (pH 6.8) and 12% separating gel (pH 8.8). Heated sample was loaded into the well of the SDS-Page gel, which was then subjected to electrophoresis in 1X running buffer (0.025M Tris-HCl, 192 mM glycine, 3 mM SDS, pH 7.4) at 200V for 60 minutes. The gel was stained with coomassie blue for 10 minutes and then destained by the solution containing acetic acid and methanol until the background of the gel became clear. A typical SDS-PAGE gel photograph is shown in Figure 4.2.



**Figure 4.2** A typical SDS-Page gel photo of *S.aureus* FtsZ. Lane 1, low molecular markers: rabbit muscle phosphorylase b (97400 Da), BSA (66200 Da), hen egg white ovalbumin (45000 Da), bovine carbonic anhydrase (31000 Da), soybean trypsin inhibitor (21500 Da), hen egg white lysozyme (14400 Da); lane 2-9, elution of *S.aureus* His-tagged FtsZ by elution buffer.

#### 4.2.3.3 Electrospray ionization-mass spectrometry (ESI-MS)

ESI-MS was used to confirm the molecular weight of *S.aureus* FtsZ. Purified *S.aureus* FtsZ was dialyzed and concentrated by 20 mM ammonium acetate. The ESI-MS spectrum was obtained using a VG Platform single quadrupole or quadrupole-time of flight (Q-TOF2) mass spectrometer (Micromass, Altrincham, Cheshire, UK) equipped with an electrospray interface. Protein samples dissolved in H<sub>2</sub>O/CH<sub>3</sub>CN (1:1 v/v) or H<sub>2</sub>O/MeOH (1:1 v/v) containing 0.2% formic acid (v/v) were injected into the electrospray source through a loop injector (Rheodyne 5717) at a flow rate of 10 µL/min. The mass spectrometer was scanned over a range of m/z 570-1600. Myoglobin (10 µmol/µL, average molecular mass 16951.15) was used as a reference to calibrate the instrument. The ESI-MS spectrum of *S.aureus* FtsZ is shown in Figure 4.3.



**Figure 4.3** ESI-mass spectrum of *S.aureus* FtsZ



#### **4.2.3.4 Determination of protein concentration**

The concentration of *S.aureus* FtsZ protein was determined by Bradford's method. 200  $\mu\text{L}$  of the Bradford's reagent (Bio-Rad) was mixed with 800  $\mu\text{L}$  of water and FtsZ protein to 1000  $\mu\text{L}$ . The mixture was then incubated at room temperature for 8 minutes. The absorbance of the sample was measured by a UV-vis spectrometer at 595 nm. The concentration of the sample can be determined by comparing a calibration curve using BSA as the standard.

#### 4.2.4 Light scattering assay

Light scattering assay was used to determine the degree of FtsZ polymerization by measuring the 90° light scattering signal using a fluorescence spectrometer (Perkin-Elmer, USA). The excitation and emission wavelengths were set to 600 nm with a slit width of 5 nm. *S.aureus* FtsZ (12 μM) was incubated with serial dilutions of the compounds in 50 mM MOPS buffer (pH 6.8) at 25°C for 10 minutes. The control sample contains 1% DMSO only. KCl (final concentration: 50 mM) and MgCl<sub>2</sub> (final concentration: 10 mM) were then added to the mixture and incubated at 37°C for 8 minutes in order to establish a baseline. A final concentration of 1 mM GTP was added and the light scattering signal was measured for 1000 seconds. The relative light scattering signals in experimental set-up were calculated with reference to the light scattering signal in control experiment. Three independent experiments were carried out for each compound concentration.

#### 4.2.5 GTPase activity assay

The GTPase activity of *S.aureus* FtsZ was determined in a 96-well microplate using a CytoPhos<sup>TM</sup> phosphate assay Biochem Kit<sup>TM</sup> (Cytoskeleton, USA) [65] which measured the concentration of inorganic phosphate released during the hydrolysis of GTP [66]. Recombiant *S.aureus* FtsZ (7.5  $\mu$ M) was incubated with serial dilutions of the compounds in 50 mM MOPS buffer (pH 6.5) at 25°C for 10 minutes. The control sample contained 1% DMSO. KCl (final concentration: 200 mM) and MgCl<sub>2</sub> (final concentration: 5 mM) were then added to the mixture. The mixture was incubated with GTP (final concentration: 500  $\mu$ M) at 37°C for 30 minutes. The insoluble polymer was removed by centrifugation at 13,500 rpm at room temperature for 1 minute. 80  $\mu$ L supernatant was transferred to a well of 96-well microplate and incubated with 120  $\mu$ L of Cytophos reagent at room temperature for 10 minutes. The inorganic phosphate in the mixture was determined by measuring the absorbance at 650 nm in a 96-well microplate reader (BioRad 680). The results from the samples were reported with reference to the control. Three independent experiments were carried out for each compound concentration.

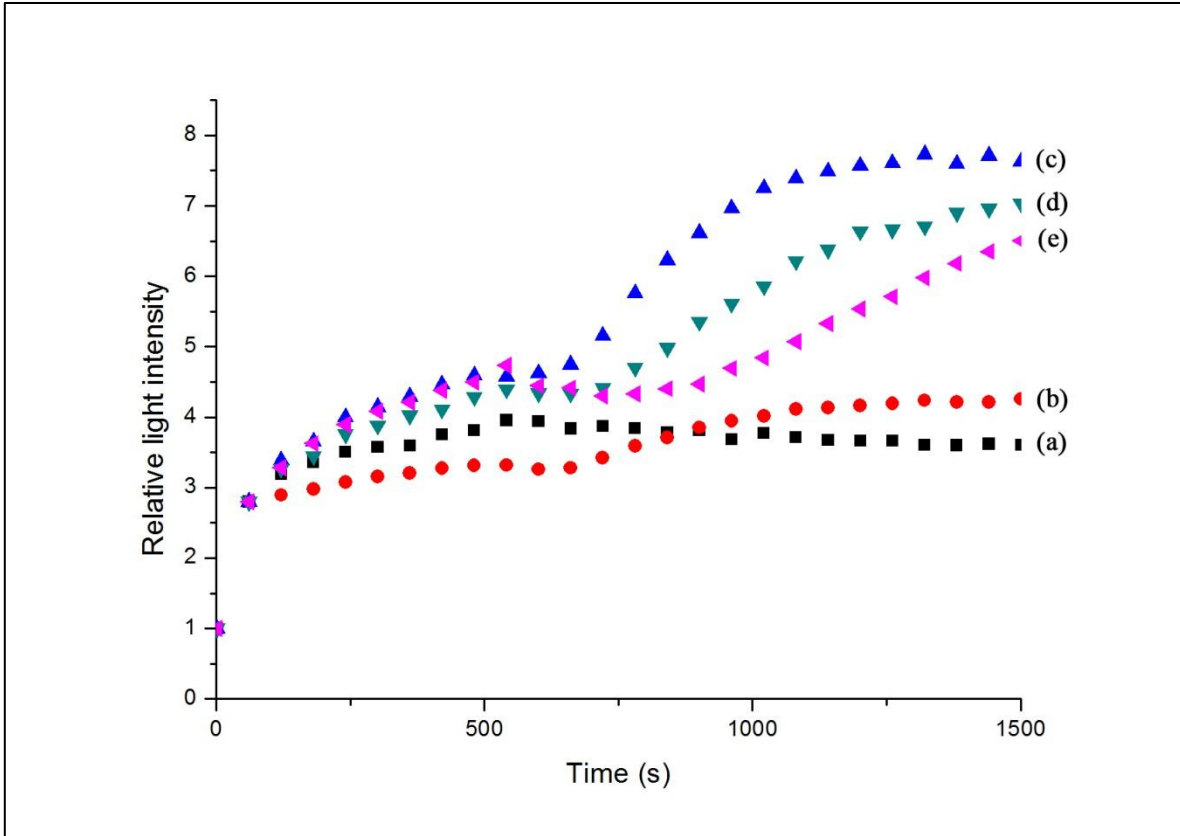
#### 4.2.6 Transmission electron microscopy (TEM)

TEM provides a direct observation of FtsZ polymer morphology. *S.aureus* FtsZ (12  $\mu$ M) was incubated with different concentrations of compounds in 50 mM MOPS buffer (pH 6.5) at 25°C for 10 minutes. The control contained 1% DMSO only. KCl (final concentration: 50 mM), MgCl<sub>2</sub> (final concentration: 5 mM) and GTP (final concentration: 1 mM) were added to the mixtures and incubated at 37°C for 15 minutes. 10  $\mu$ L reaction mixtures were applied on a glow-discharged Formvar carbon-coated copper grid (400 meshes) at 25°C for 10 minutes. 10  $\mu$ L of 0.5% phosphotungstic acid (PTA) was applied on the copper grid in order to negatively stain the proteins. The copper grid was allowed to air dry overnight. The FtsZ polymer morphology was observed with a transmission electron microscope (JEOL model JEM 2010) operated at 200 kV and equipped with a Gatan MSC 794 CCD camera.

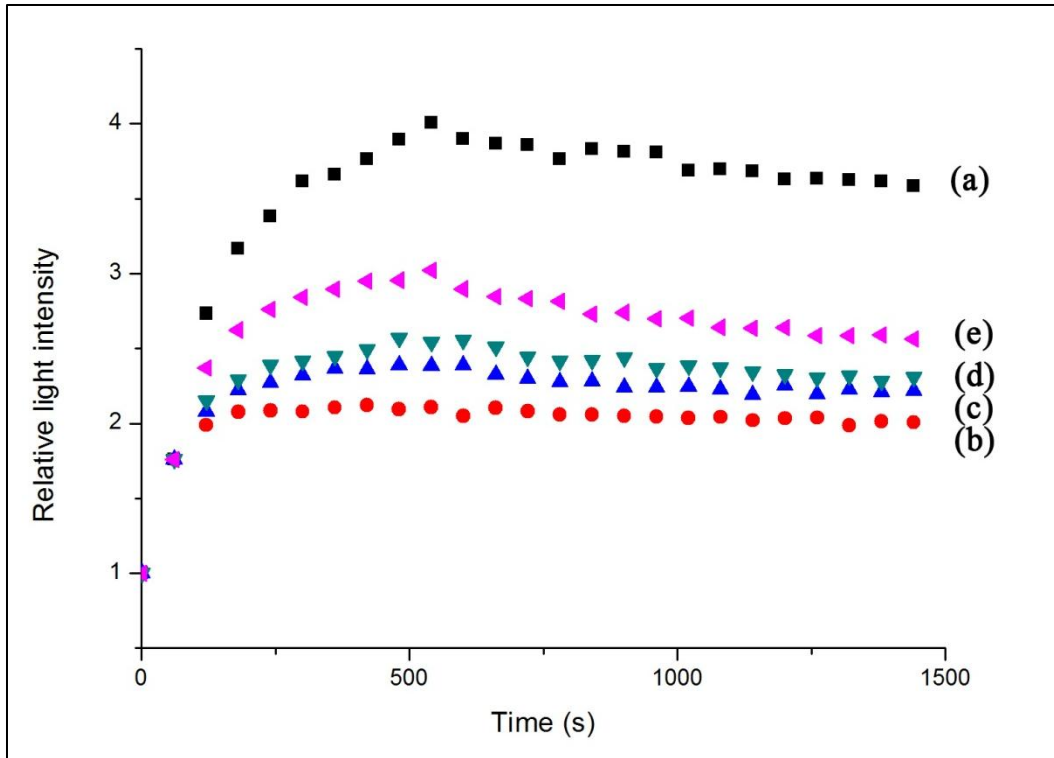
## 4.3 Results and discussion

### 4.3.1 Light scattering assay

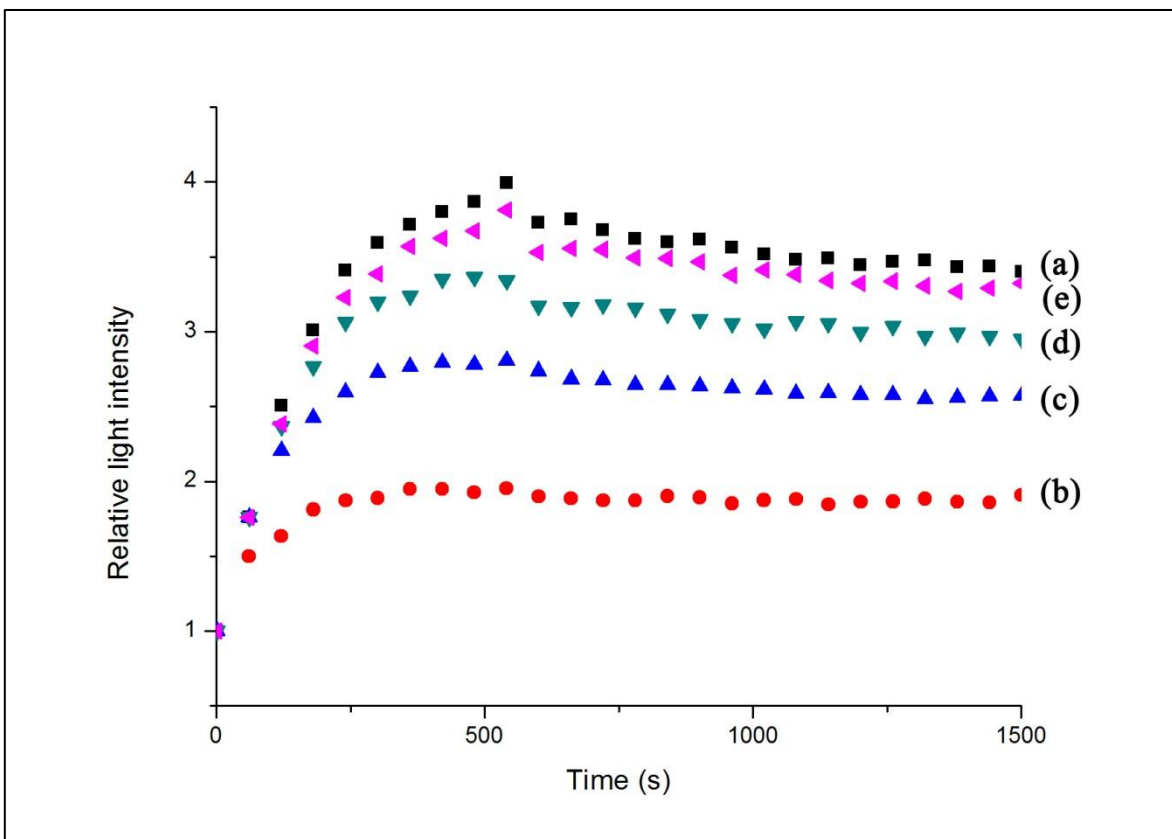
The effect of compounds on FtsZ polymerization and depolymerization can be traced by light scattering assay. In the assay, the light scattering signal scattered by FtsZ polymer was measured at 600 nm. As the polymer mass of FtsZ is directly proportional to the magnitude of light scattering signal, the dynamics of FtsZ assembly can be investigated *in vitro* [67]. **4-F332** and **4-F361** were evaluated for their ability to perturb the polymerization of recombinant *S.aureus* FtsZ while a published FtsZ inhibitor, **F327** (**PC190723**) acts as a positive control in this assay. **F327** can promote the light scattering of FtsZ assembly, which has been reported in a previous study [68]. **4-F332** and **4-F361** can inhibit the light scattering of FtsZ assembly. The decreased light scattering signal indicates that both compounds can reduce the polymer mass of FtsZ protofilament in a dose-dependent manner. The results are summarized in Figure 4.4-4.6. Figure 4.4 shows the effect of **F327** on *S.aureus* FtsZ assembly. Figure 4.5 shows the effect of **4-F332** on FtsZ assembly *in vitro*, about 47%, 39%, 34% inhibition were observed at 100  $\mu$ M, 50  $\mu$ M and 25  $\mu$ M of **4-F332** respectively. Figure 4.6 shows the effect of **4-F361** on the FtsZ assembly *in vitro*, about 51%, 29%, 17% inhibition were observed at 100  $\mu$ M, 50  $\mu$ M and 25  $\mu$ M of **4-F361** respectively.



**Figure 4.4** Effect of **F327** on FtsZ assembly *in vitro*. *S.aureus* FtsZ (5  $\mu$ M) was polymerized in 50 mM MOPS, pH 6.5, 50 mM KCl, 10 mM MgCl<sub>2</sub> and 1 mM GTP in the absence of **F327** (a), in the presence of 100  $\mu$ M (b), 50  $\mu$ M (c), 25  $\mu$ M (d) and 12.5  $\mu$ M (e) of **F327**. Appropriate blanks were subtracted from all the traces. Each experiment was repeated three times.



**Figure 4.5** Effect of **4-F332** on FtsZ assembly *in vitro*. *S.aureus* FtsZ (5  $\mu$ M) was polymerized in 50 mM MOPS, pH 6.5, 50 mM KCl, 10 mM MgCl<sub>2</sub> and 1 mM GTP in the absence of **4-F332** (a), in the presence of 100  $\mu$ M (b), 50  $\mu$ M (c), 25  $\mu$ M (d) and 12.5  $\mu$ M (e) of **4-F332**. Appropriate blanks were subtracted from all the traces. Each experiment was repeated three times.



**Figure 4.6** Effect of **4-F361** on FtsZ assembly *in vitro*. *S.aureus* FtsZ (5  $\mu$ M) was polymerized in 50 mM MOPS, pH 6.5, 50 mM KCl, 10 mM MgCl<sub>2</sub> and 1 mM GTP in the absence of **4-F361** (a), in the presence of 100  $\mu$ M (b), 50  $\mu$ M (c), 25  $\mu$ M (d), 12.5  $\mu$ M (e) of **4-F361**. Appropriate blanks were subtracted from all the traces. Each experiment was repeated three times.



### 4.3.2 GTPase activity

The GTPase activity of FtsZ is important to regulate the dynamic assembly of FtsZ protein. As a result, the effect of chemical compounds on the GTPase activity of FtsZ is usually investigated in FtsZ inhibitor discovery. **4-F332** and **4-F361** were diluted in a serial two-fold manner and their effect on the GTPase activity were tested. A 1% DMSO solution was used as the blank. A FtsZ inhibitor developed from our research group, a pyrimidine substituted quinuclidines 10, was used as a positive control [66]. F327 is **PC190723**, which has been reported to have inhibitory effect on GTPase activity of *S.aureus* FtsZ and *B.subtilis* FtsZ. [40, 68]. The results of the effect of **F327**, **4-F332** and **4-F361** on the GTPase activity of *S.aureus* FtsZ are summarized in Table 4.1.

**F327 (PC190723)** was reported to inhibit the GTPase activity of *S.aureus* FtsZ in a dose-dependent manner with a half-maximal inhibitory concentration ( $IC_{50}$ ) of 0.15  $\mu$ M [40]. Surprisingly, no inhibitory effect on the GTPase activity of *S.aureus* FtsZ was observed by **F327** in our assay. Several published GTPase activity assay methods had been tried, but still no inhibitory effect by **F327** was observed. The result is in contrast to that of the original published paper [40]. Anderson et al. reviewed the results of reported FtsZ inhibitors, they did not observe any inhibitory effect on the GTPase activity of *B.subtilis* FtsZ by F327 in both enzyme-coupled or malachite green assays [31]. In fact, Anderson et al. found that F327 increased the GTPase activity of *S.aureus* FtsZ in a dose-dependent manner. Similar result was also obtained in our GTPase assay (Figure 4.7). On the other hand, no significant change of the GTPase activity of *S.aureus* FtsZ was observed by **4-F332** and **4-F361** (Figure 4.8 & Figure 4.9.) Based on the results in light scattering and

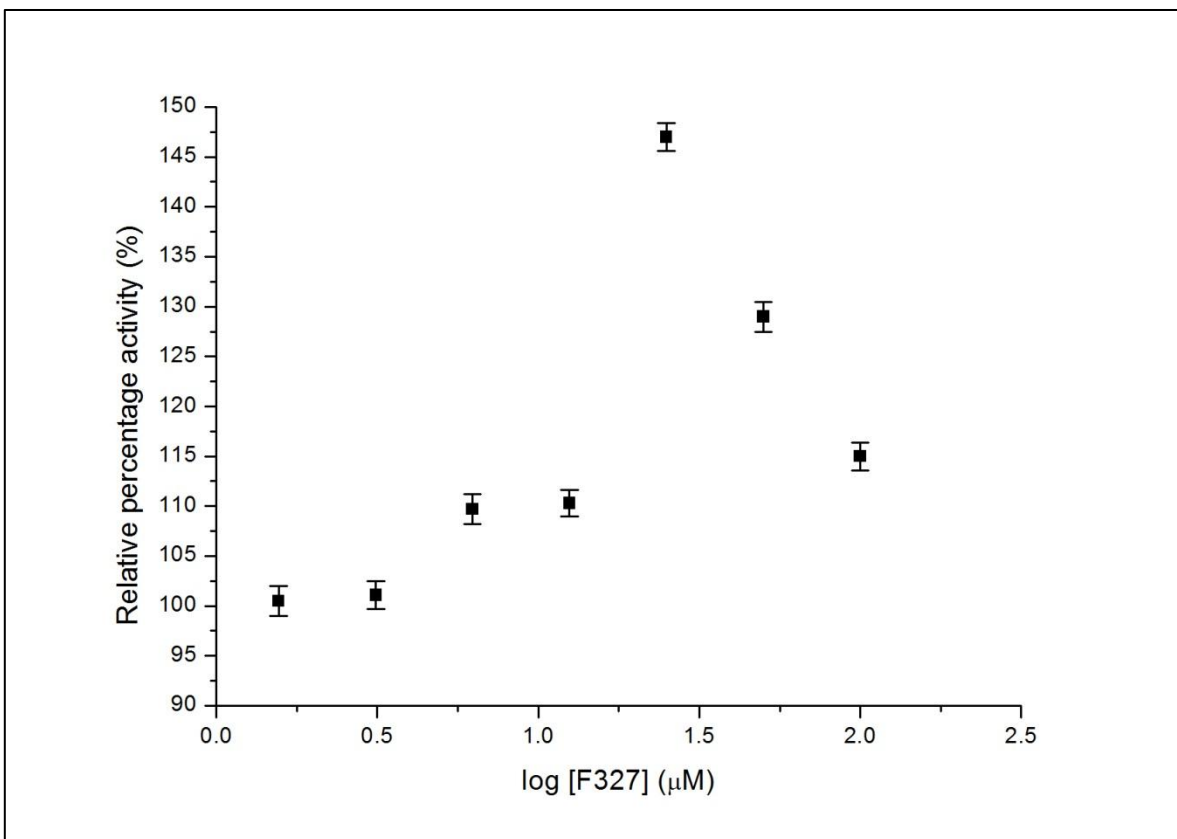
GTPase activity measurement, **4-F332** and **4-F361** inhibit the polymerization of FtsZ without affecting its GTPase activity.

**Table 4.1** Relative percentage inhibition on the GTPase activity of *S.aureus* FtsZ by **F327**, **4-F332** and **4-F361**

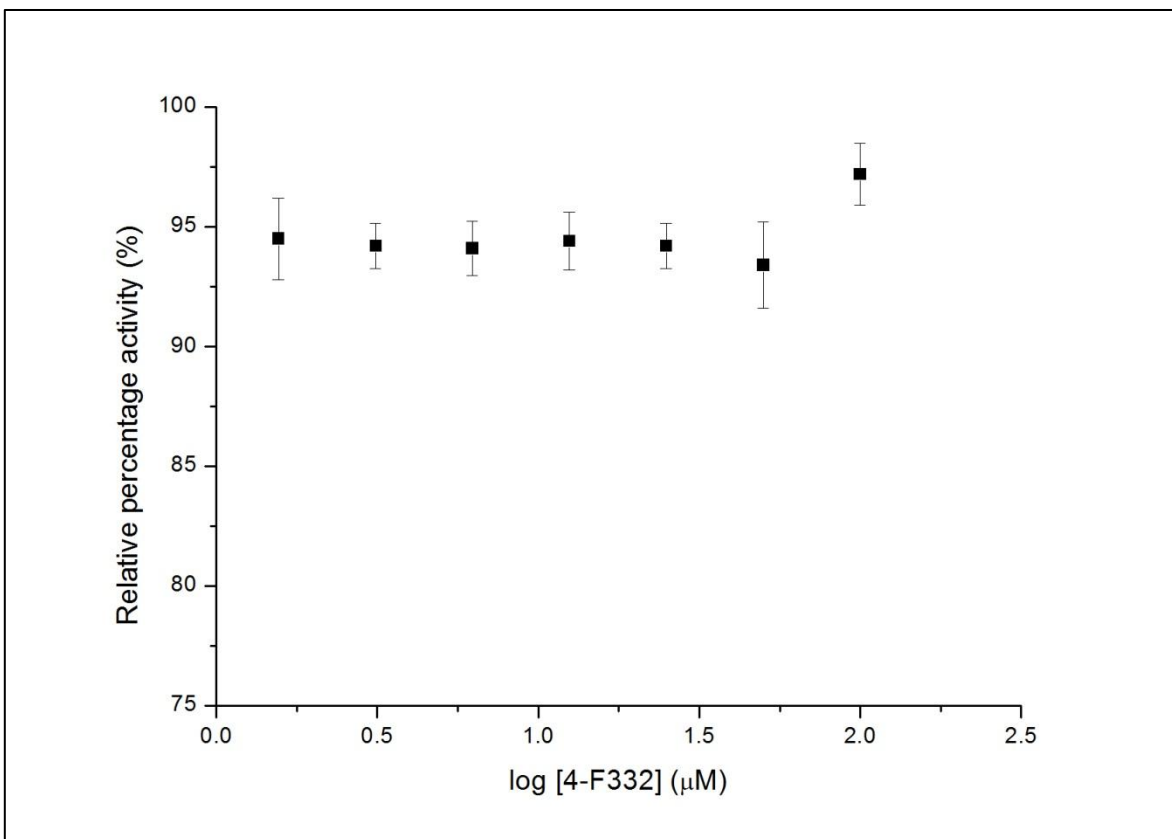
Compound	Relative percentage activity (%)
DMSO only	100
<b>F327</b> (100 $\mu$ M)	114.8 $\pm$ 1.4
<b>F327</b> (50 $\mu$ M)	112.9 $\pm$ 1.5
<b>F327</b> (25 $\mu$ M)	114.8 $\pm$ 1.4
<b>F327</b> (12.5 $\mu$ M)	110.3 $\pm$ 1.3
<b>F327</b> (6.25 $\mu$ M)	109.7 $\pm$ 1.5
<b>F327</b> (3.13 $\mu$ M)	101.1 $\pm$ 1.4
<b>F327</b> (1.56 $\mu$ M)	100.5 $\pm$ 1.5

Compound	Relative percentage activity (%)
DMSO only	100
<b>4-F332</b> (100 $\mu$ M)	97.2 $\pm$ 1.3
<b>4-F332</b> (50 $\mu$ M)	93.4 $\pm$ 1.8
<b>4-F332</b> (25 $\mu$ M)	94.2 $\pm$ 1.0
<b>4-F332</b> (12.5 $\mu$ M)	94.4 $\pm$ 1.2
<b>4-F332</b> (6.25 $\mu$ M)	94.1 $\pm$ 1.1
<b>4-F332</b> (3.13 $\mu$ M)	94.2 $\pm$ 1.0
<b>4-F332</b> (1.56 $\mu$ M)	94.5 $\pm$ 1.7

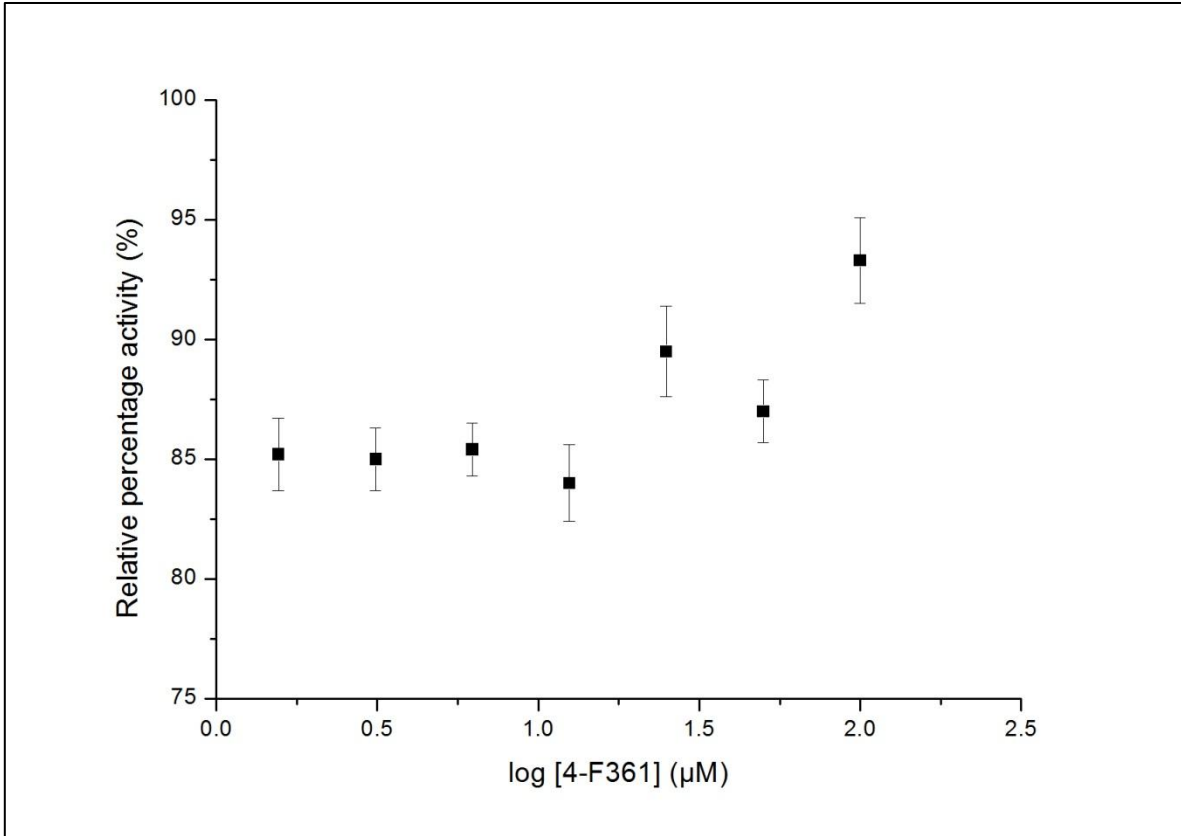
Compound	Relative percentage activity (%)
DMSO only	100
<b>4-F361</b> (100 $\mu$ M)	93.3 $\pm$ 1.8
<b>4-F361</b> (50 $\mu$ M)	87.0 $\pm$ 1.3
<b>4-F361</b> (25 $\mu$ M)	89.5 $\pm$ 1.9
<b>4-F361</b> (12.5 $\mu$ M)	84.0 $\pm$ 1.6
<b>4-F361</b> (6.25 $\mu$ M)	85.4 $\pm$ 1.1
<b>4-F361</b> (3.13 $\mu$ M)	85.0 $\pm$ 1.3
<b>4-F361</b> (1.56 $\mu$ M)	85.2 $\pm$ 1.5



**Figure 4.7** Effect of **F327** on the GTPase activity of *S.aureus* FtsZ assays.



**Figure 4.8** Effect of **4-F332** on the GTPase activity of *S.aureus* FtsZ



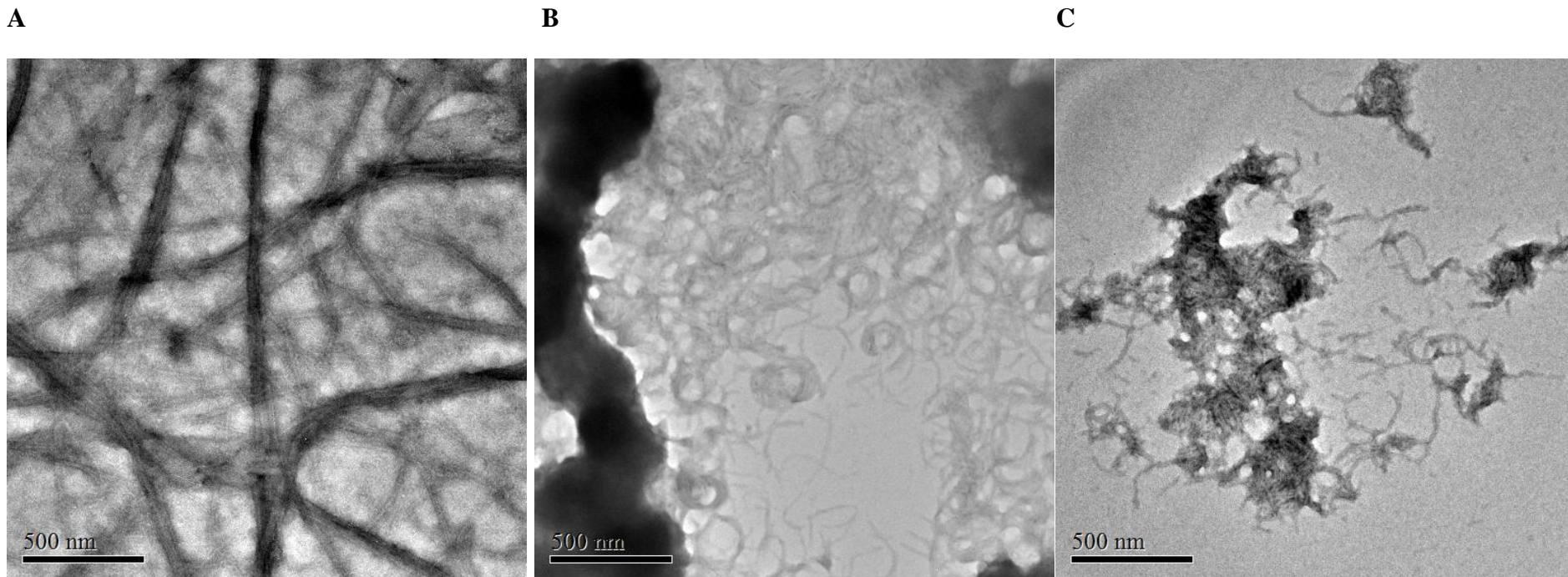
**Figure 4.9** Effect of **4-F361** on the GTPase activity of *S.aureus* FtsZ

### 4.3.3 Transmission electron microscopy (TEM)

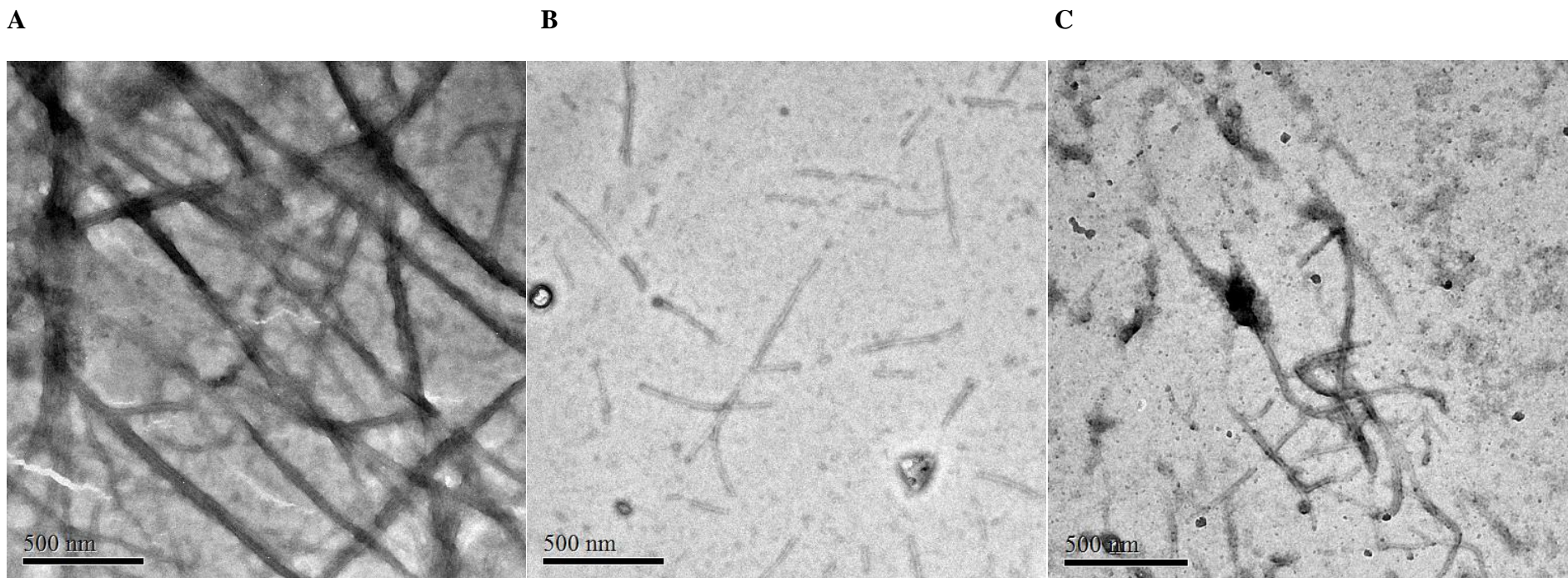
The effect of **F327**, **4-F332** and **4-F361** on the polymerization of *S.aureus* FtsZ protofilament were studied by transmission electron microscopy. The electron micrographs of **F327**, **4-F332** and **4-F361** are shown in Figures 4.10-4.12 respectively. An extensive network of thick bundles formed by FtsZ protofilaments was observed in the absence of inhibitor (Figure 4.10 (A), Figure 4.11 (A) and Figure 4.12(A)). Compared with FtsZ filaments in the absence of inhibitors, single strand coiled FtsZ filaments with shorter length were observed when *S.aureus* FtsZ was allowed to polymerize in the presence of **F327** at 50  $\mu$ M and 100  $\mu$ M respectively (Figure 4.10 (B) (C)). Similar filament morphology was also observed in the previous report [68]. Protein aggregates were also observed at both concentrations of **F327**. Therefore, **F327** induces the formation of protein aggregates by enhancing FtsZ polymerization, which explains the enhanced signal observed in light scattering assay (Figure 4.4). Comparing with protofilaments obtained in the absence of inhibitor, short and straight single strand FtsZ protofilaments were obtained when FtsZ was polymerized in the presence of 100  $\mu$ M of **4-F332** (Figure 4.11 (B) (C)). Relatively thicker bundles were observed in the presence of 50  $\mu$ M of **4-F332**. This phenomenon coincides with the light scattering assay, where **4-F332** was shown to inhibit FtsZ polymerization in a dose-dependent manner (Figure 4.5). The short and thin protofilaments observed in electron micrographs implies that **4-F332** inhibits both longitudinal and lateral association of protofilaments in a dose-dependent manner. Similar to the FtsZ protofilaments obtained in the presence of **4-F332**, short and straight single strand protofilaments were also observed in the presence of 100  $\mu$ M of **4-F361**. However, **4-F361** has stronger inhibitory effects on inhibition of both longitudinal and lateral

associations of protofilaments. Comparing with the same concentrations of **4-F332**, the length and the thickness of protofilaments were relatively shorter and thinner when FtsZ was polymerized in the presence of **4-F361**. This phenomenon is similar to that observed in light scattering assay, where **4-F361** also inhibits polymerization of FtsZ in the presence of **4-F361** in a dose-dependent manner.

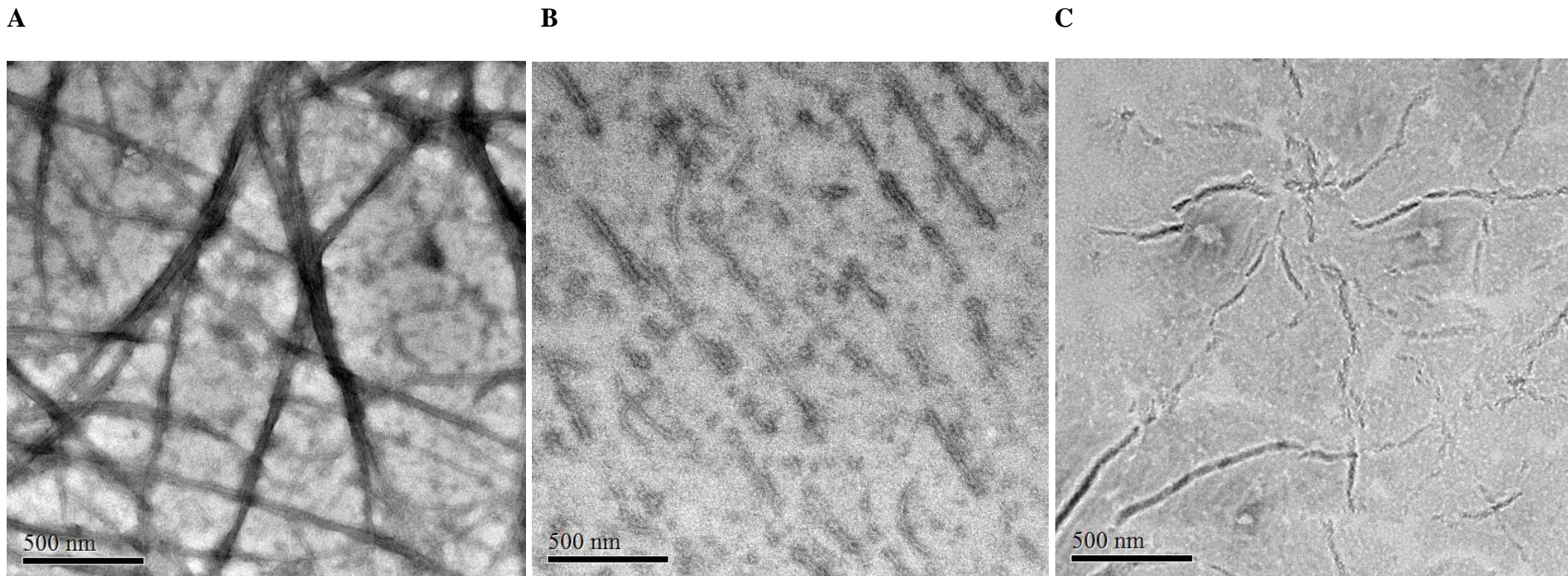




**Figure 4.10** Electron micrographs of FtsZ polymers. *S.aureus* FtsZ (12  $\mu$ M) was polymerized in 50 mM MOPS buffer, pH 6.5, containing 50 mM KCl, 5 mM MgCL<sub>2</sub> and 1 mM GTP in the absence and presence of **F327** at 37°C for 15 minutes. The pictures above are the electron micrographs of FtsZ polymers formed in the absence (A) and presence of 100  $\mu$ M (B) and 50  $\mu$ M (C) of F327 (**PC190723**). The scale bar is 500 nm.



**Figure 4.11** Electron micrographs of FtsZ polymers. *S.aureus* FtsZ (12  $\mu$ M) was polymerized in 50 mM MOPS buffer, pH 6.5, containing 50 mM KCl, 5 mM MgCL<sub>2</sub> and 1 mM GTP in the absence and presence of **4-F332** at 37°C for 15 minutes. The pictures above are the electron micrographs of FtsZ polymers formed in the absence (A) and presence of 100  $\mu$ M (B) and 50  $\mu$ M (C) of 4-F332. The scale bar is 500 nm.



**Figure 4.12** Electron micrographs of FtsZ polymers. *S.aureus* FtsZ (12  $\mu$ M) was polymerized in 50 mM MOPS buffer, pH 6.5, containing 50 mM KCl, 5 mM MgCL<sub>2</sub> and 1 mM GTP in the absence and presence of **4-F361** at 37°C for 15 minutes. The pictures above are the electron micrographs of FtsZ polymers formed in the absence (A) and presence of 100  $\mu$ M (B) and 50  $\mu$ M (C) of 4-F361. The scale bar is 500 nm.

#### 4.4 Concluding remarks

In this chapter, **F327 (PC190723)**, **4-F332** and **4-F361** were tested to see if they can perturb the FtsZ protein *in vitro*. A previous reported FtsZ inhibitor, **F327**, was found to promote FtsZ polymerization by enhancing the GTPase activity of *S.aureus* FtsZ in our assays. Although this finding is in contrary to the original published paper, another research group also obtained similar results when reviewing published FtsZ inhibitors. Transmission electron microscopy (TEM) showed coiled single strand filaments and protein aggregates when *S.aureus* FtsZ was polymerized in the presence of **F327**, which explained the enhanced light scattering signal obtained in light scattering assay.

**4-F332** and **4-F361** were found to inhibit *S.aureus* FtsZ polymerization in a dose-dependent manner without affecting the GTPase activity of FtsZ proteins. TEM showed that short and single strand filaments were observed when *S.aureus* FtsZ was polymerized in the presence of 100  $\mu$ M of **4-F332** and **4-F361** respectively. However, relatively shorter and thinner FtsZ protofilaments were observed in the presence of 50  $\mu$ M of **4-F361** comparing with the same concentration of **4-F332**.

Our results indicated that **F327** may have different mechanism to interact with *S.aureus* FtsZ compared to **4-F332** and **4-F361**. Further experiments should be carried out to investigate the mechanism of their interactions with FtsZ.

## Chapter 5

### Conclusions

The emergence of antibiotic-resistant bacteria in community becomes a public concern in recent years. From the report of World Health Organization (WHO) and Department of Health of Hong Kong, there is an increasing percentage of antibiotic-resistant bacteria found in the community. A common bacterial infection might become life-threatening if we cannot develop novel antibacterial agents in the 21<sup>st</sup> century.

FtsZ is a target with great potential for developing novel antibacterial agents. The FtsZ protein has only shared limited sequence with tubulin in human. The structure of FtsZ from different bacterial species are known. Various FtsZ inhibitors have been identified from natural and synthetic sources. These inhibitors are either targeting at the GTP-binding site or the T7-loop of FtsZ. Many inhibitors targeting at the GTP-binding site of FtsZ have high toxicity to animal cells. It is possible that some of these inhibitors also interfere with the GTPase activity of enzymes such as tubulin. On the other hand, those inhibitors targeting at the less conserved T7-loop are usually less toxic to animal cells. Protein X-ray crystallography has shown that **PC190723**, a **3-MBA** derivative, binds to the T7-loop of *S.aureus* FtsZ [41]. Derivatives of **3-MBA**, alkoxybenzamides, have been shown to be potential potent FtsZ inhibitors in a previous publication [58]. In our study, **4-F332** and **4-F361** were shown to inhibit the growth of *B.subtilis* 168 and *S.aureus* 29213 with low MICs. Filamentous cells of *B.subtilis* 168 were observed when the cells were grown in the presence of 0.5X MIC of **4-F332** and **4-F361** respectively, suggesting cytoplasmic division proteins of *B.subtilis* 168 cells were inhibited by these compounds. Light scattering assay

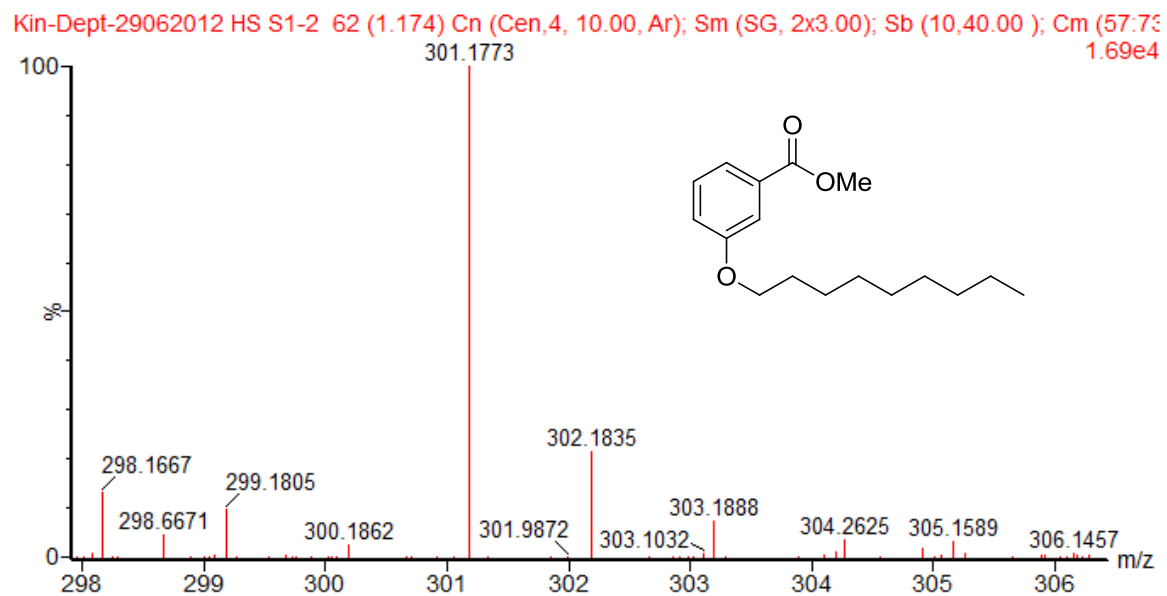
showed that both compounds can inhibit the polymerization of FtsZ in a concentration-dependent manner. GTPase activity assay showed that both compounds did not affect the GTPase activity of *S.aureus* FtsZ *in vitro*. Single strand and short FtsZ protofilaments were observed when the protein was allowed to polymerize at a concentration of 100  $\mu$ M of **4-F332** or **4-F361**. Relatively thinner FtsZ bundles were observed at 50  $\mu$ M of **4-F361**. TEM suggested that **4-F332** and **4-F361** inhibit both the longitudinal and lateral associations of FtsZ polymers to give thinner and shorter protofilaments. In addition, **4-F361** shows higher inhibitory effects on both longitudinal and lateral associations compared with **4-F332**. Although both compounds have similar chemical structures and *in vitro* activity, **4-F361** is less toxic to animal cells. The selectivity indices of **4-F332** and **4-F361** are 8 and 20 respectively. As a potential drug should have selectivity index greater than 10, it is worthwhile to further investigate **4-F361** in future study.

Although **4-F361** was identified as a potential potent FtsZ inhibitor, it still requires further optimization to reduce its MIC against *S.aureus* 29213. The methyl group on the amino group of **4-F361** was found to enhance the antibacterial activity significantly. Therefore, the methyl group could be further replaced with aliphatic chains of various lengths to study their effect on antibacterial activity. An extra alkyl chain on the amino group of **4-F361** may further enhance its potency to inhibit the growth of various antibiotic-resistant bacteria strains, though it will also affect its hydrophobicity hence ClogP and its binding to FtsZ. In addition, X-ray crystallography can be employed to study the interaction between **4-F361** and FtsZ. The synergistic effect of **4-F361** with commonly used antibiotics such as ampicillin should also be investigated. Ampicillin, oxacillin, ceftazidime and vancomycin are commonly used in clinical treatment. However, the emergence of antibiotic-

resistant strains has weakened the effectiveness of these four antibiotics. By using **4-F361** and commonly used antibiotics synergistically, one may be able to find a new direction to treat antibiotic-resistant bacteria.

## Appendix I: High resolution mass spectra of compounds

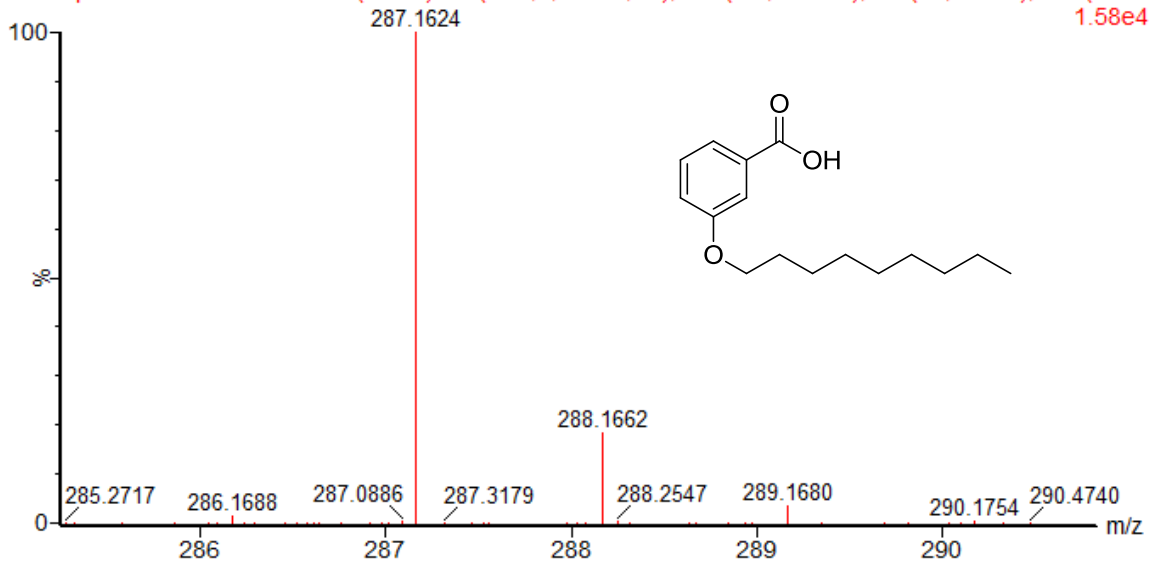
---



I-1 High resolution mass spectrum of **1-F300**

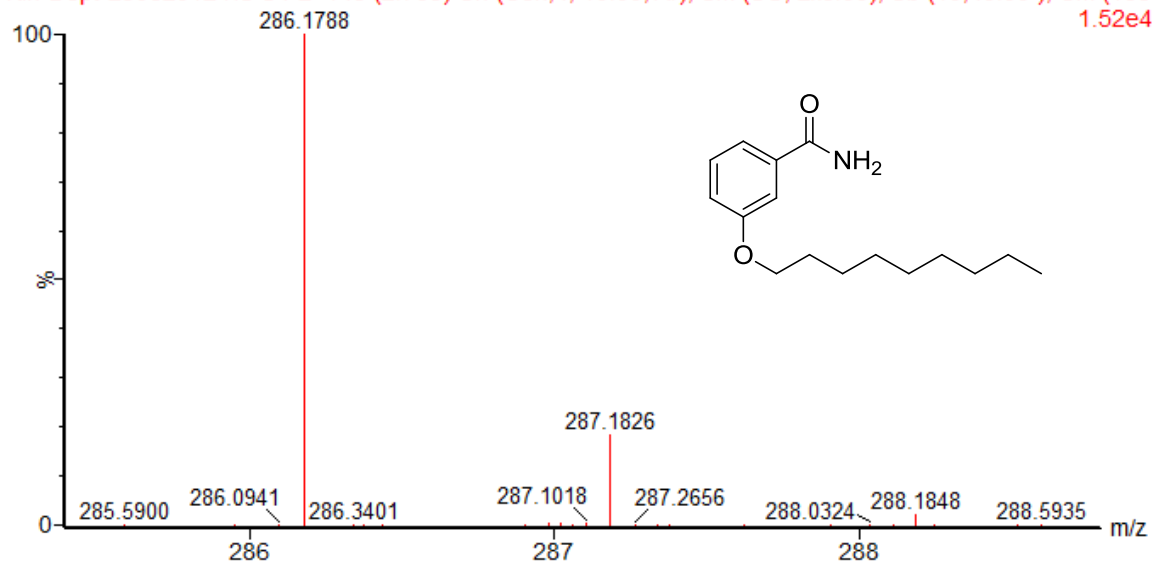


Kin-Dept-29062012 HS S2-2 88 (1.663) Cn (Cen,4, 10.00, Ar); Sm (SG, 2x3.00); Sb (10,40.00 ); Cm (81:9E  
1.58e4



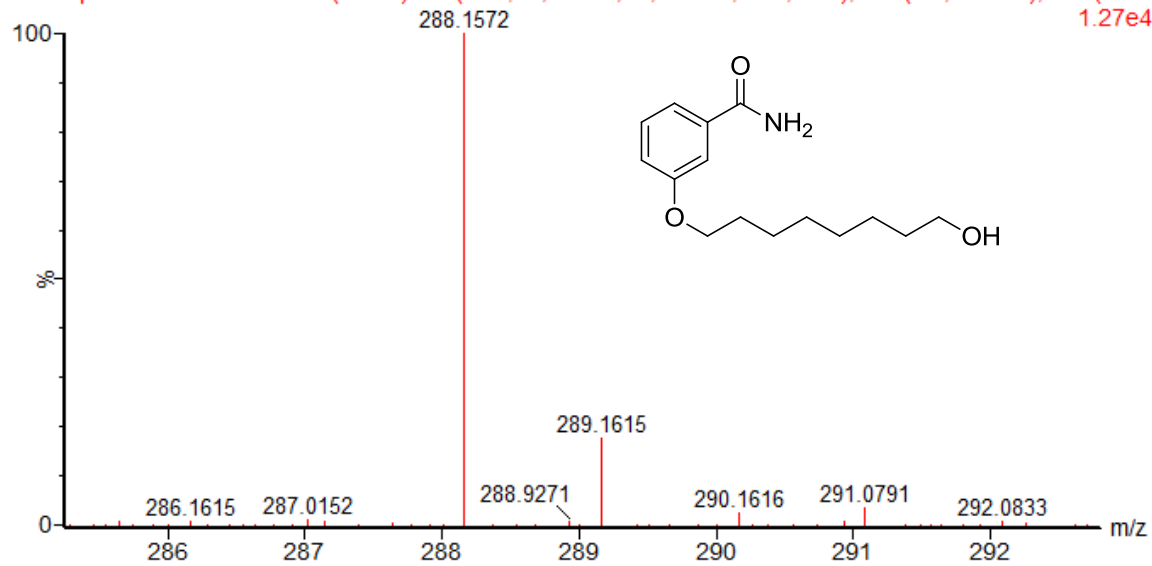
I-2 High resolution mass spectrum of **1-F301**

Kin-Dept-29062012 HS S4-2 145 (2.735) Cn (Cen,4, 10.00, Ar); Sm (SG, 2x3.00); Sb (10,40.00 ); Cm (136  
1.52e4



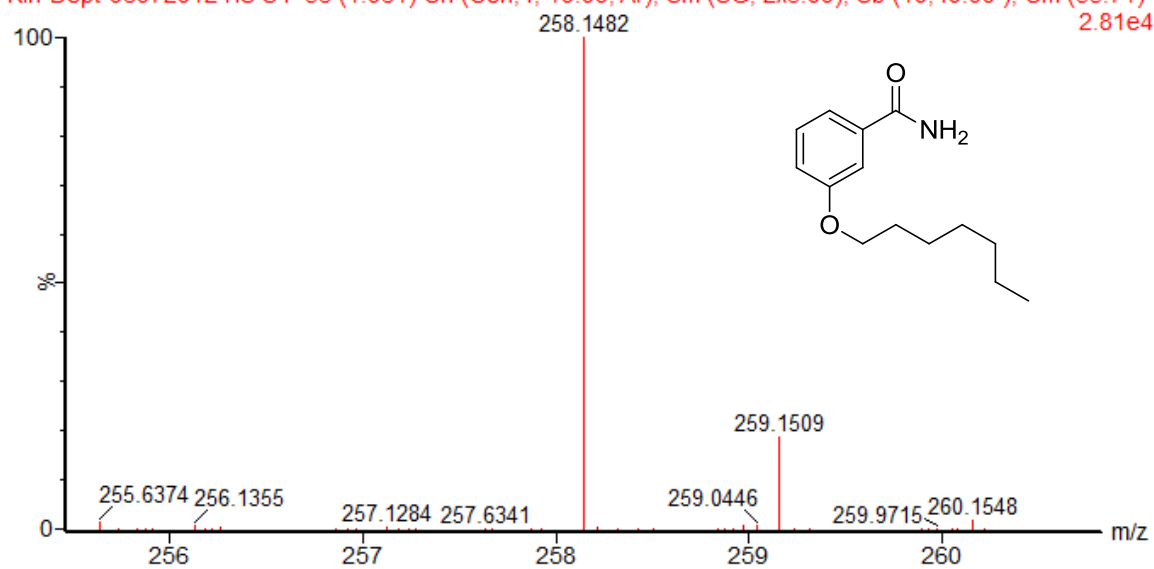
I-3 High resolution mass spectrum of compound **1-F302**

Kin-Dept-29062012 HS S6 38 (0.722) AM (Cen,10, 80.00, Ar,7000.0,0.00,1.00); Sm (Mn, 2x3.00); Cm (37:4; 1.27e4



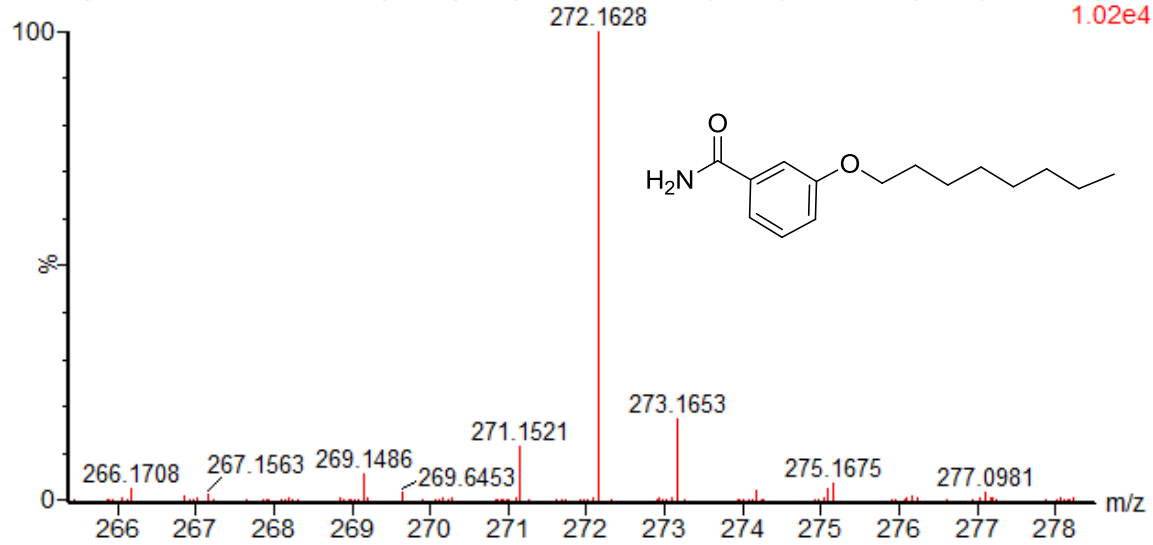
I-4 High resolution mass spectrum of compound **1-F304**

Kin-Dept-06072012 HS S4 56 (1.061) Cn (Cen,4, 10.00, Ar); Sm (SG, 2x3.00); Sb (10,40.00 ); Cm (55:71)  
2.81e4



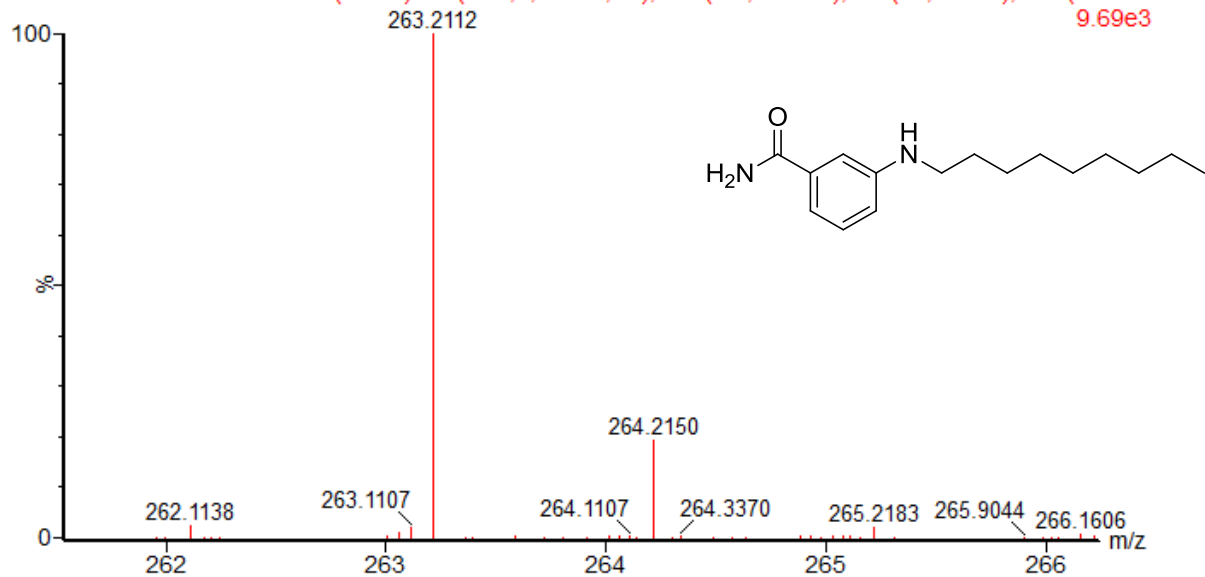
I-5 High resolution mass spectrum of compound **1-F313**

Kin-Dept-18072012 HS S13 85 (1.606) Cn (Cen,4, 10.00, Ar); Sm (SG, 2x3.00); Sb (10,40.00 ); Crr 1.02e4

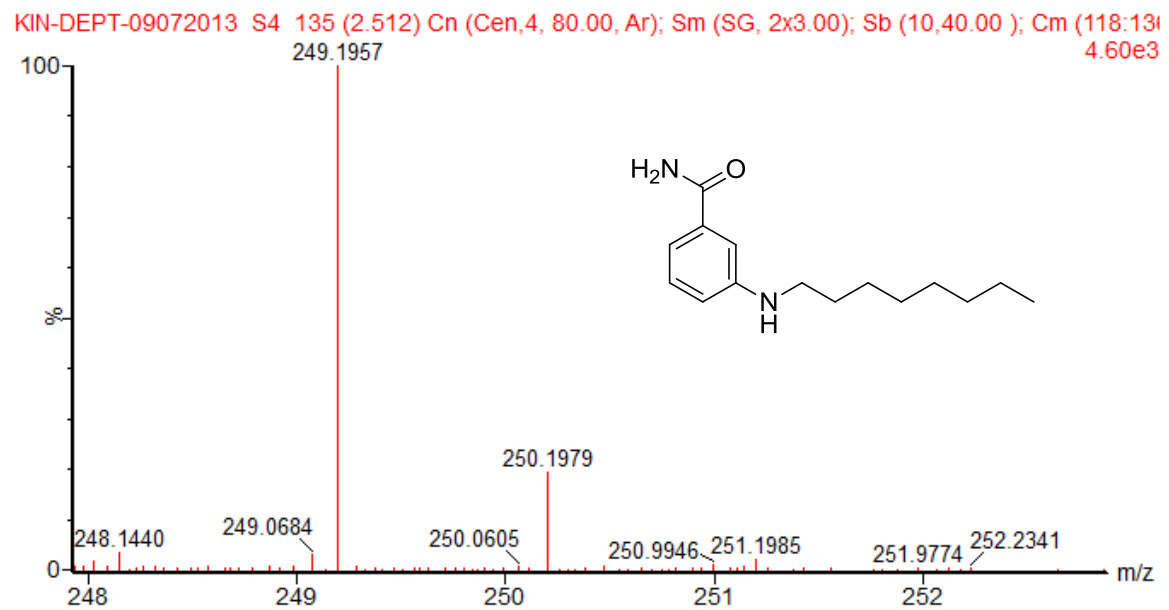


I-6 High resolution mass spectrum of compound **1-F320**

KIN-DEPT-09072013 S5 186 (3.458) Cn (Cen,4, 80.00, Ar); Sm (SG, 2x3.00); Sb (10,40.00 ); Cm (186:20  
9.69e3

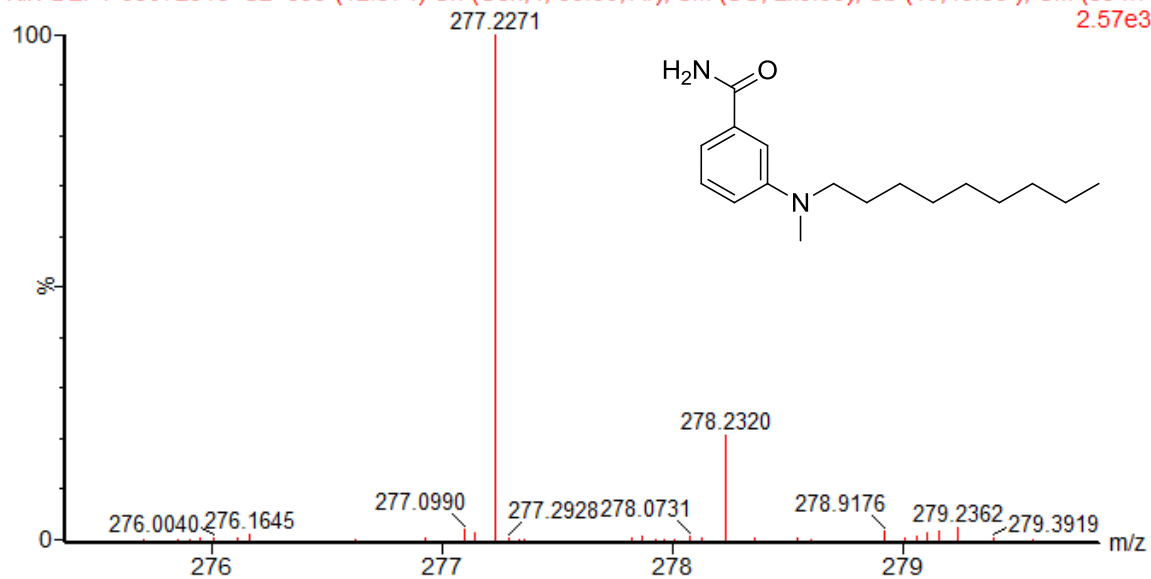


I-7 High resolution mass spectrum of compound **2-F411**



I-8 High resolution mass spectrum of compound **2-F412**

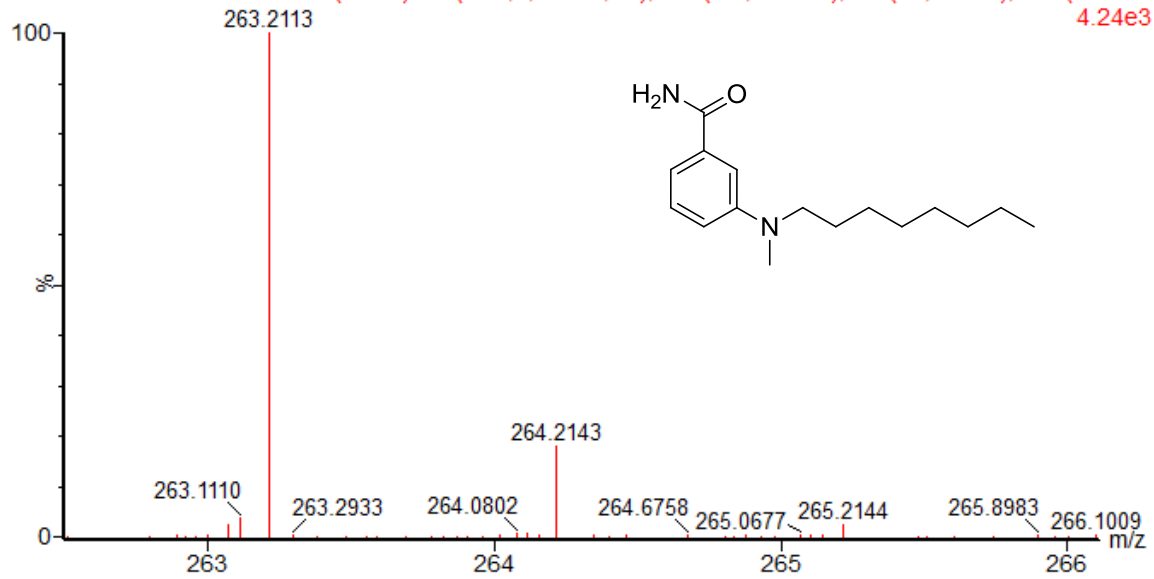
KIN-DEPT-09072013 S2 699 (12.974) Cn (Cen,4, 80.00, Ar); Sm (SG, 2x3.00); Sb (10,40.00 ); Cm (694:7 2.57e3



I-8 High resolution mass spectrum of compound **2-F413**

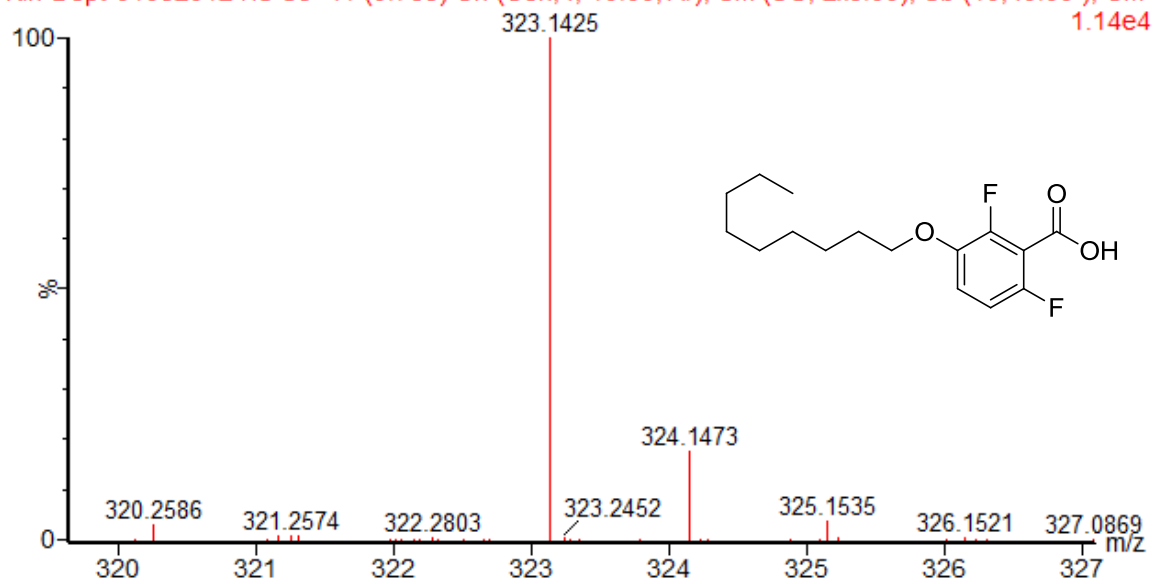


KIN-DEPT-09072013 S3 108 (2.011) Cn (Cen,4, 80.00, Ar); Sm (SG, 2x3.00); Sb (10,40.00 ); Cm (104:116  
4.24e3



I-9 High resolution mass spectrum of compound **2-F414**

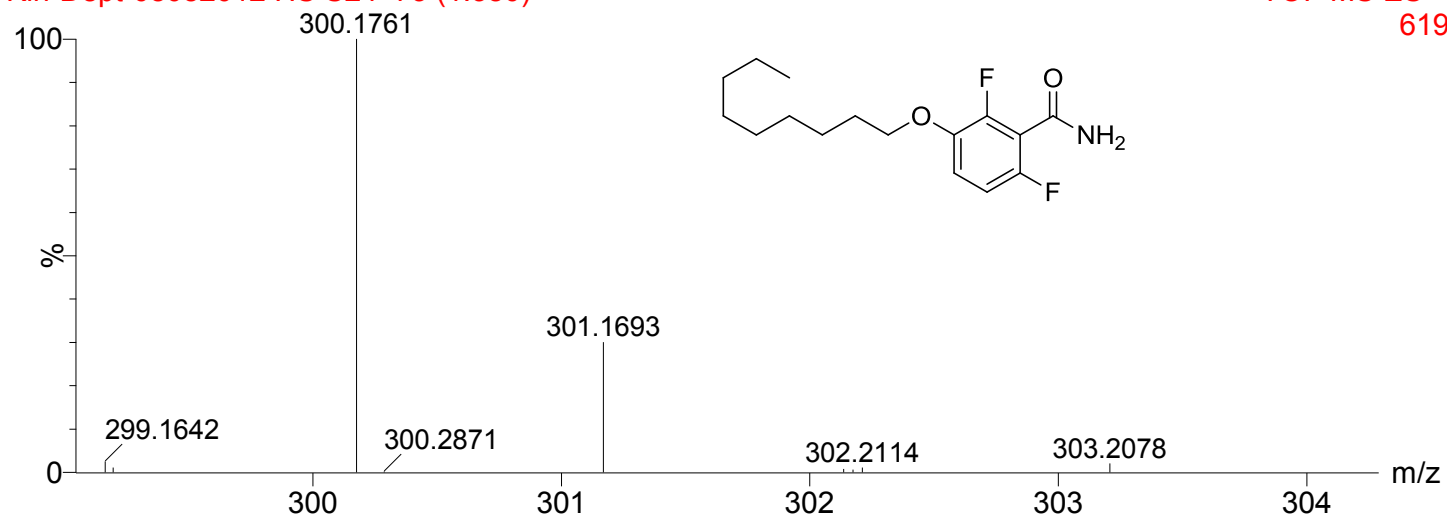
Kin-Dept-01082012 HS S8 41 (0.768) Cn (Cen,4, 10.00, Ar); Sm (SG, 2x3.00); Sb (10,40.00 ); Cm 1.14e4



I-10 High resolution mass spectrum of compound **3-F325**

Kin-Dept-08082012 HS S24 73 (1.380)

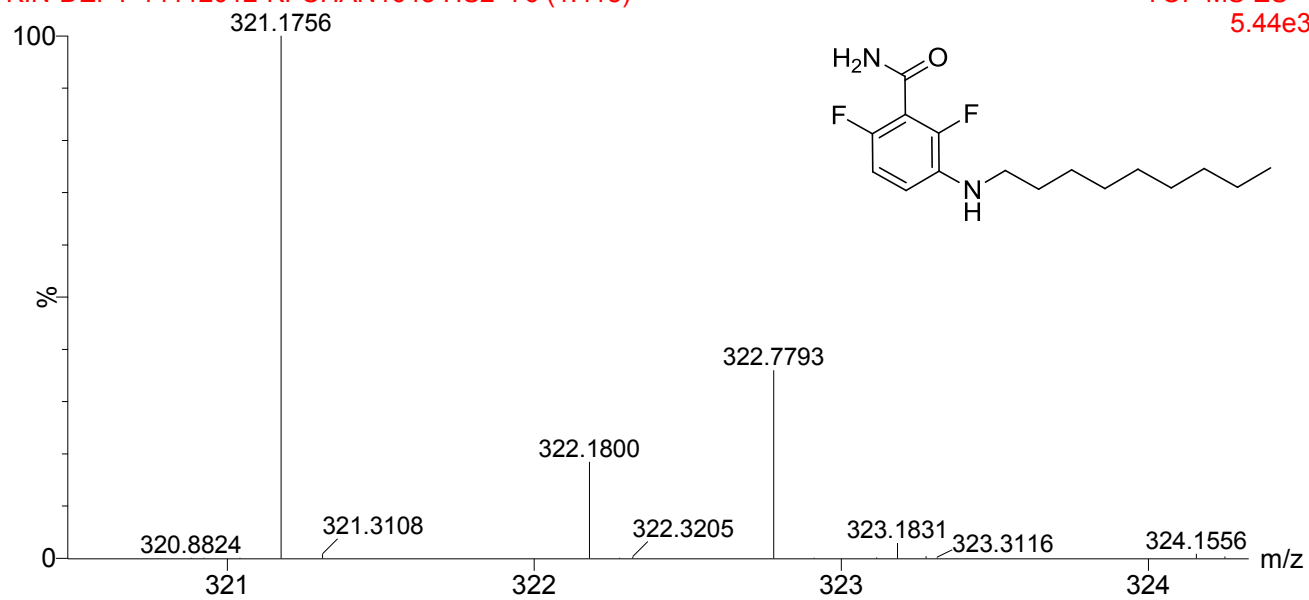
TOF MS ES+  
619



I-11 High resolution mass spectrum of compound **3-F326**

KIN-DEPT-14112012-KFCHAN1648 HS2 76 (1.418)

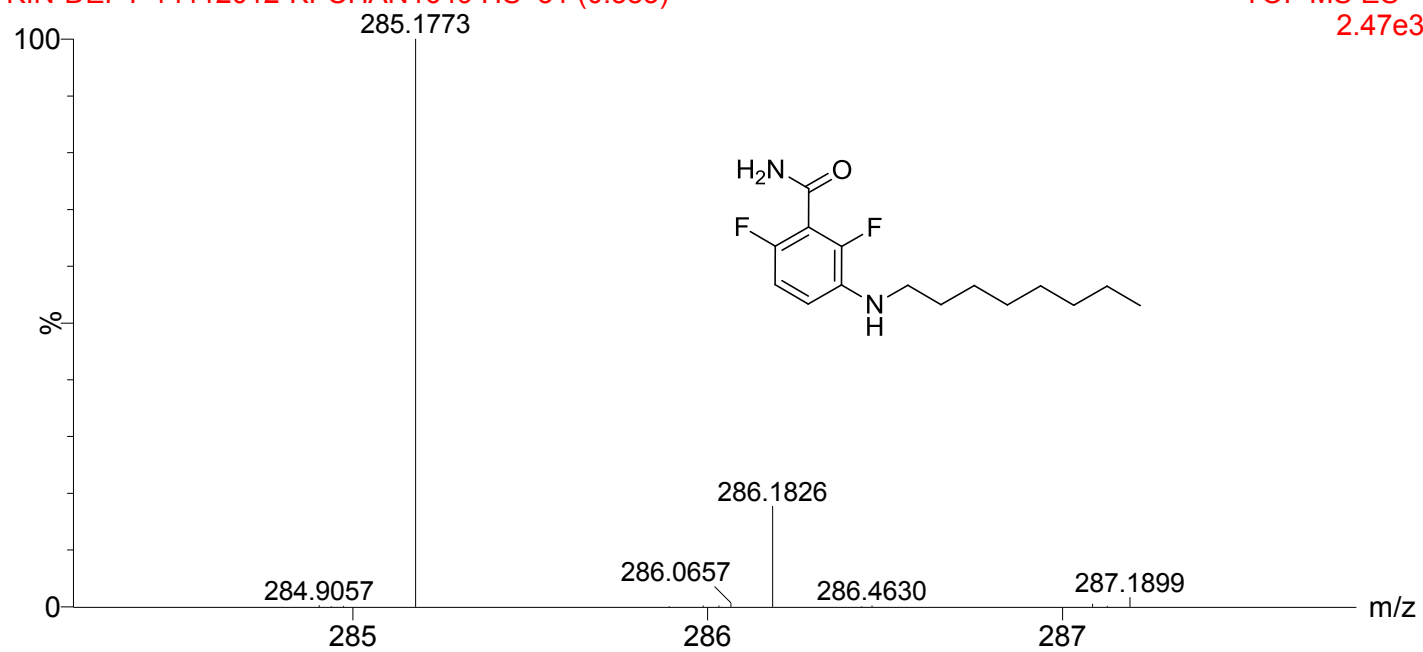
TOF MS ES+  
5.44e3



I-12 High resolution mass spectrum of compound **4-F332**

KIN-DEPT-14112012-KFCHAN1649 HS 31 (0.583)

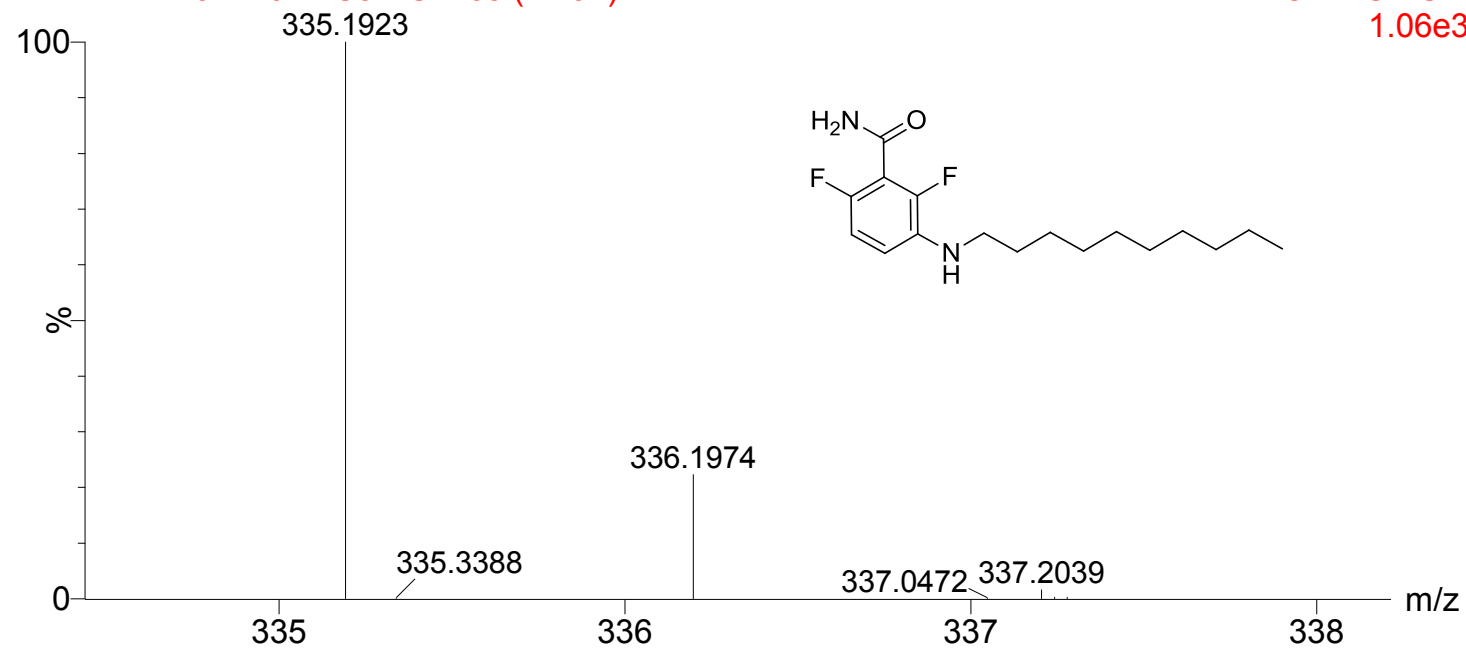
TOF MS ES+  
2.47e3



I-13 High resolution mass spectrum of compound **4-F333**

KIN-DEPT-23112012-S5 HS2 63 (1.192)

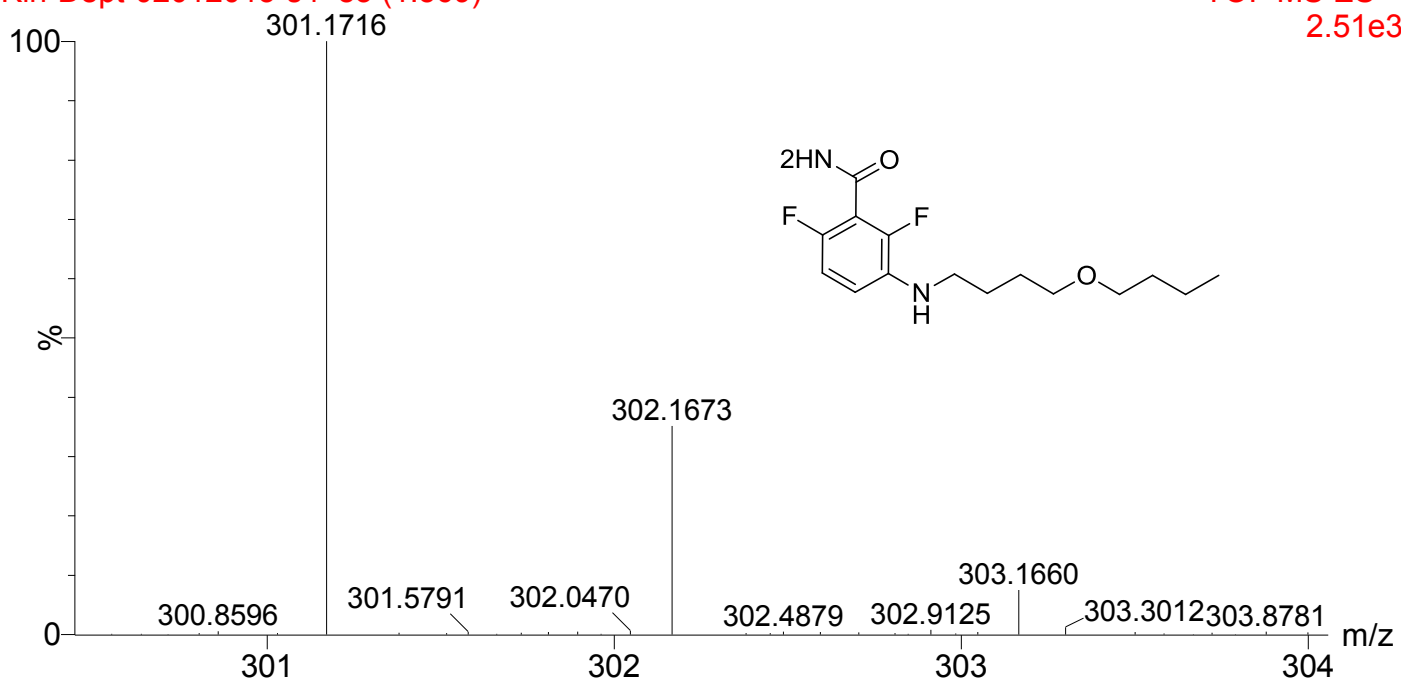
TOF MS ES+  
1.06e3



I-14 High resolution mass spectrum of compound **4-F334**

Kin-Dept-02012013-s4 83 (1.569)

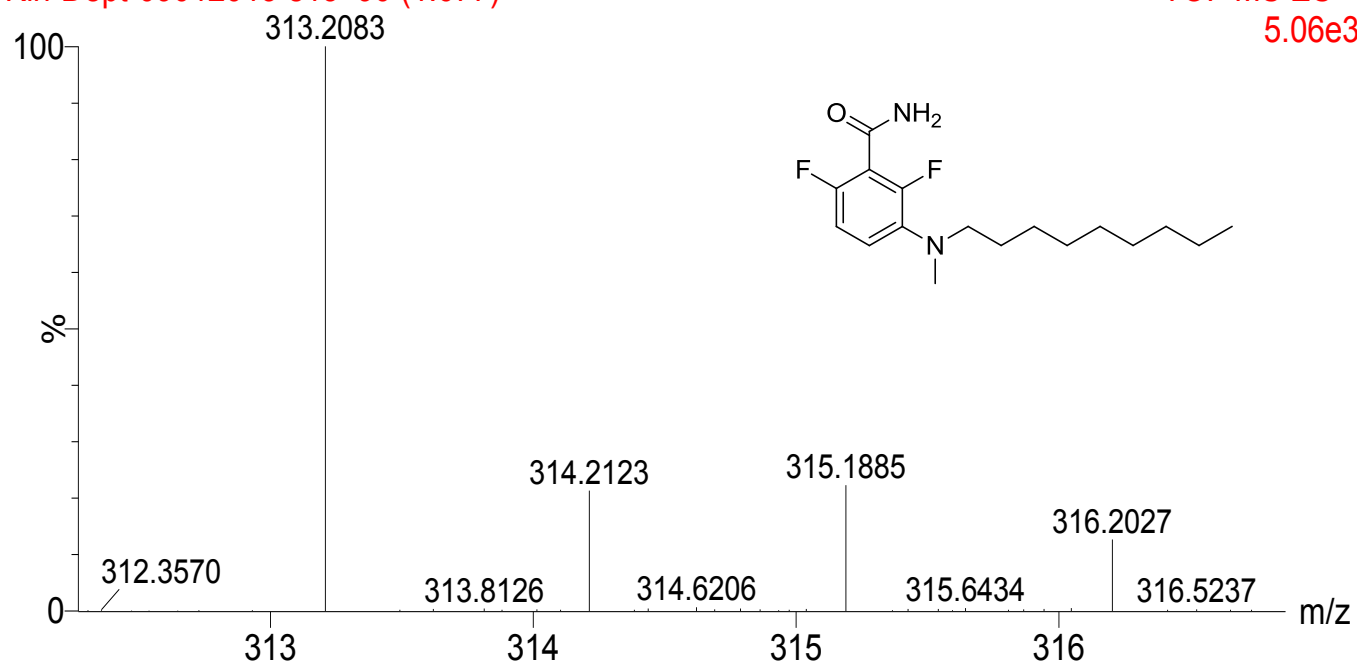
TOF MS ES+  
2.51e3



I-15 High resolution mass spectrum of compound **4-F350**

Kin-Dept-09012013-s13 90 (1.677)

TOF MS ES+  
5.06e3

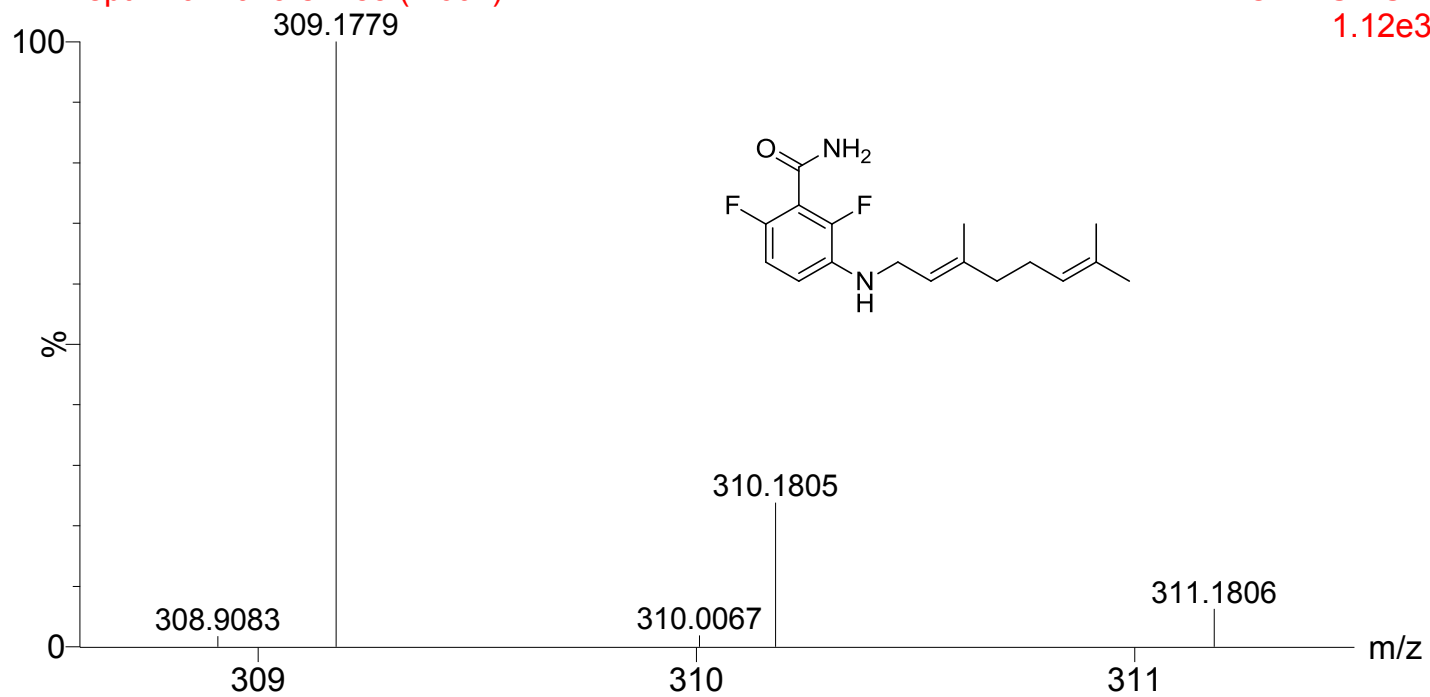


I-16 High resolution mass spectrum of compound **4-F361**



Kin-Dept-24012013-s2 85 (1.607)

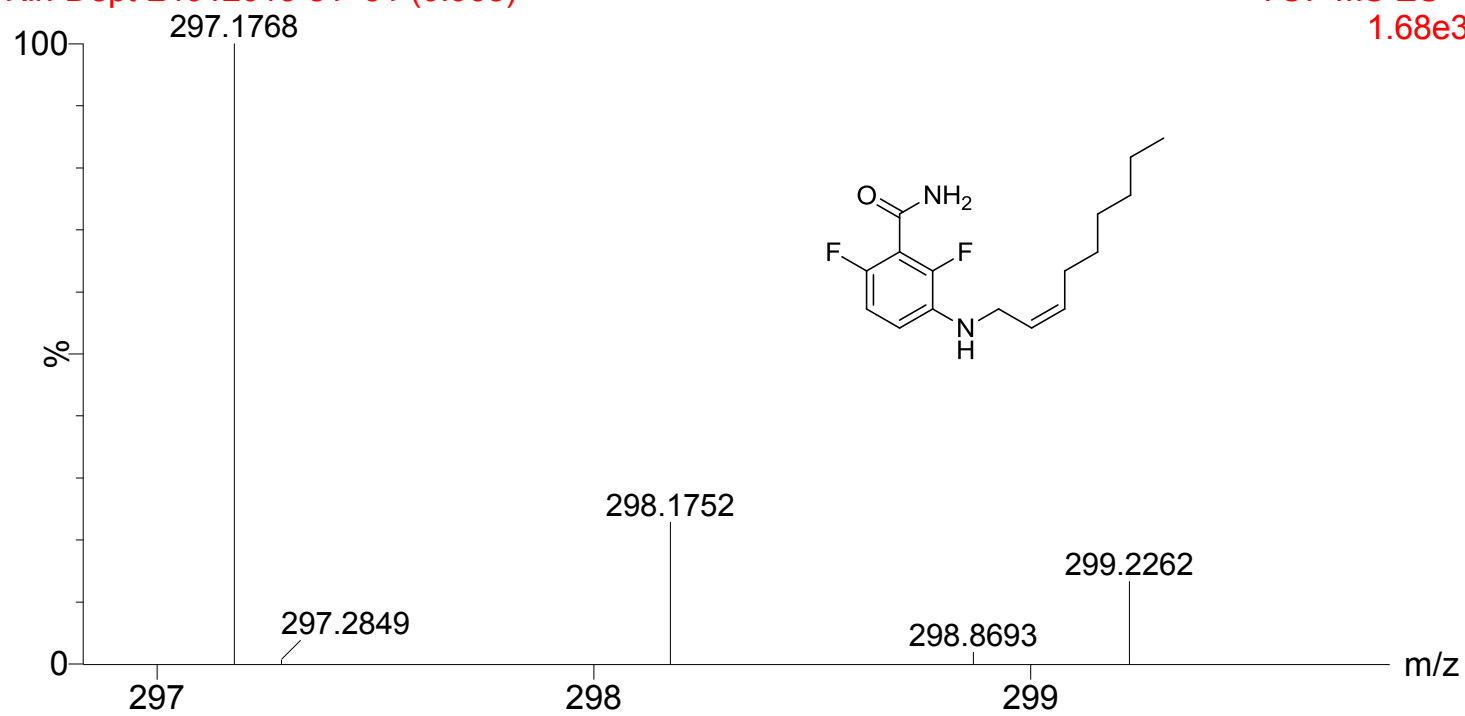
TOF MS ES+  
1.12e3



I-17 High resolution mass spectrum of compound **4-F369**

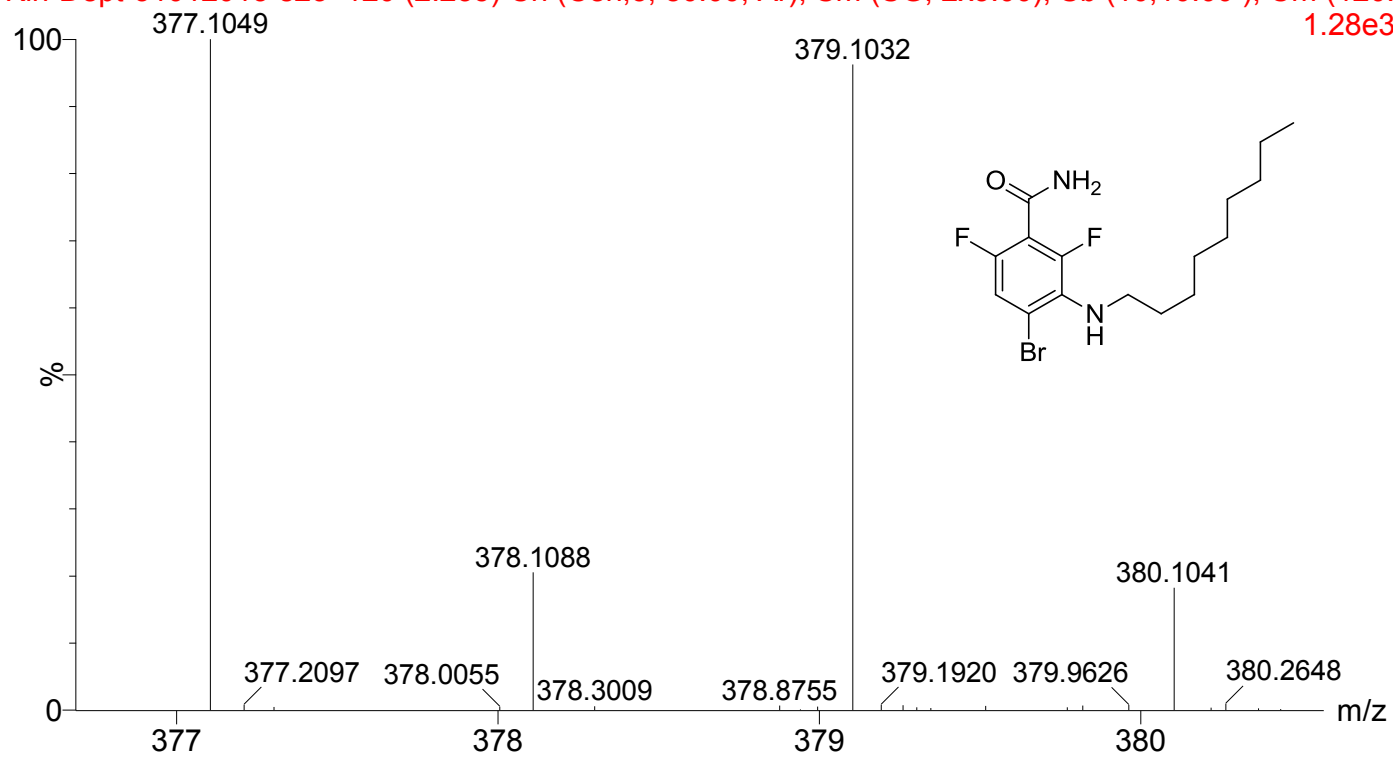
Kin-Dept-24012013-s1 51 (0.968)

TOF MS ES+  
1.68e3



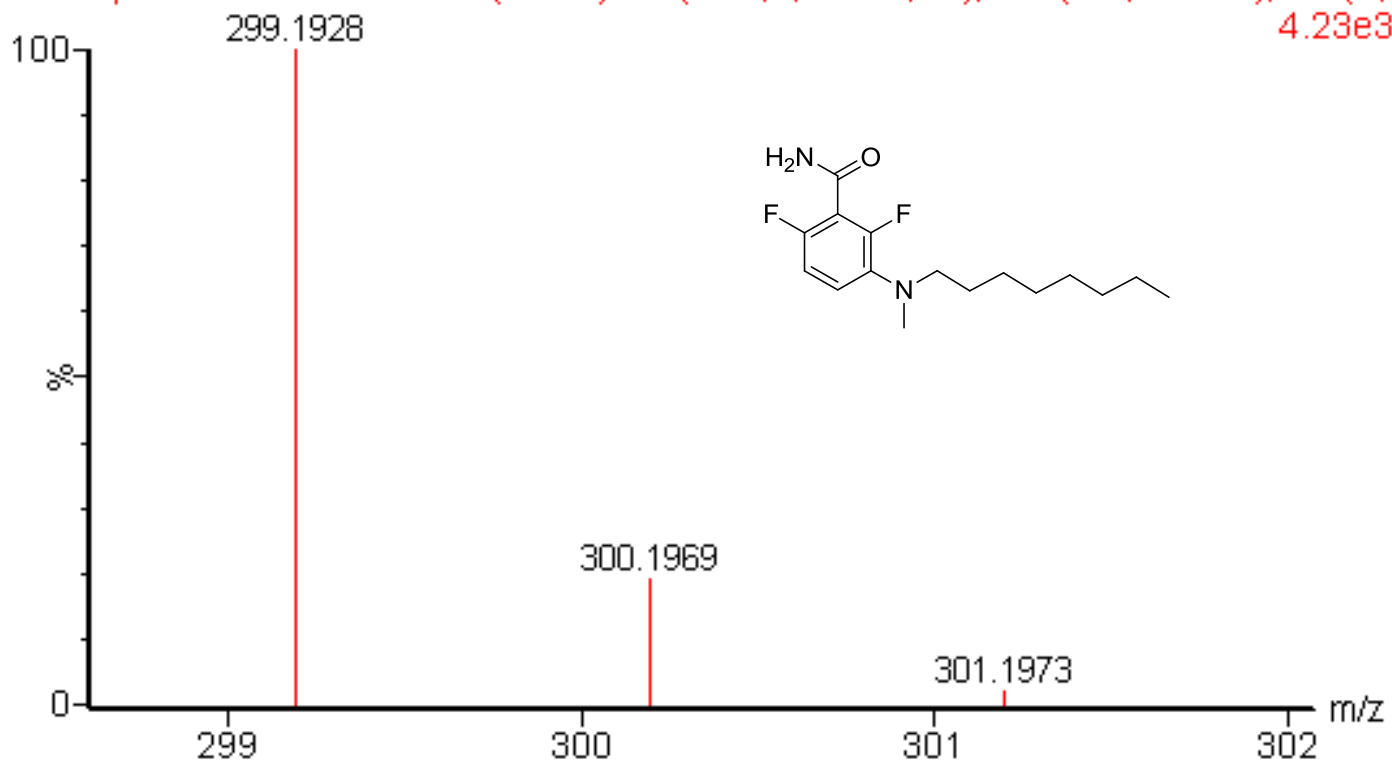
I-18 High resolution mass spectrum of compound **4-F370**

Kin-Dept-31012013-s23 120 (2.235) Cn (Cen,5, 80.00, Ar); Sm (SG, 2x3.00); Sb (10,10.00 ); Cm (120: 1.28e3



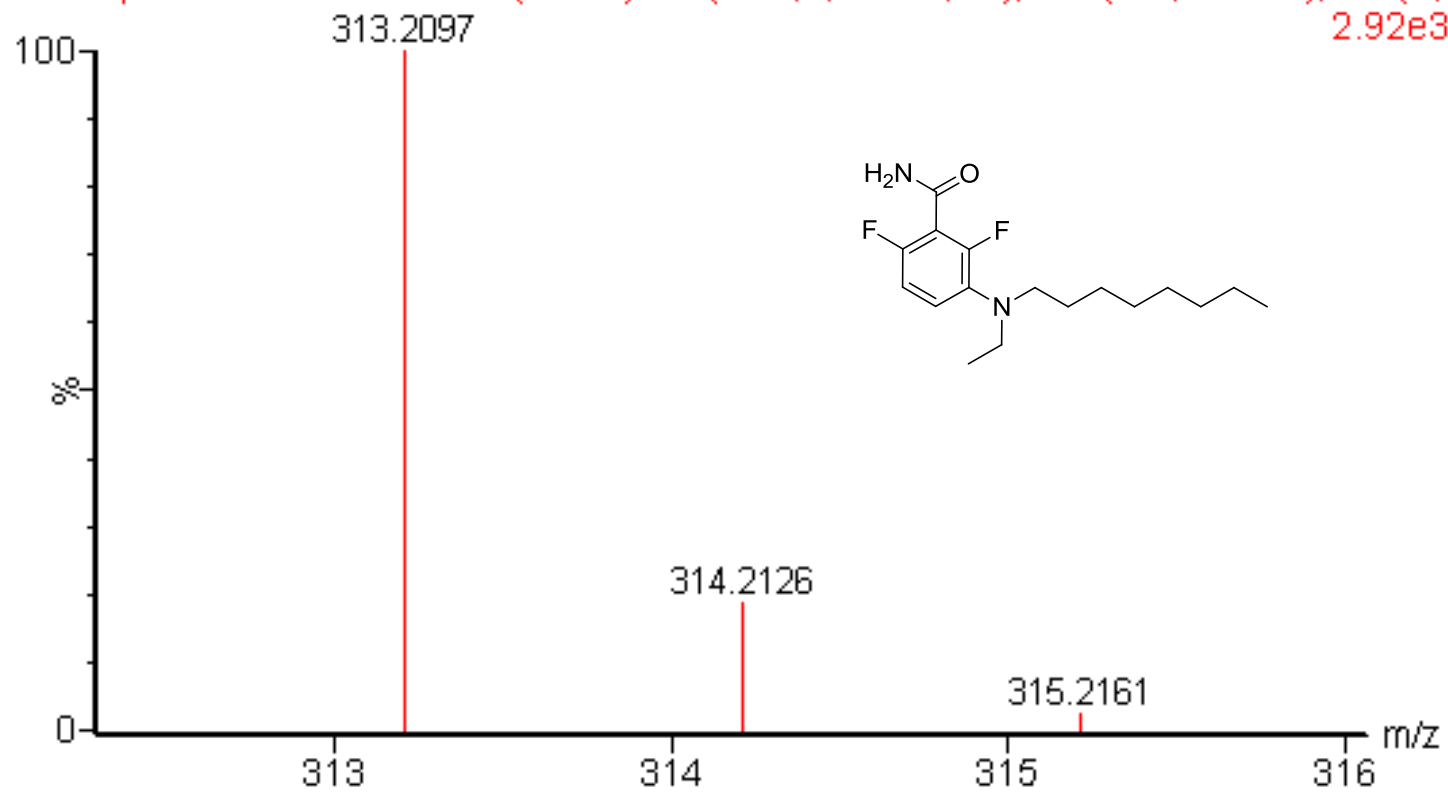
I-19 High resolution of mass spectrum of compound **4-F371**

Kin-Dept-02072013-s11 111 (2.068) Cn (Cen,4, 80.00, Ar); Sm (SG, 2x3.00); Sb (5, 4.23e3)



I-20 High resolution of mass spectrum of compound **4-F409**

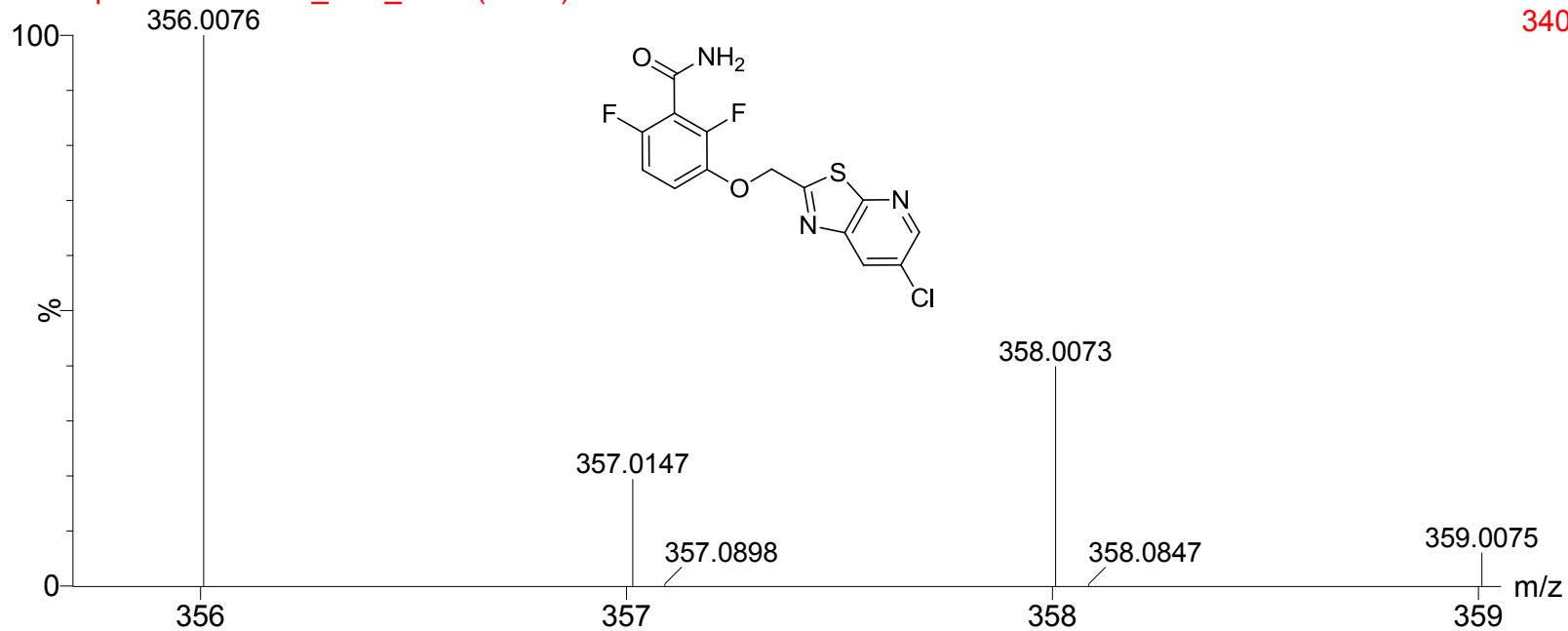
Kin-Dept-02072013-s10 113 (2.105) Cn (Cen,4, 80.00, Ar); Sm (SG, 2x3.00); Sb (5, 2.92e3)



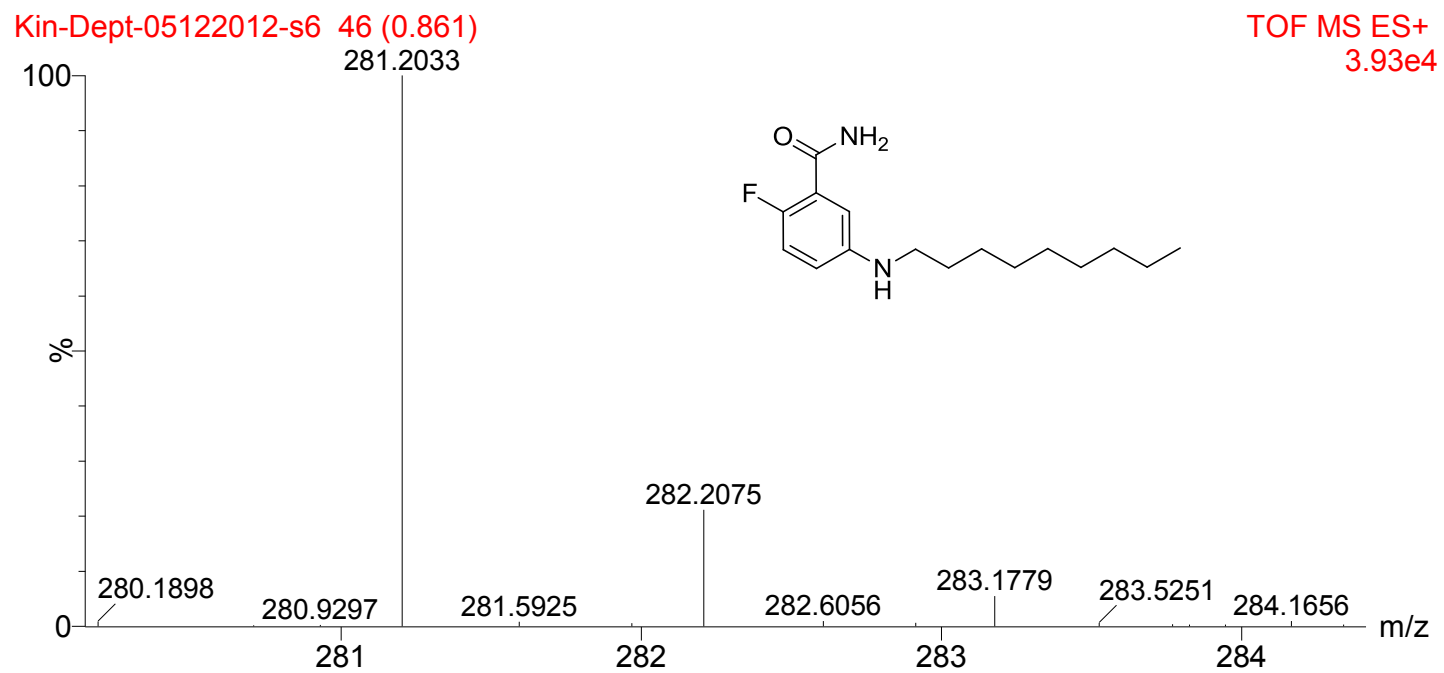
I-21 High resolution of mass spectrum of compound **4-F410**

Kin-Dept-11092012 HS\_2 s6\_2 48 (0.903)

TOF MS ES+  
340



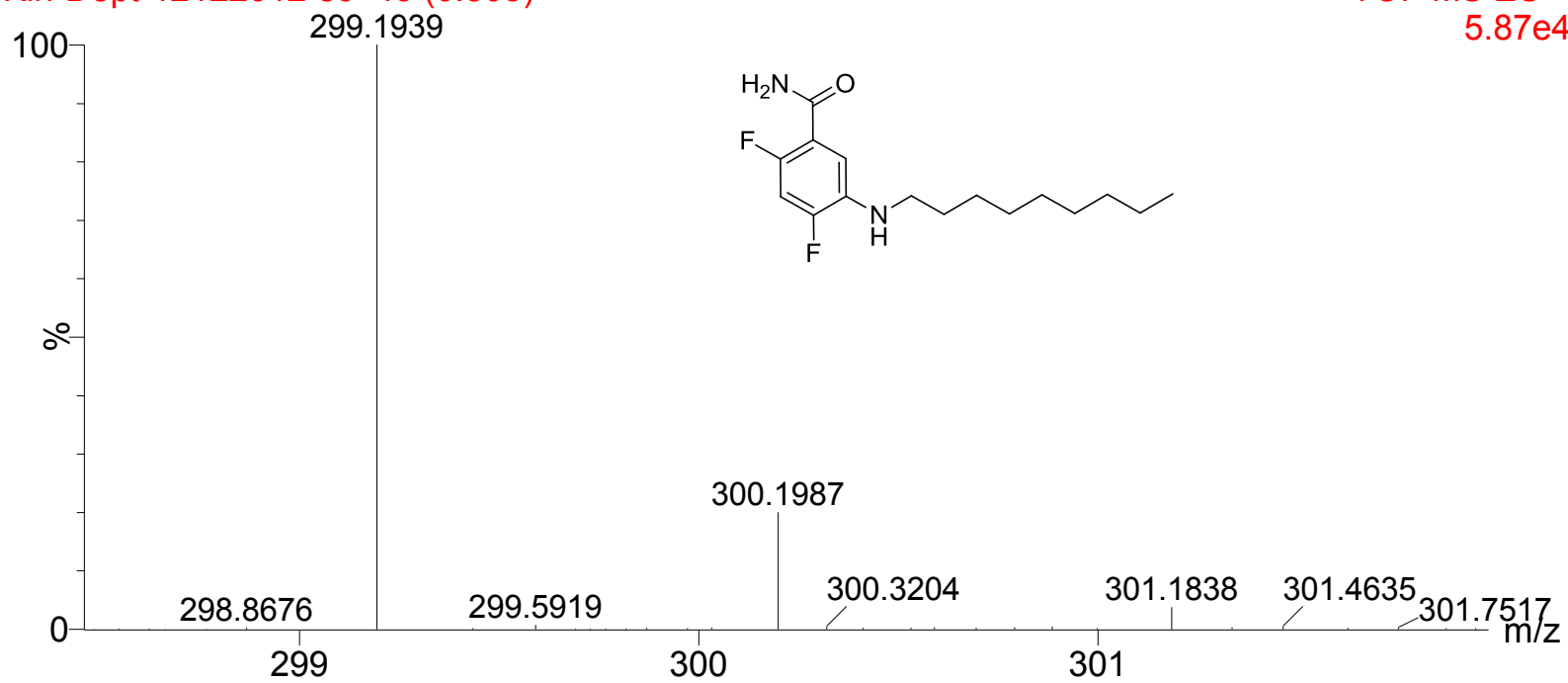
I-22 High resolution of mass spectrum of compound **F327**



I-23 High resolution of mass spectrum of compound **F342**

Kin-Dept-12122012-s3 43 (0.805)

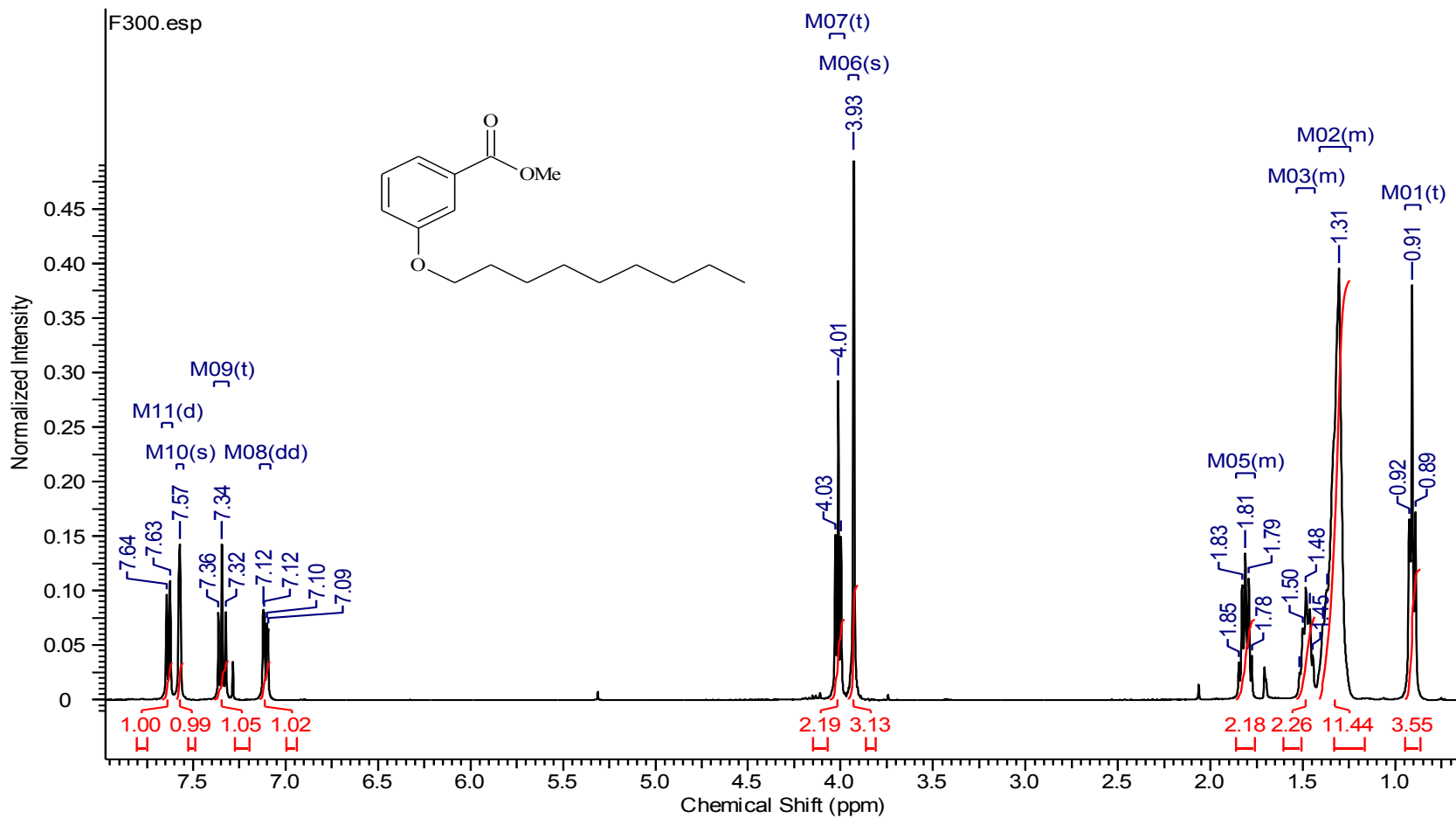
TOF MS ES+  
5.87e4



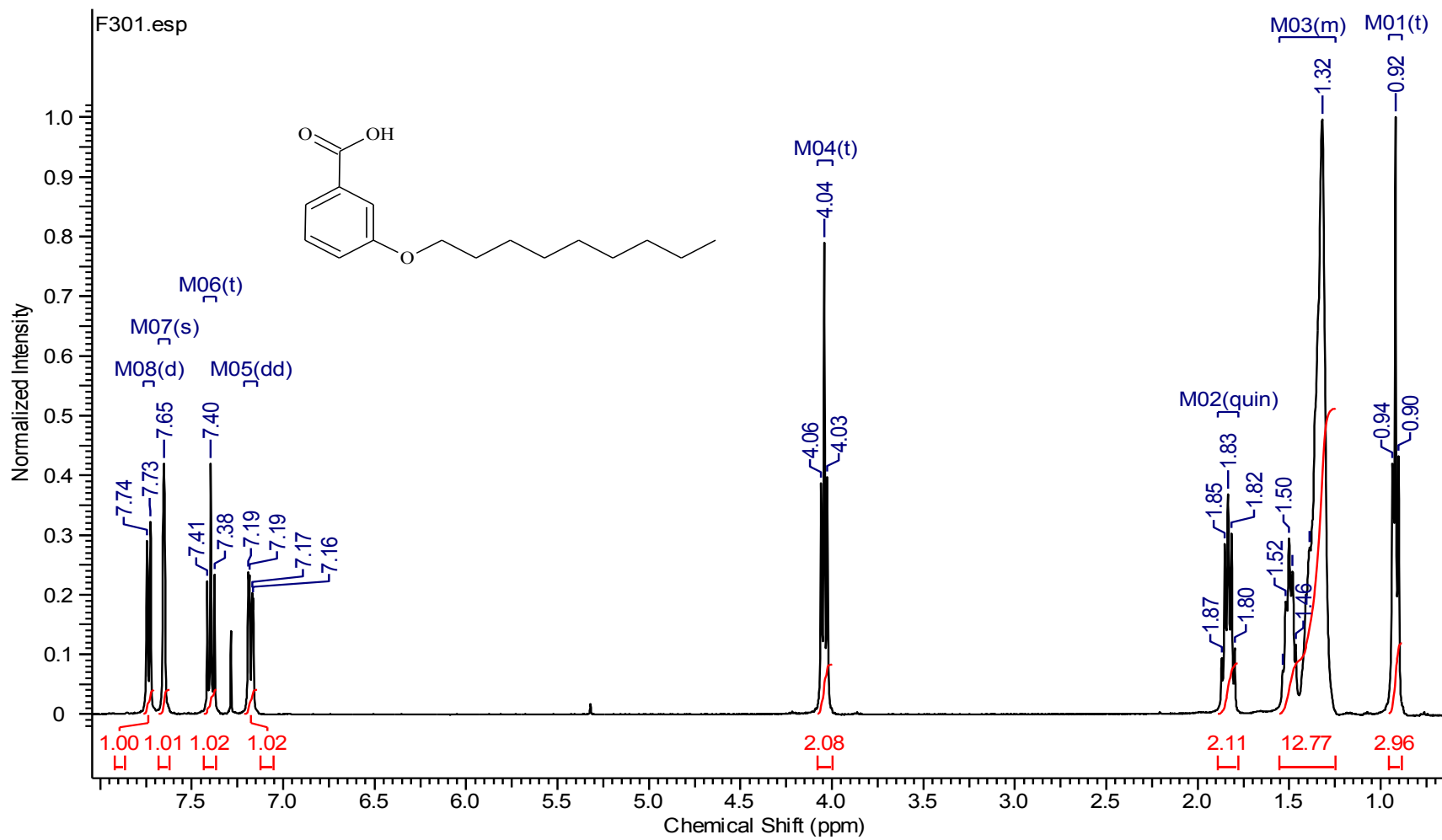
I-24 High resolution of mass spectrum of compound **F345**



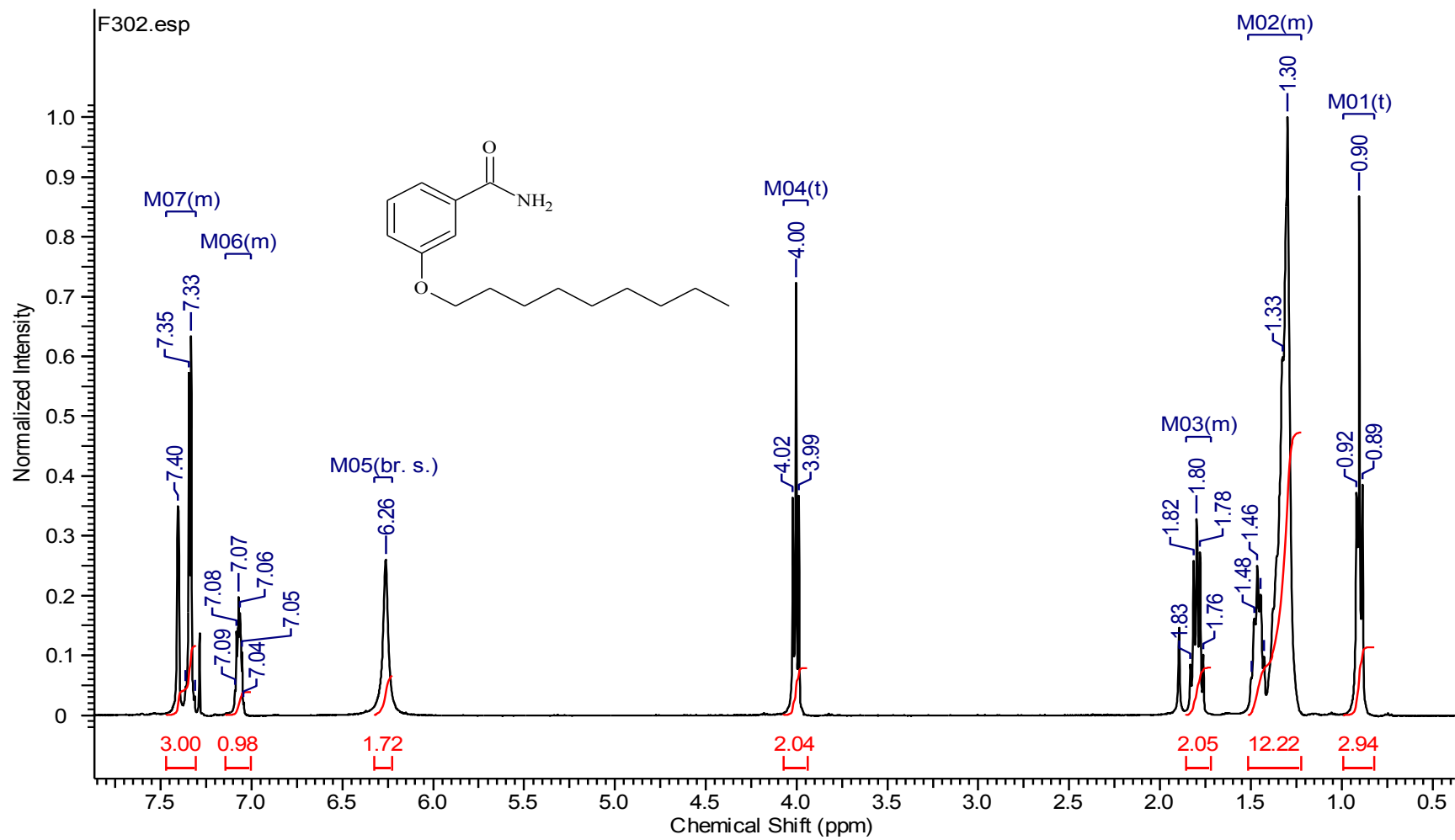
## Appendix II: $^1\text{H}$ NMR spectra of compounds



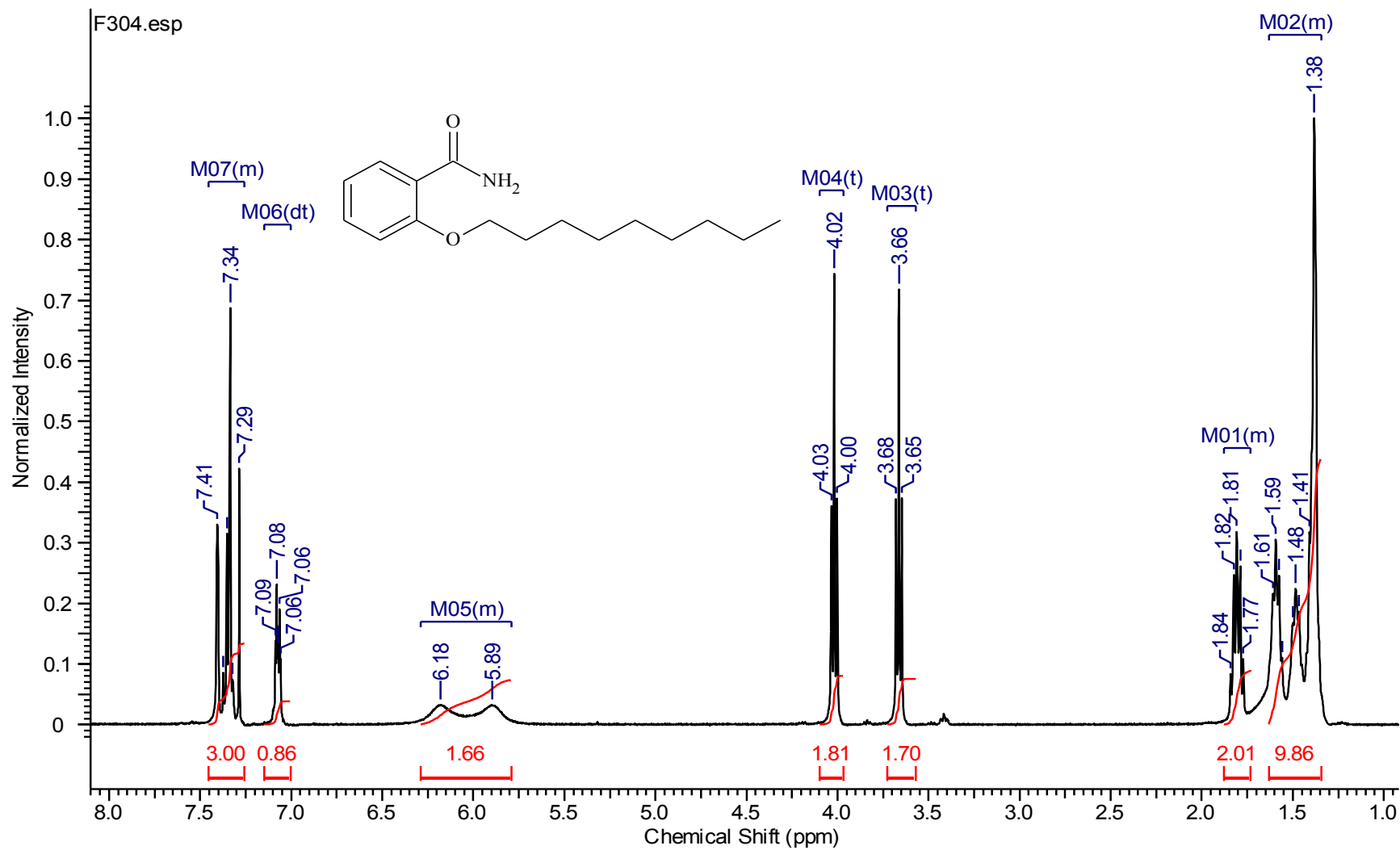
II-1  $^1\text{H}$  NMR spectrum of compound 1-F300



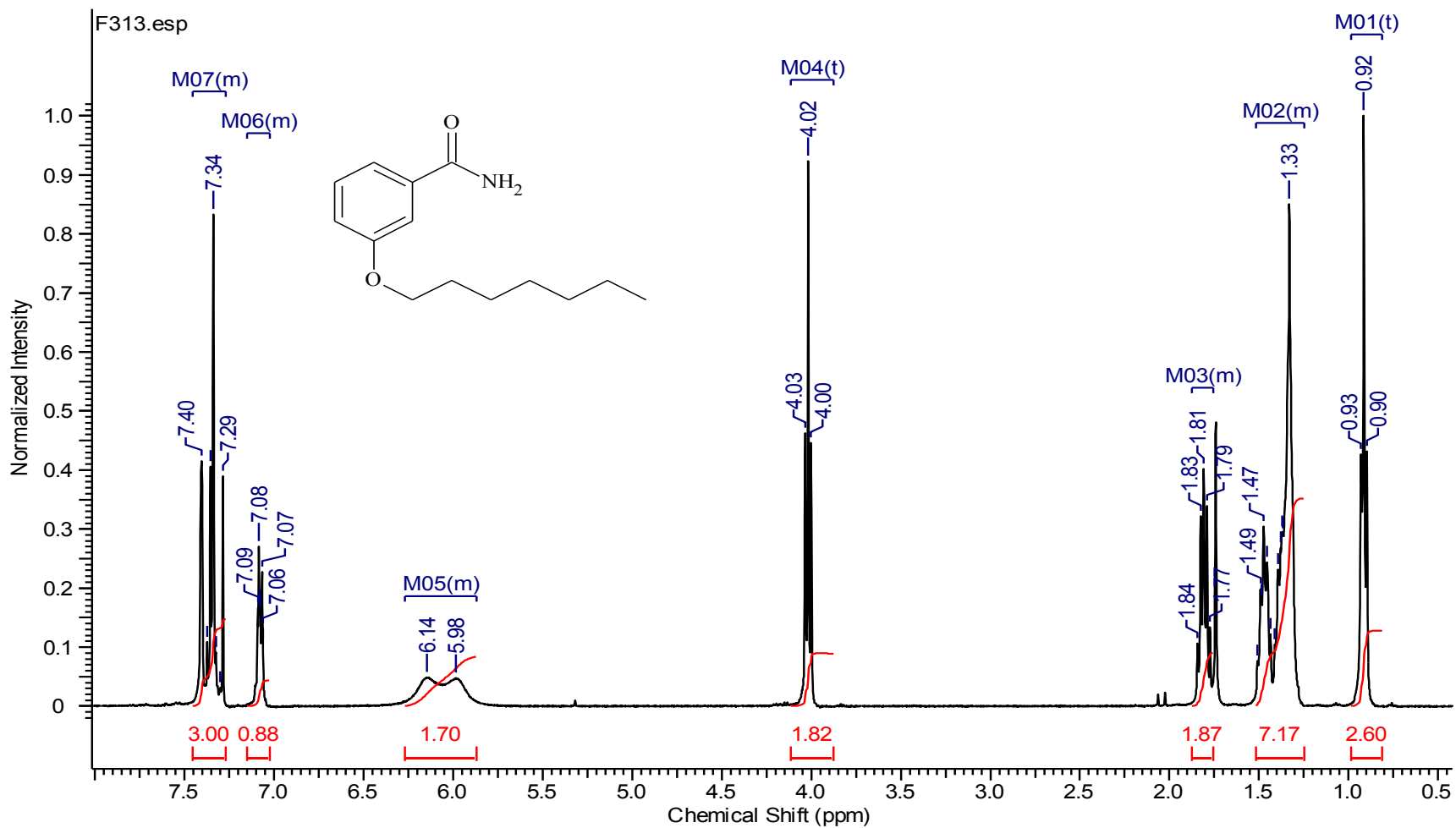
II-2  $^1\text{H}$  NMR spectrum of compound **1-F301**



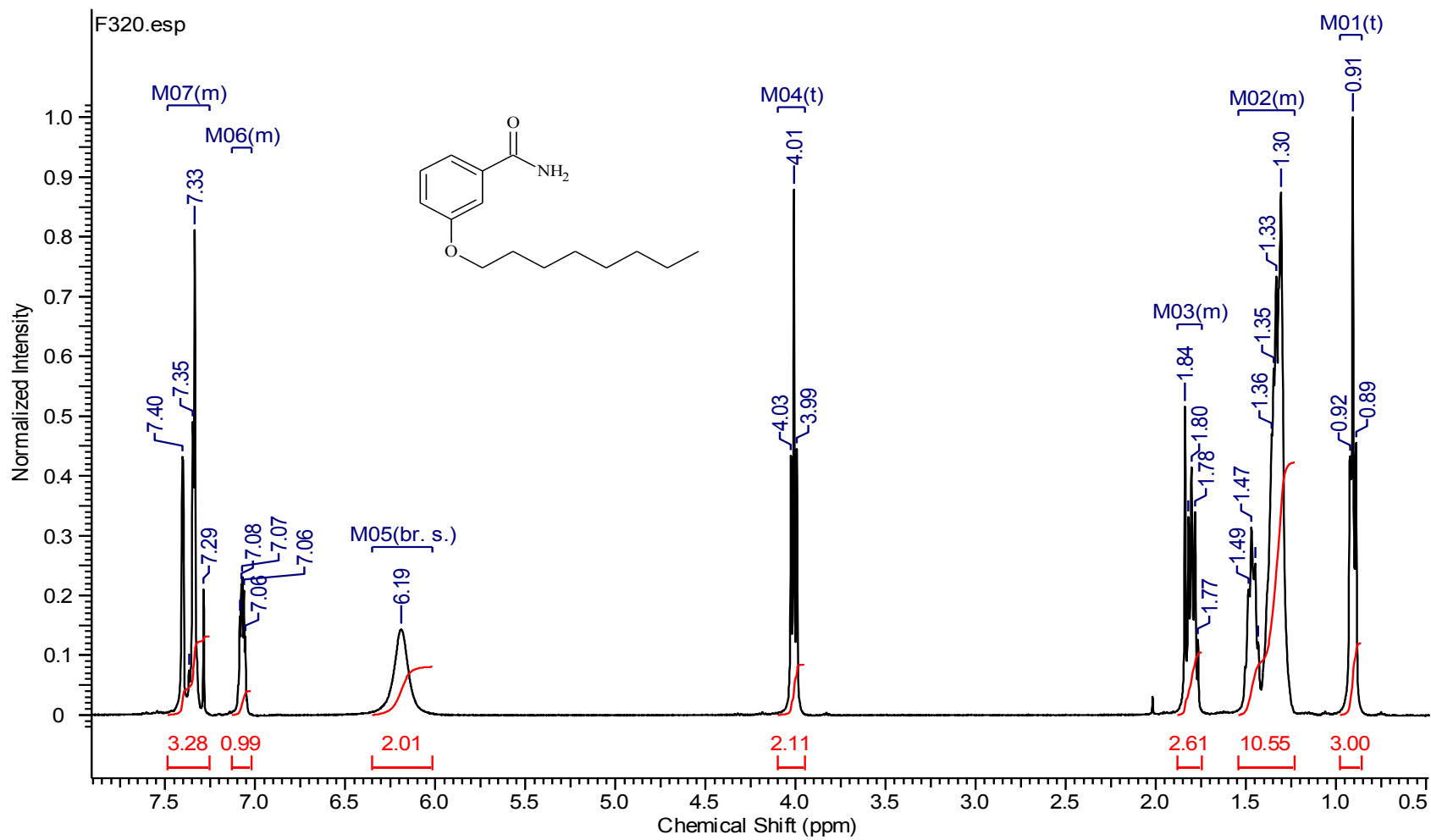
II-3  $^1\text{H}$  NMR spectrum of compound **1-F302**



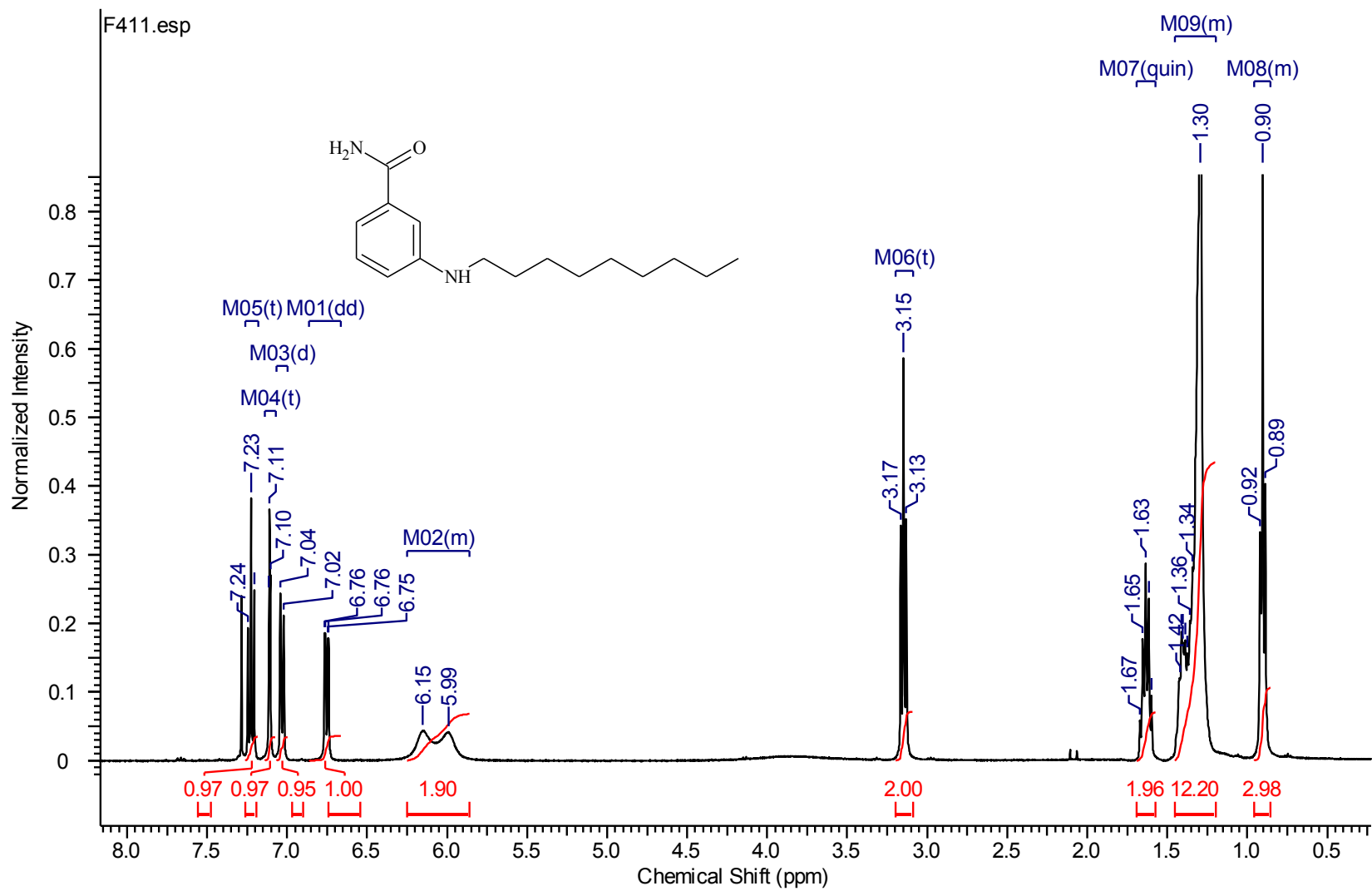
II-4  $^1\text{H}$  NMR spectrum of compound 1-F304



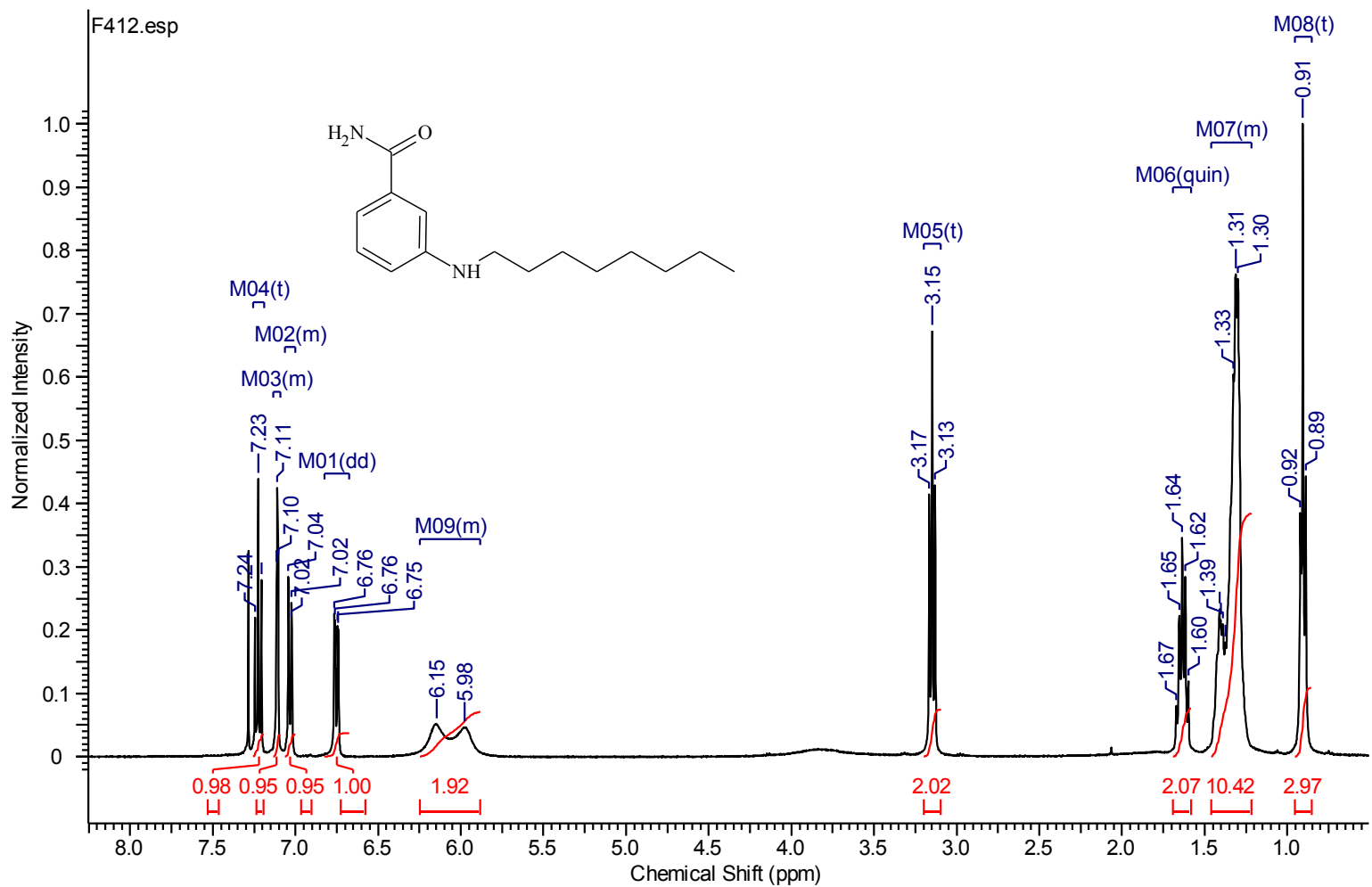
II-5  $^1\text{H}$  NMR spectrum of compound **1-F313**



II-6  $^1\text{H}$  NMR spectrum of compound 1-F320

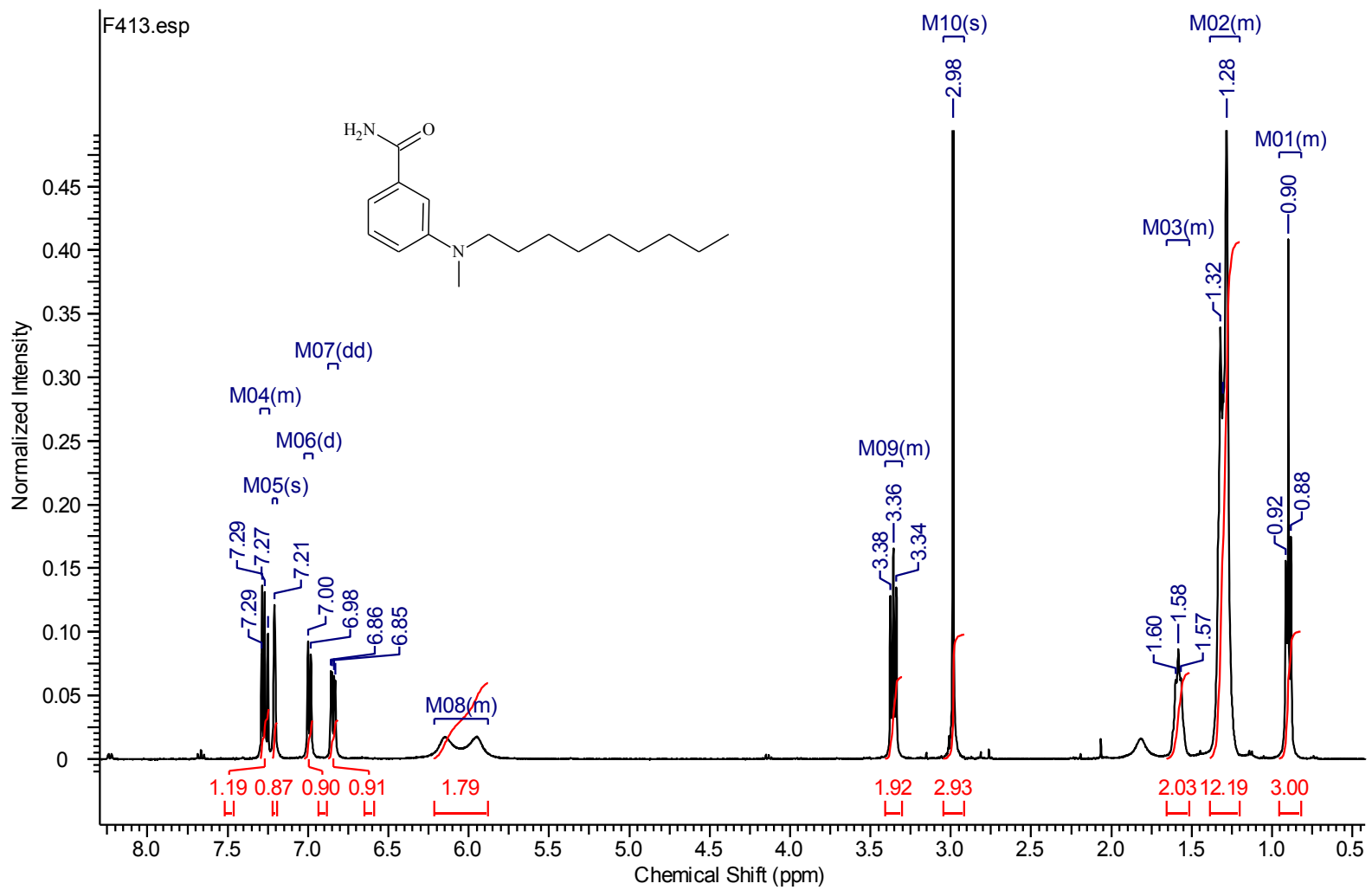


II-7  $^1\text{H}$  NMR spectrum of compound 2-F411

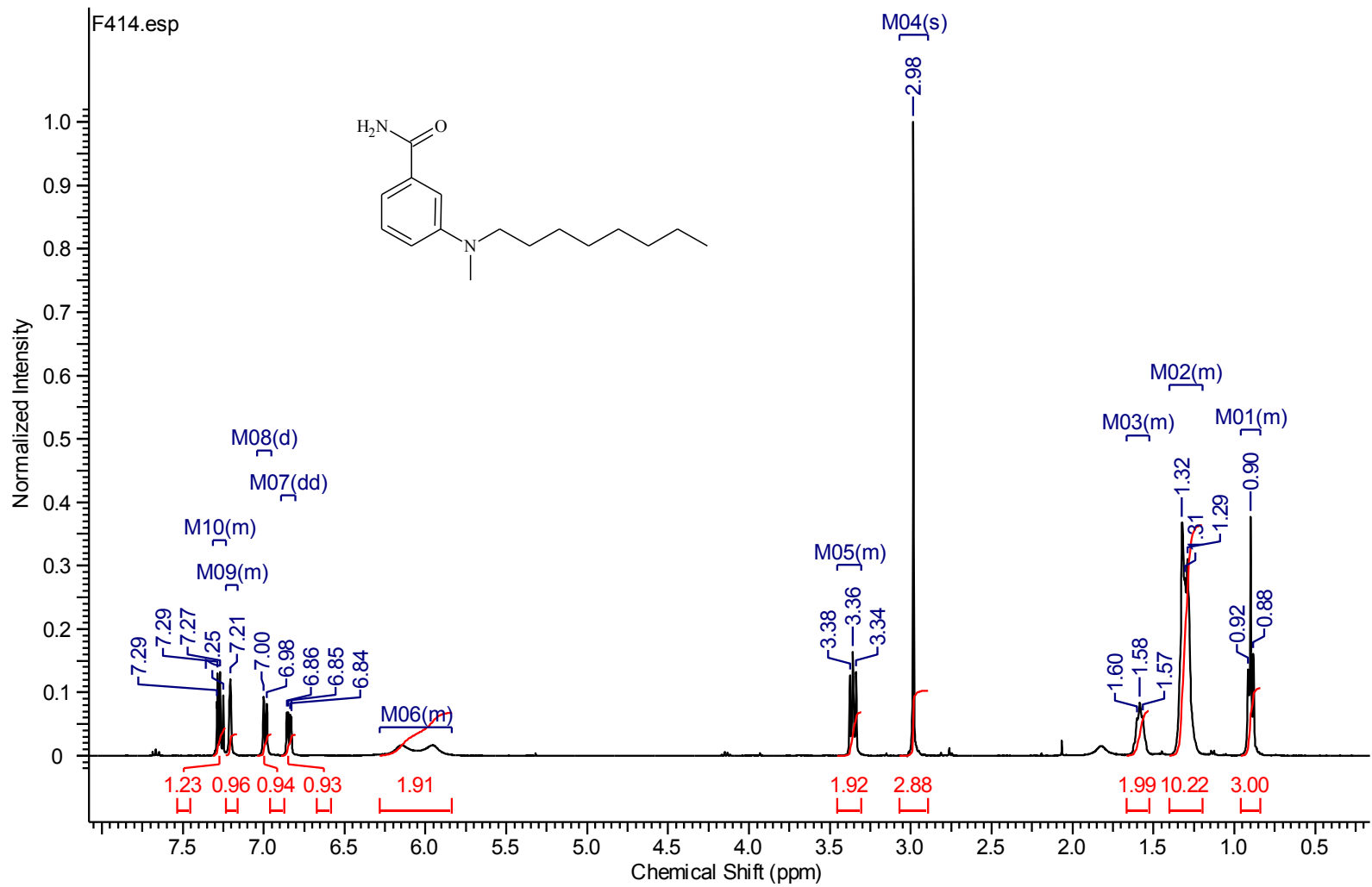


II-8  $^1\text{H}$  NMR spectrum of compound 2-F412

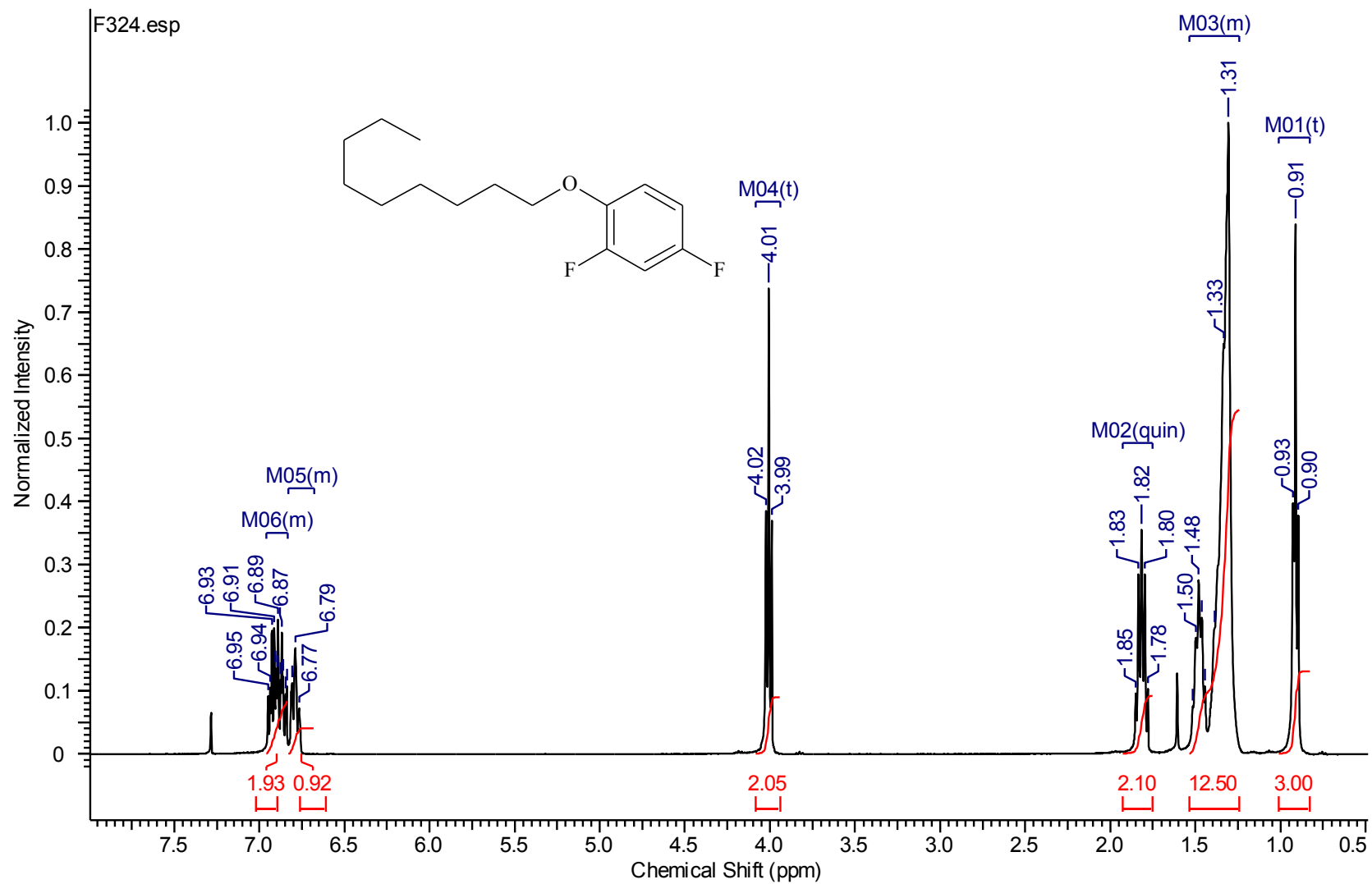




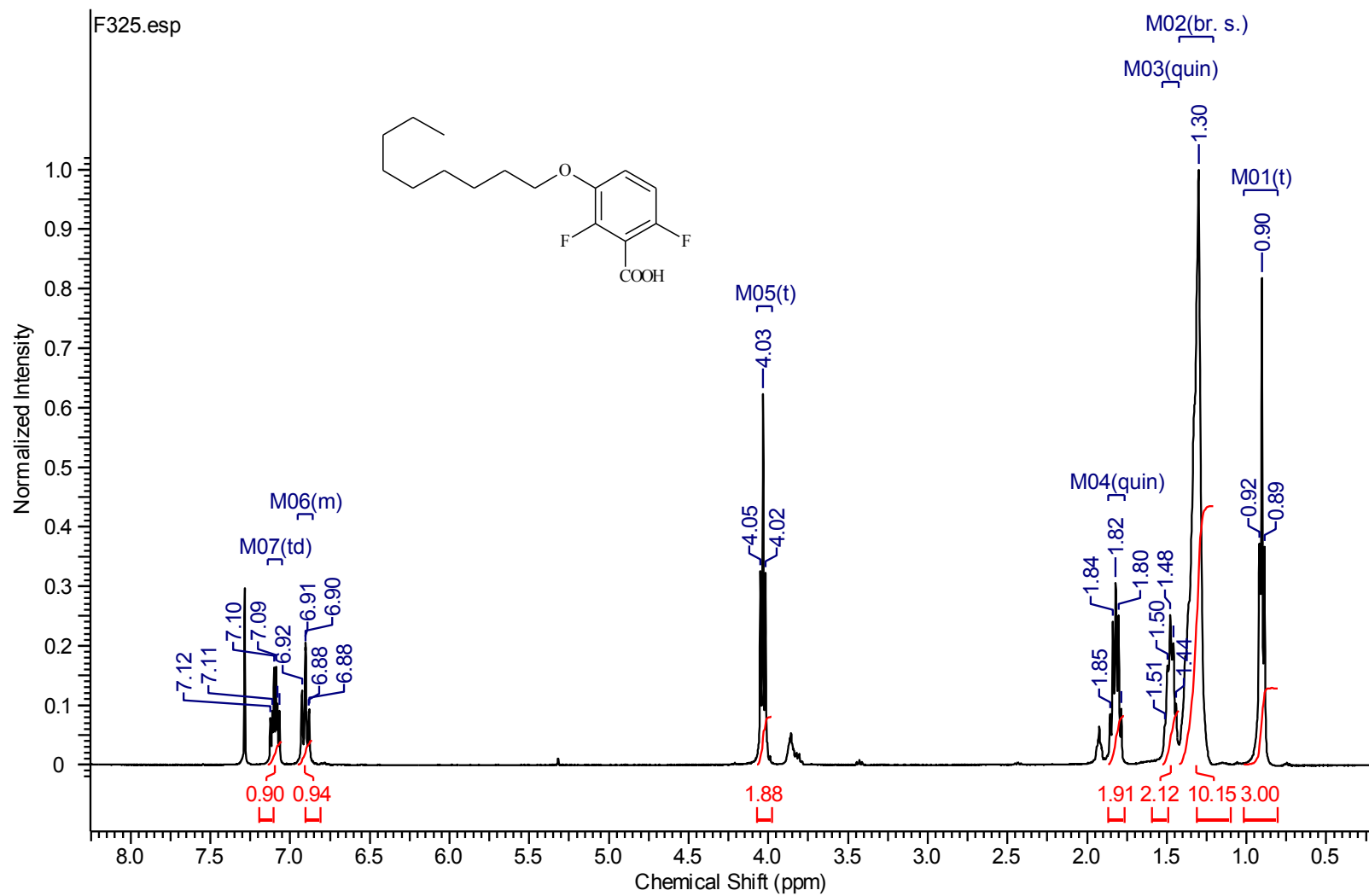
II-9  $^1\text{H}$  NMR spectrum of compound 2-F413



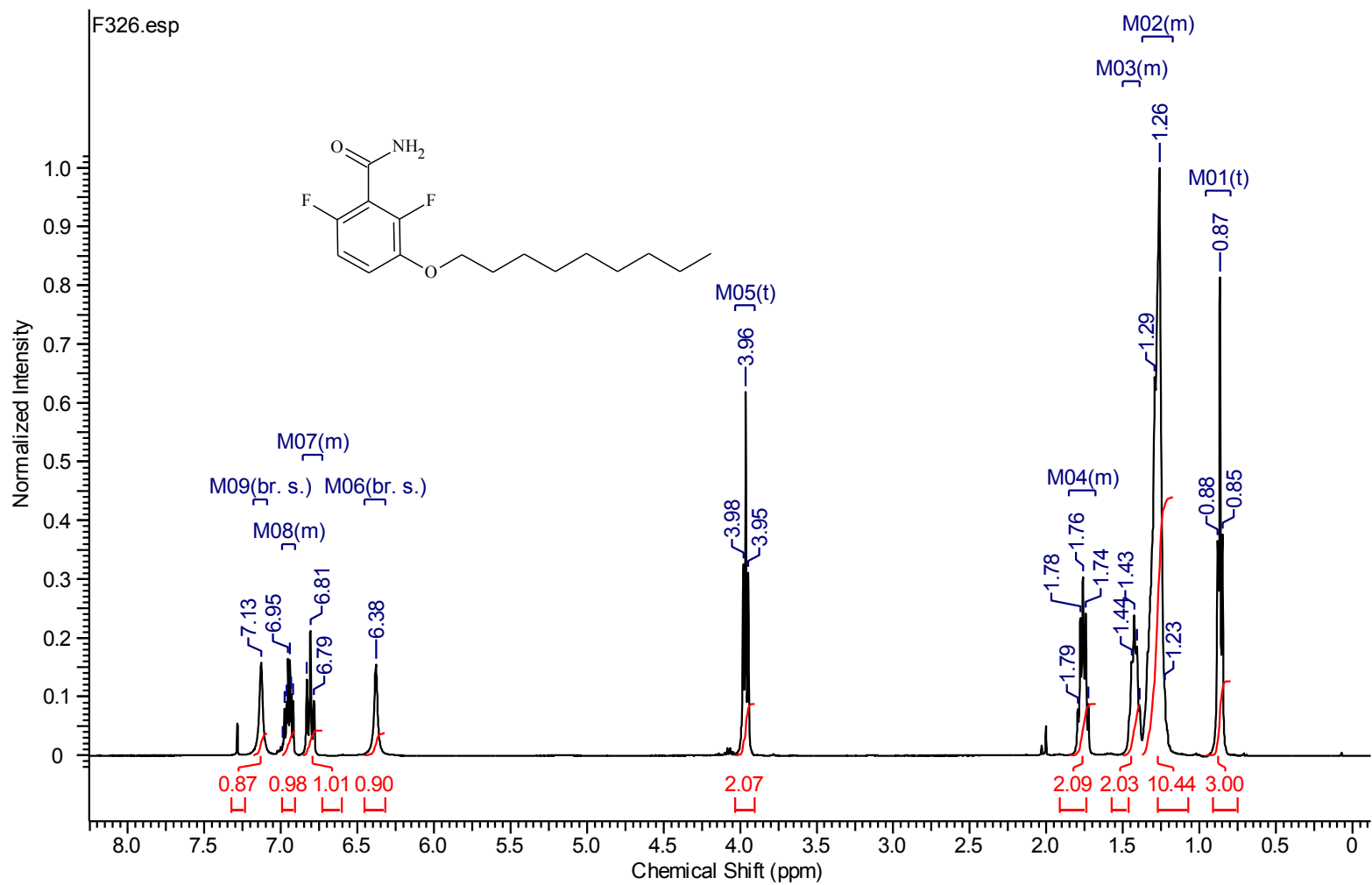
II-10  $^1\text{H}$  NMR spectrum of compound 2-F414



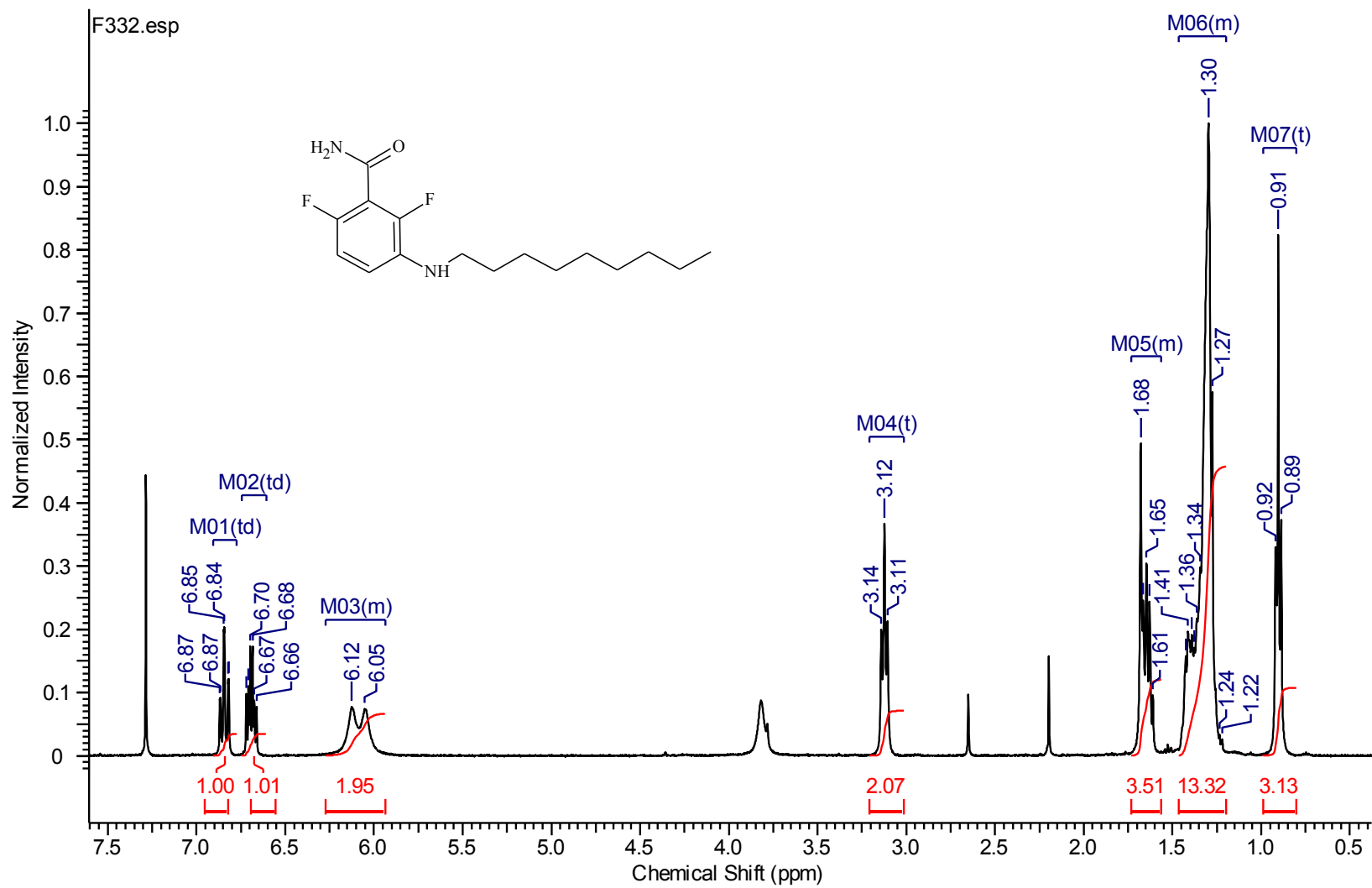
II-11  $^1\text{H}$  NMR spectrum of compound **3-F324**



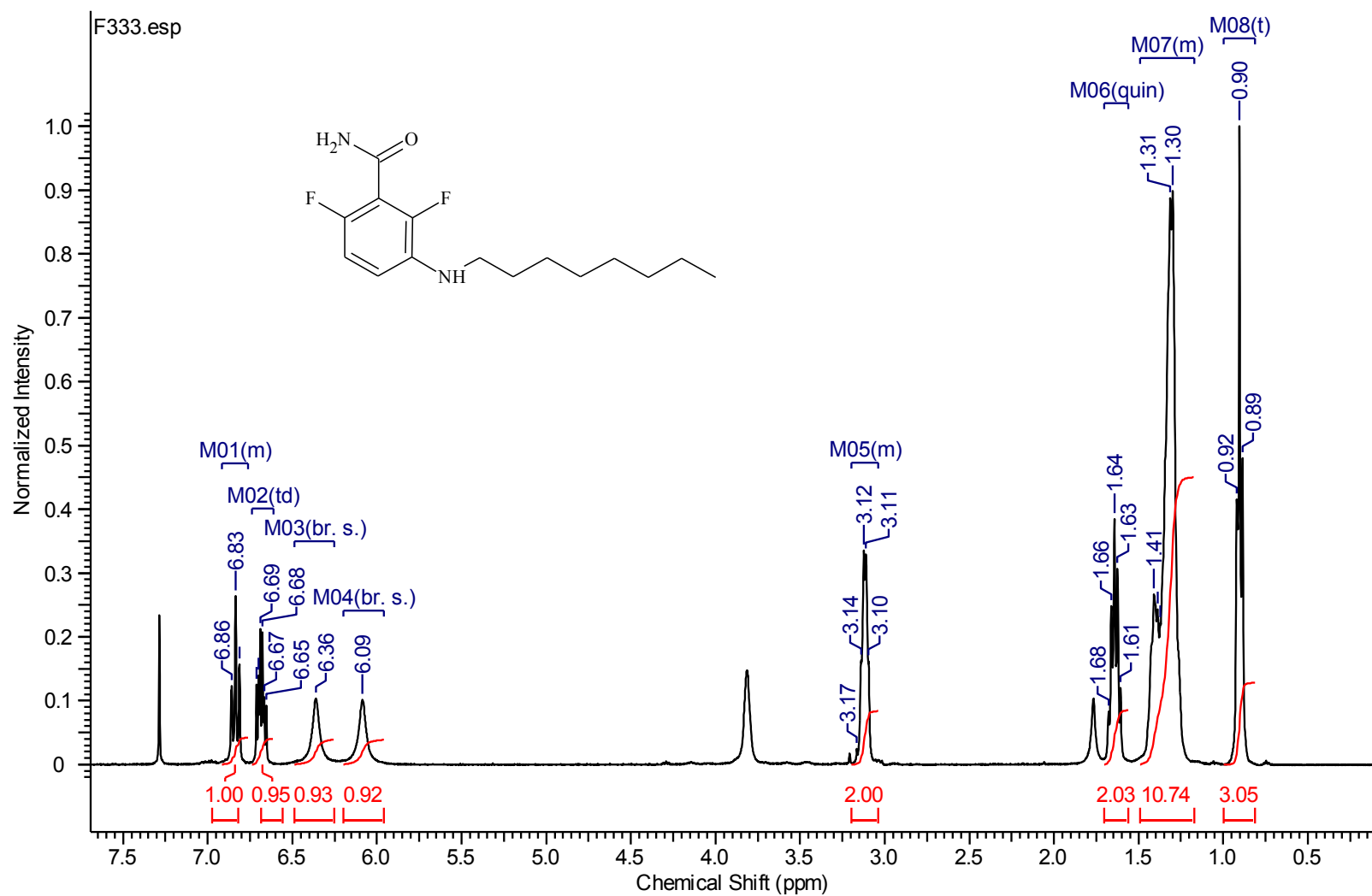
II-12  $^1\text{H}$  NMR spectrum of compound **3-F325**



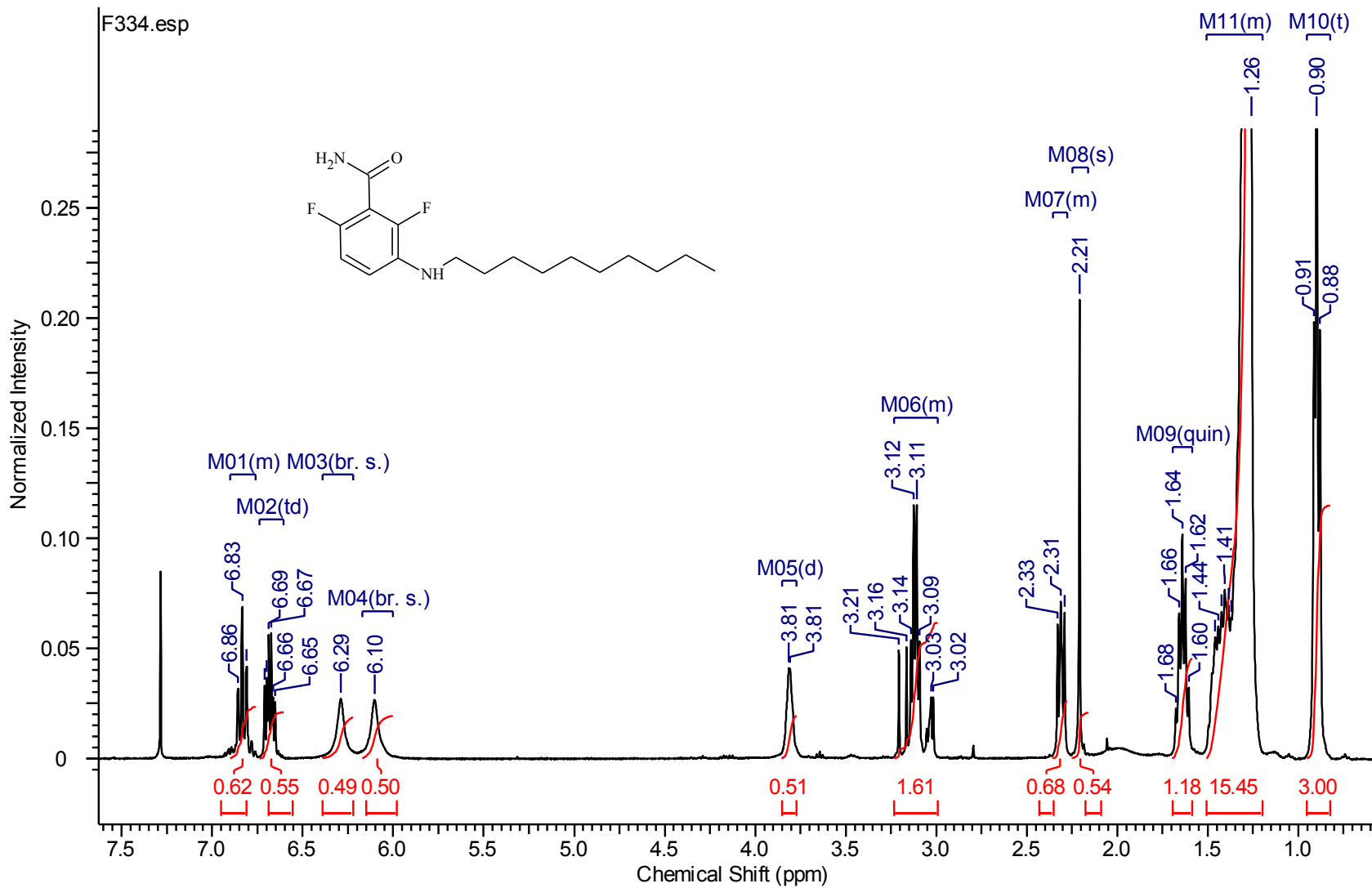
II-13  $^1\text{H}$  NMR spectrum of compound 3-F326



II-14  $^1\text{H}$  NMR spectrum of compound 4-F332

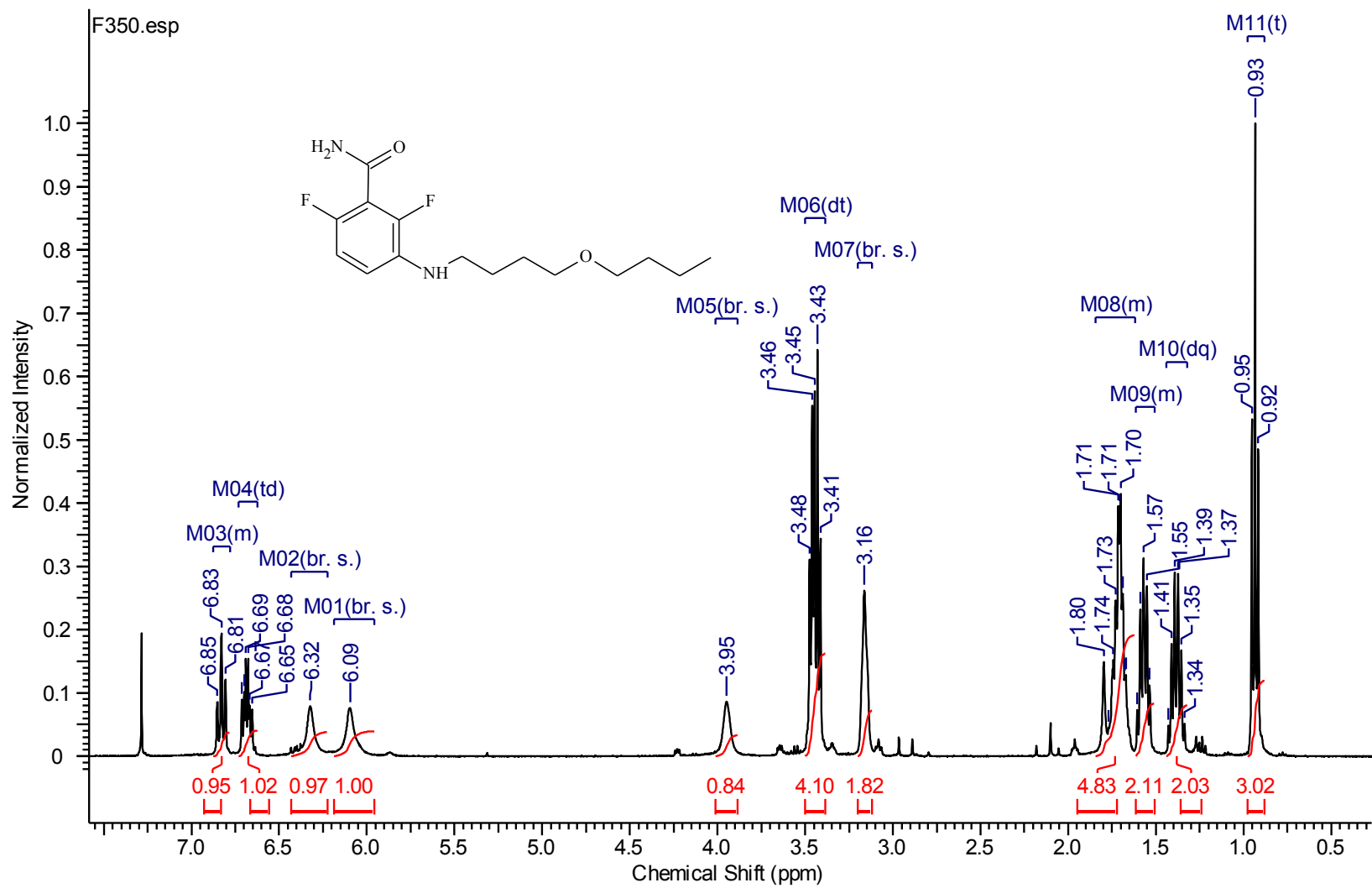


II-15  $^1\text{H}$  NMR spectrum of compound 4-F333

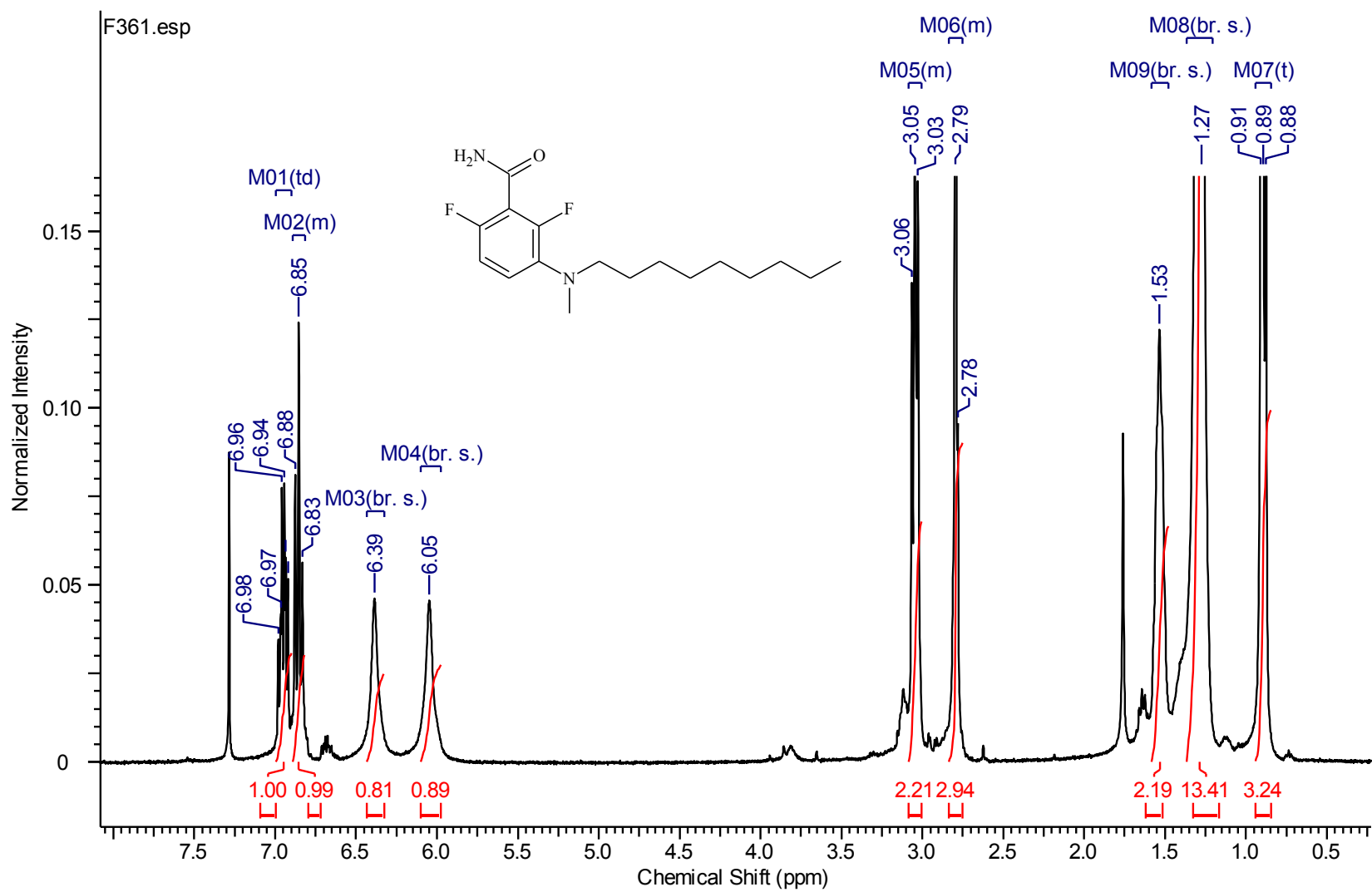


II-16  $^1\text{H}$  NMR spectrum of compound 4-F334

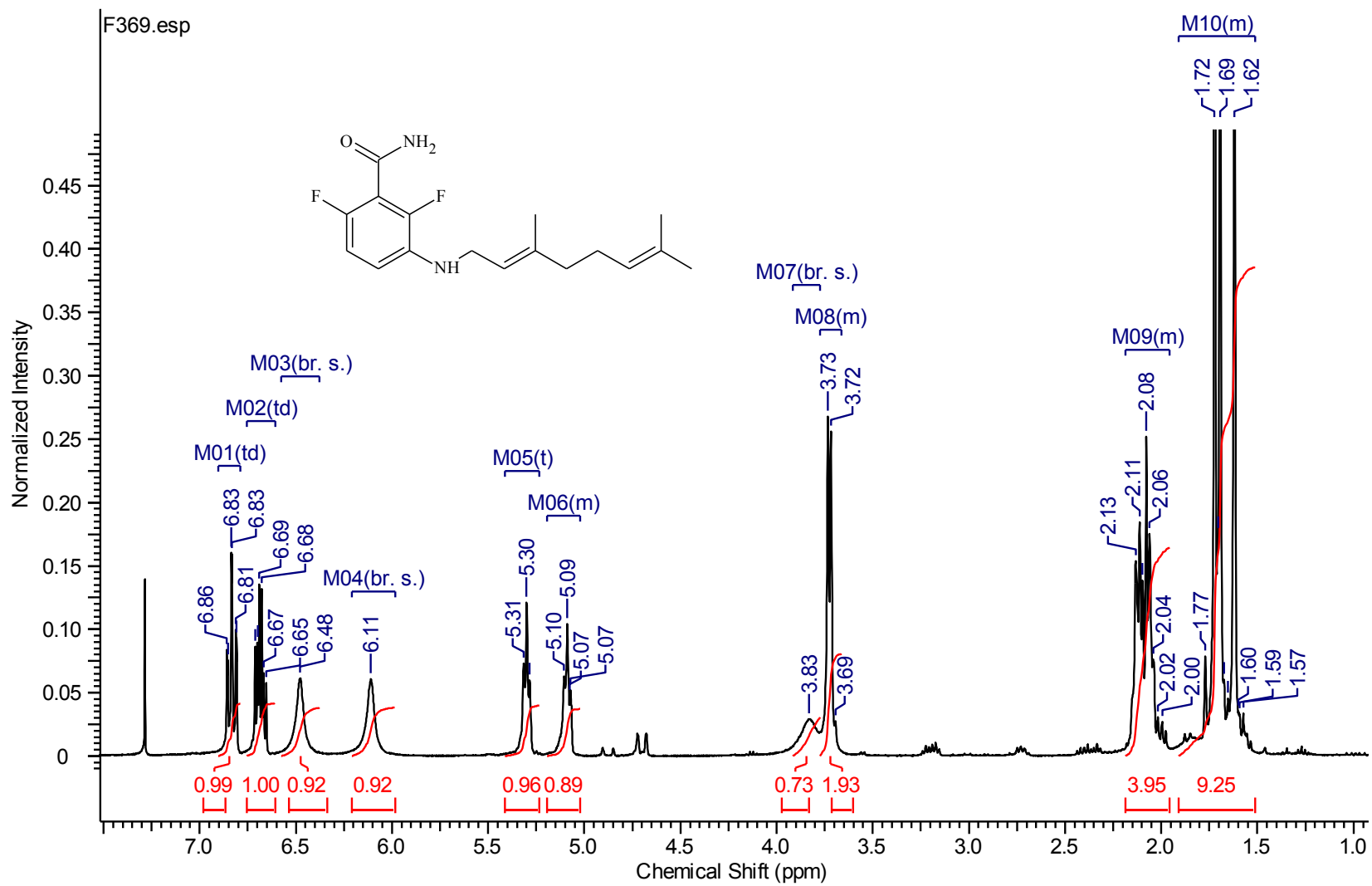




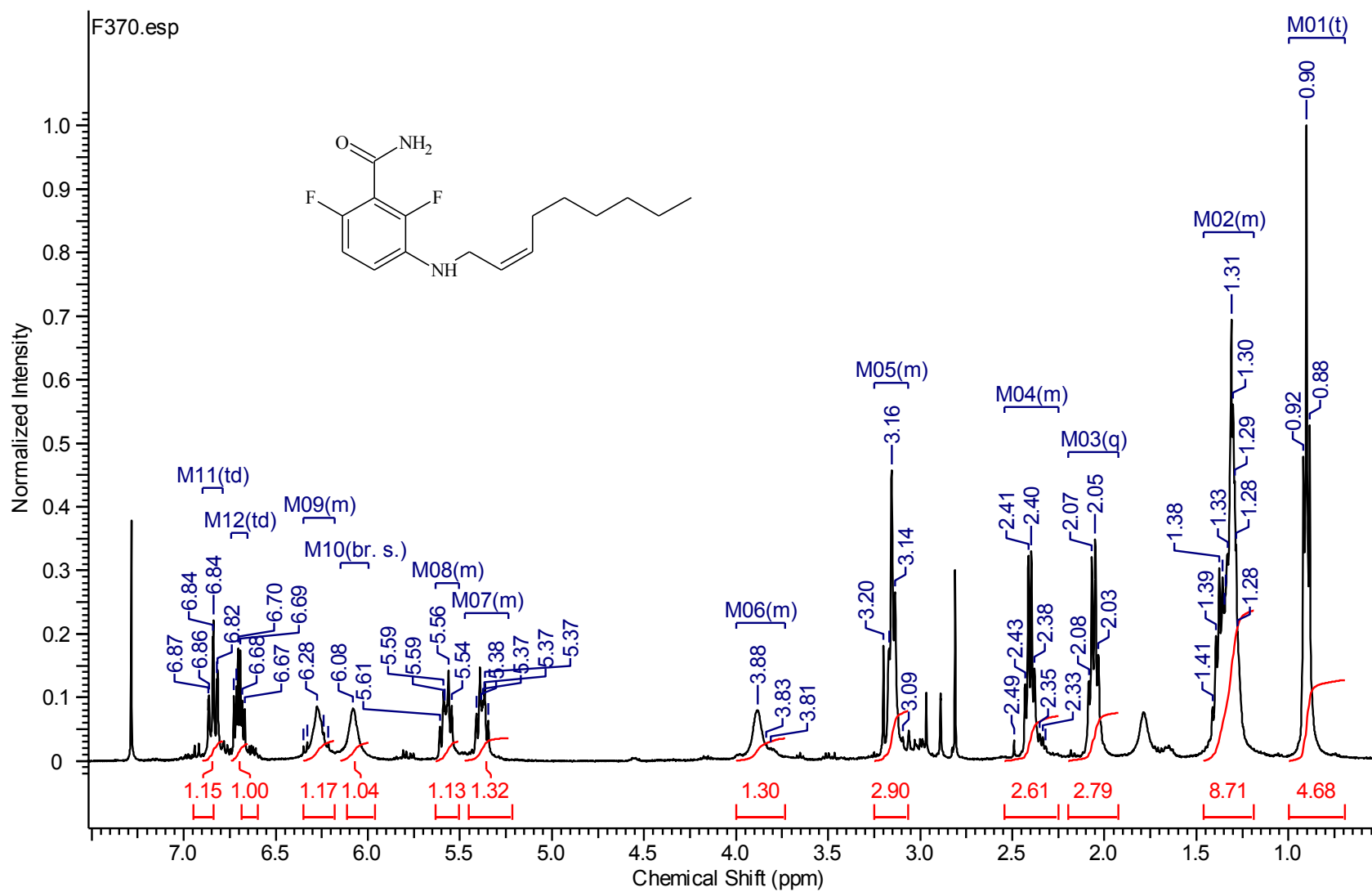
II-17  $^1\text{H}$  NMR spectrum of compound 4-F350



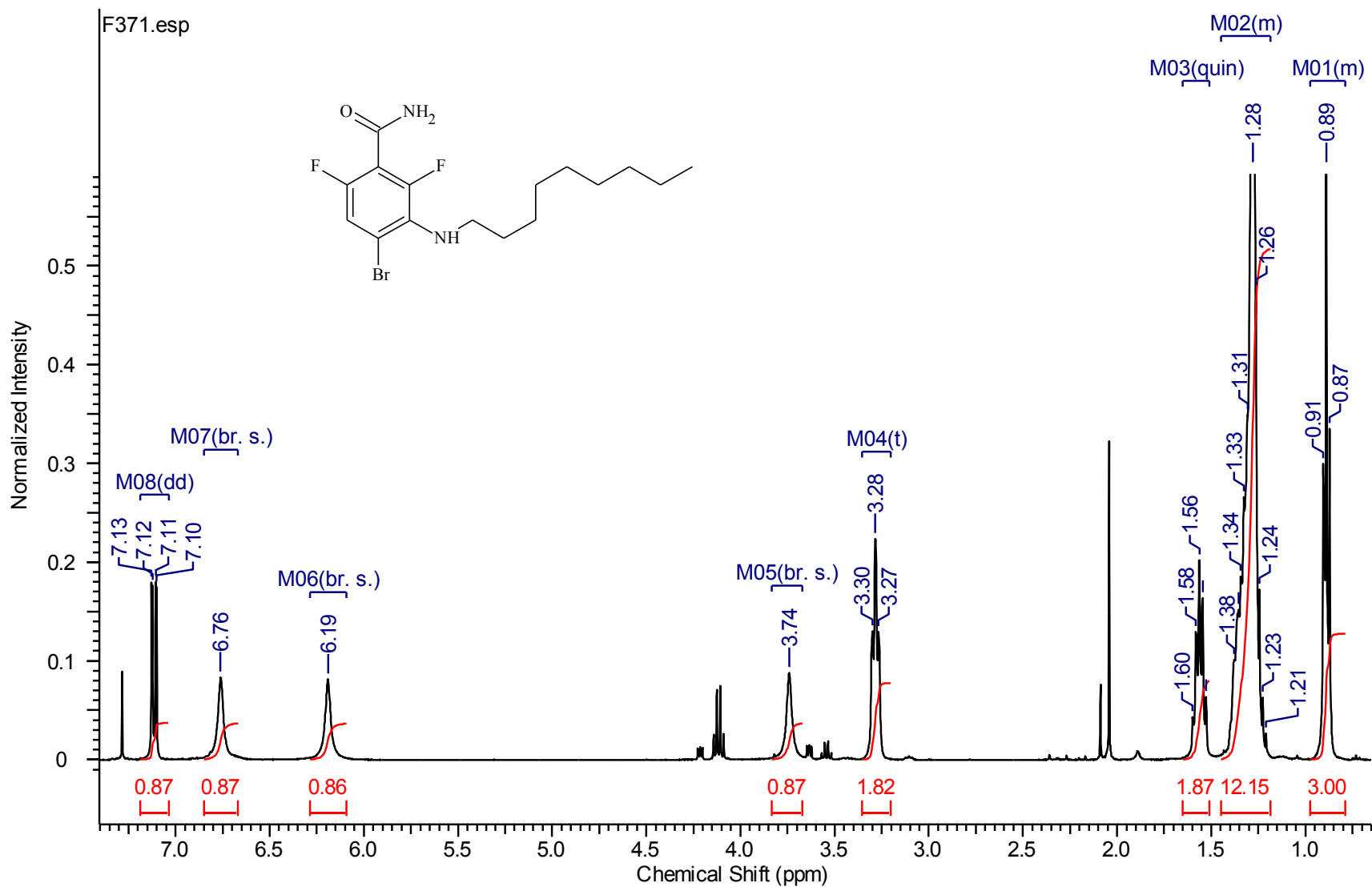
II-18  $^1\text{H}$  NMR spectrum of compound 4-F361



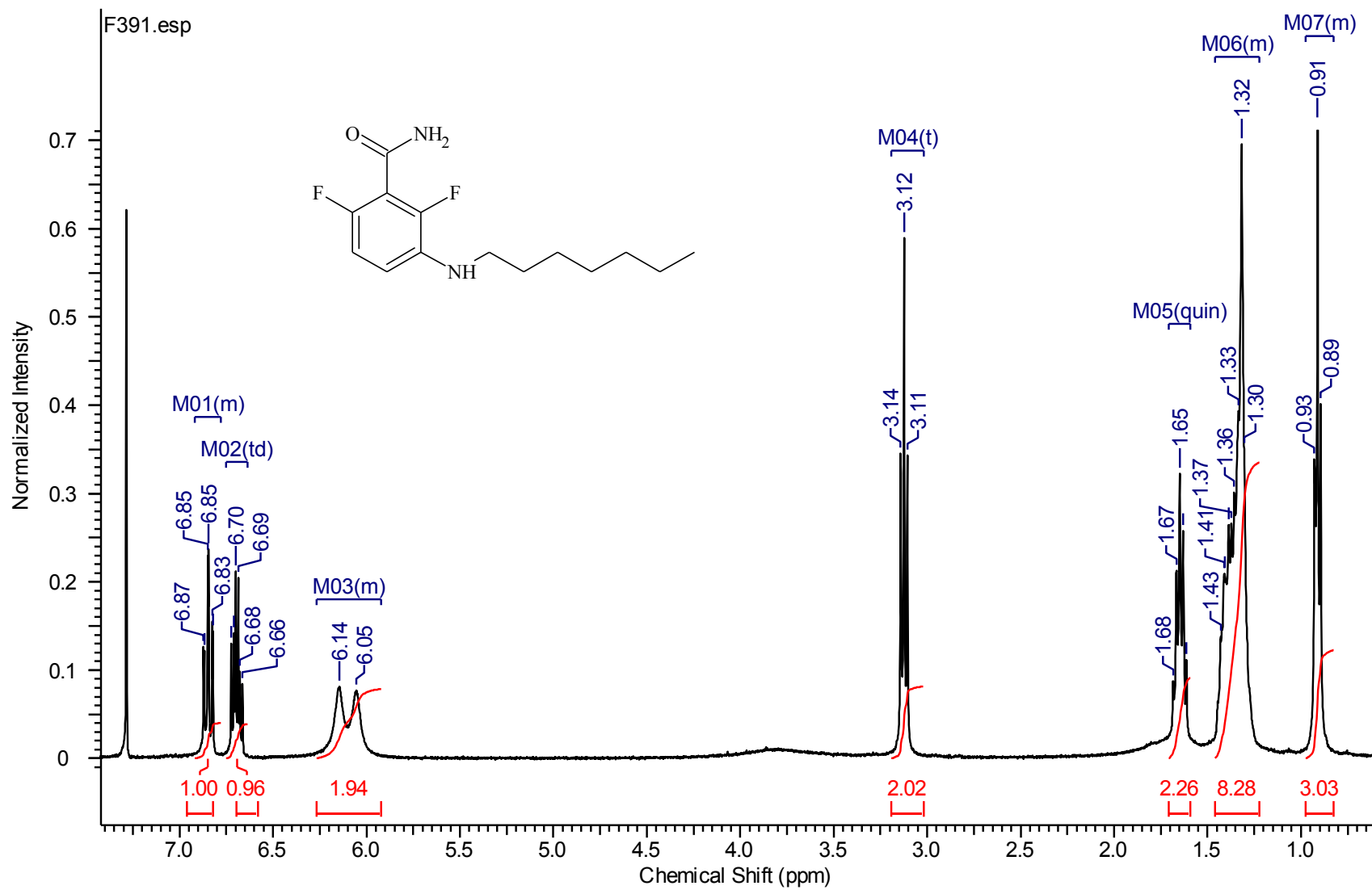
II-19  $^1\text{H}$  NMR spectrum of compound 4-F369



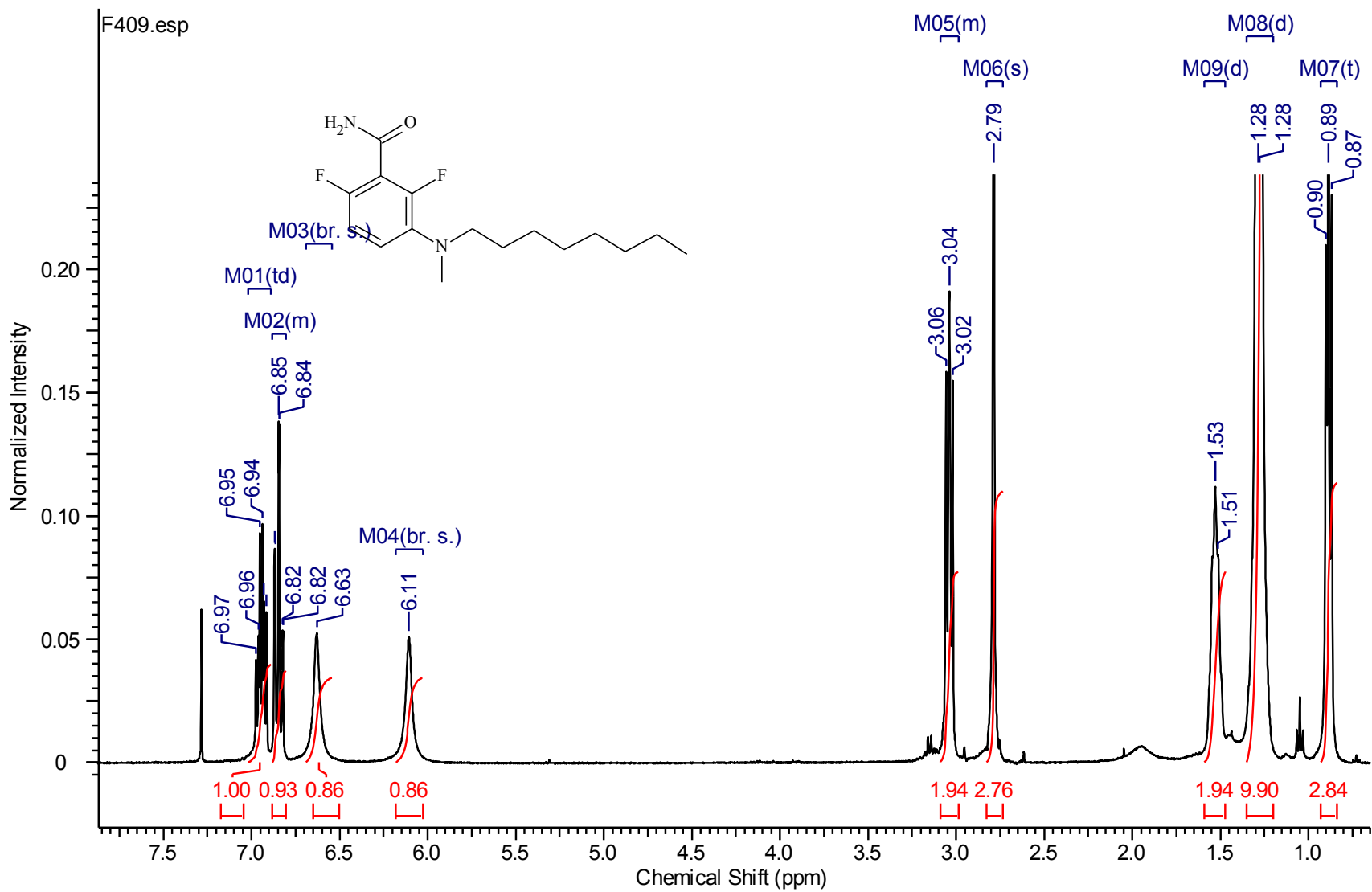
II-20  $^1\text{H}$  NMR spectrum of compound 4-F370



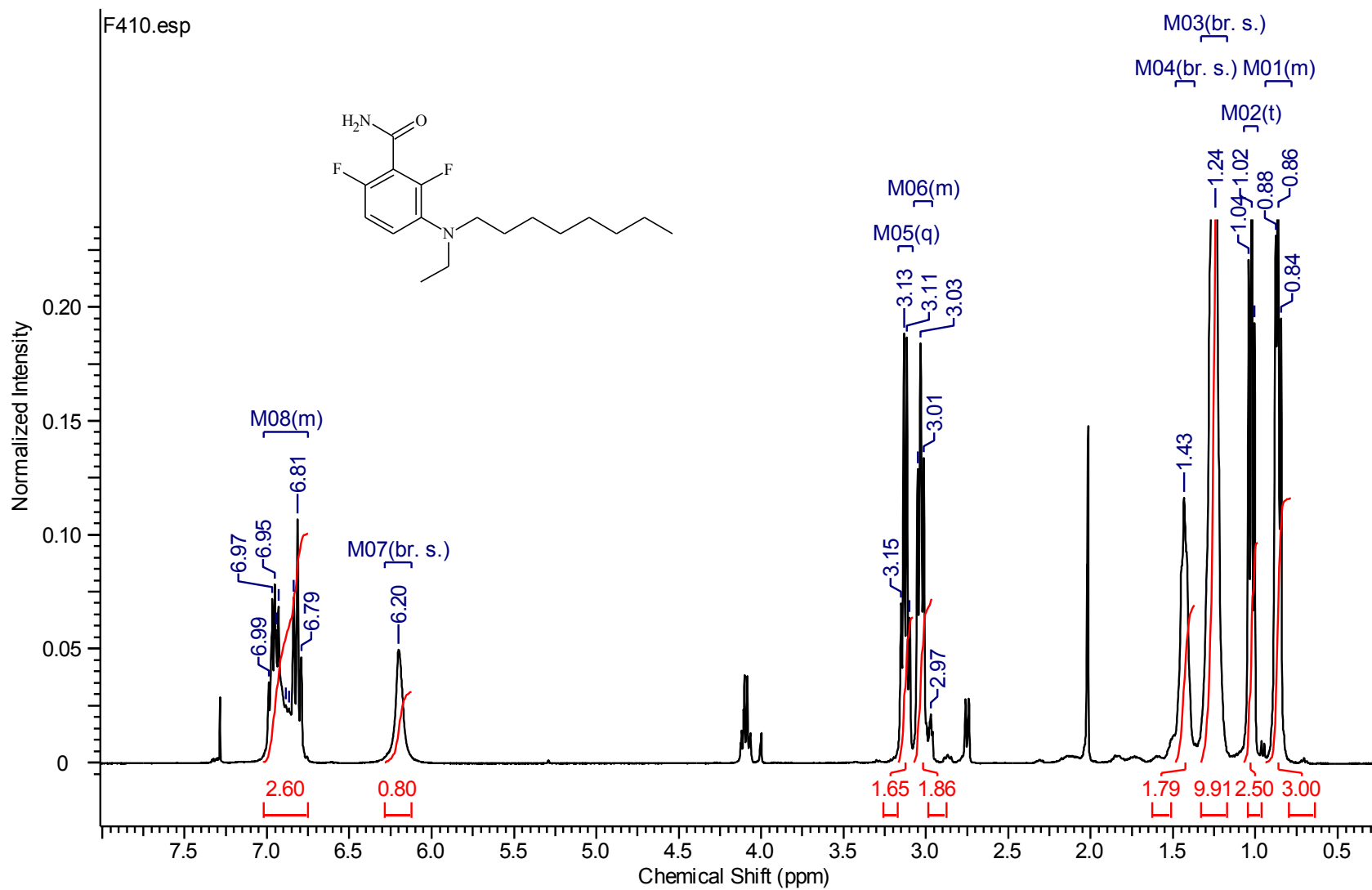
II-21  $^1\text{H}$  NMR spectrum of compound **4-F371**



II-22  $^1\text{H}$  NMR spectrum of compound 4-F391

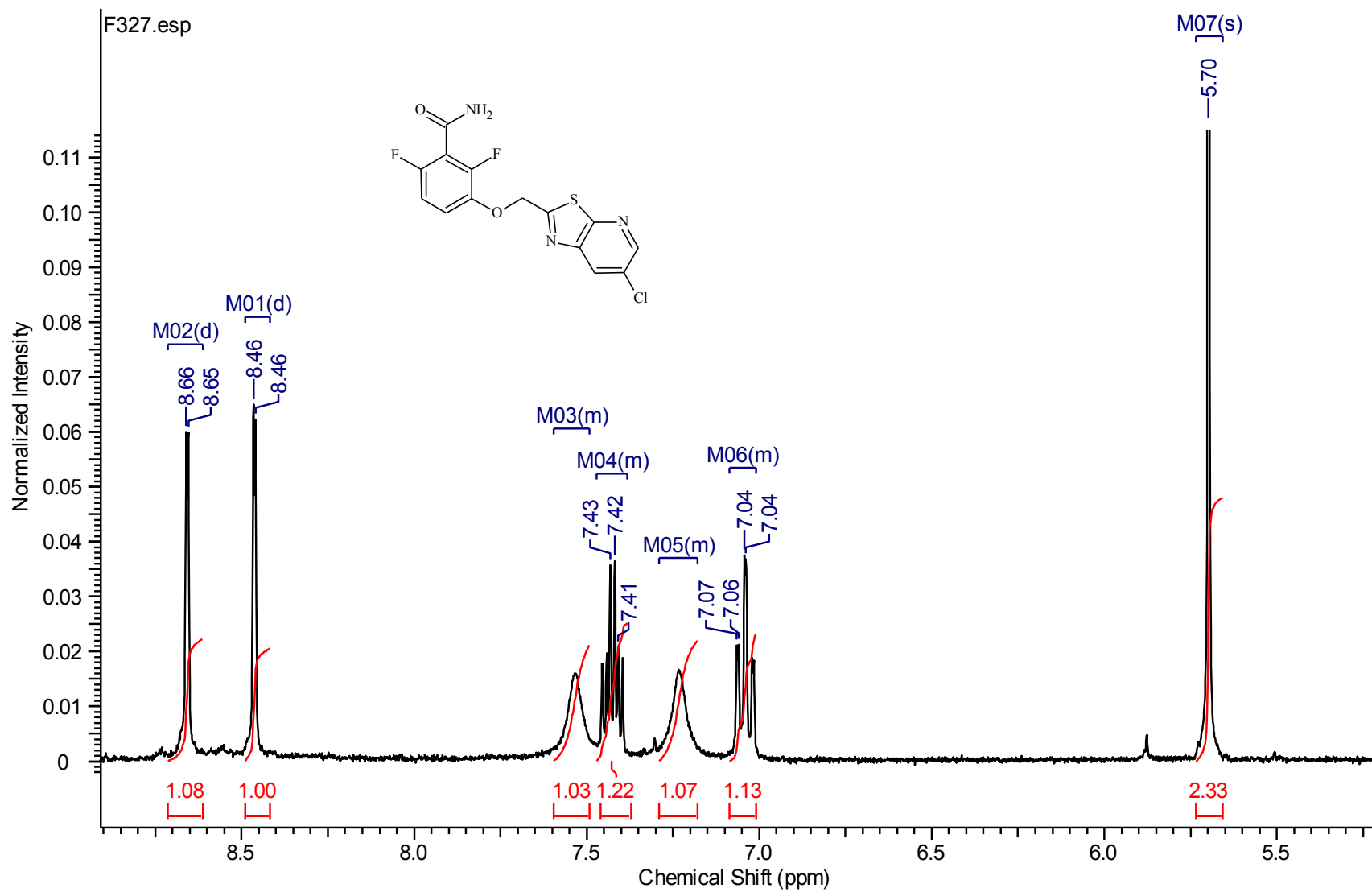


II-23  $^1\text{H}$  NMR spectrum of compound 4-F409

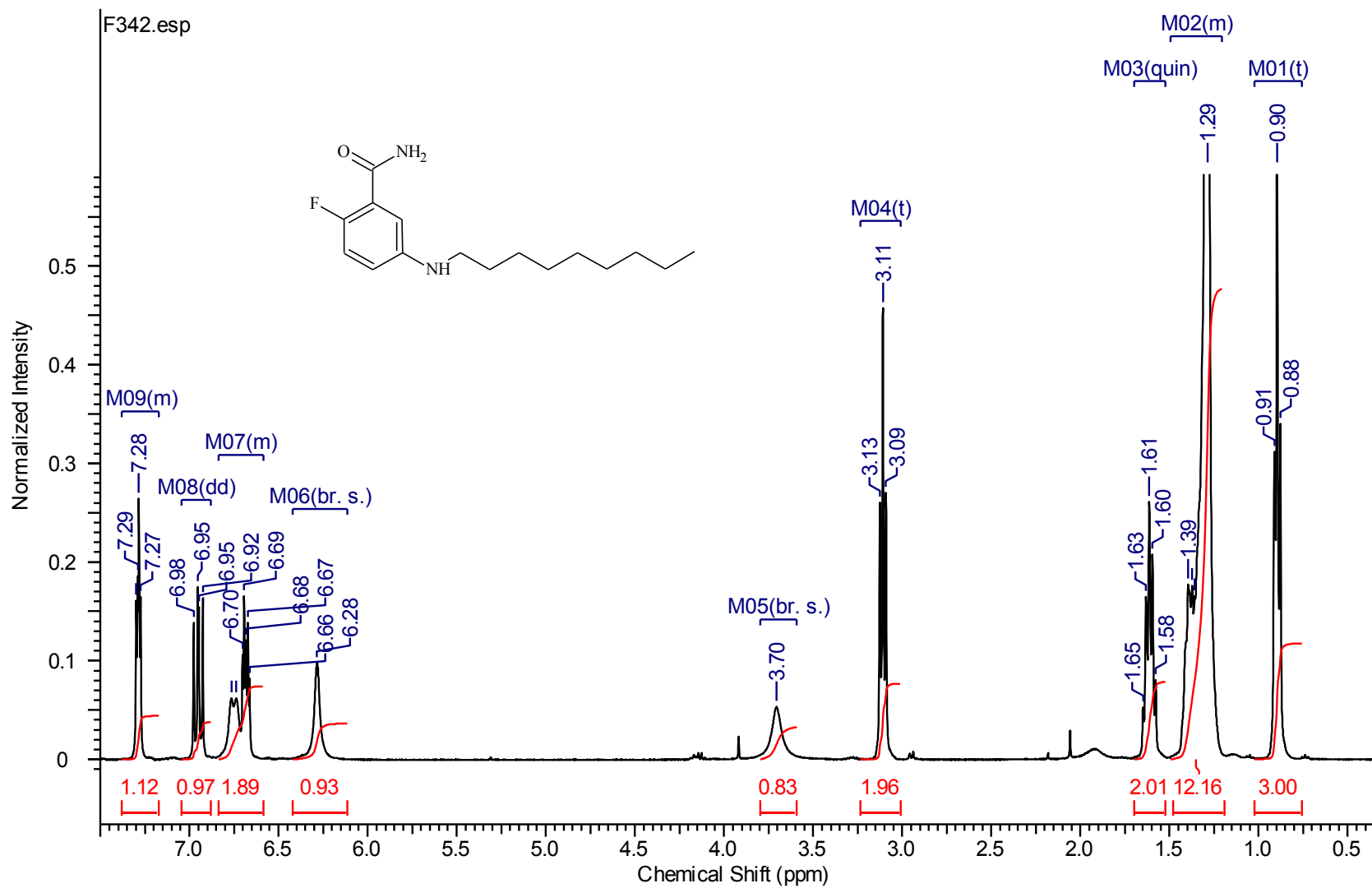


II-24  $^1\text{H}$  NMR spectrum of compound 4-F410

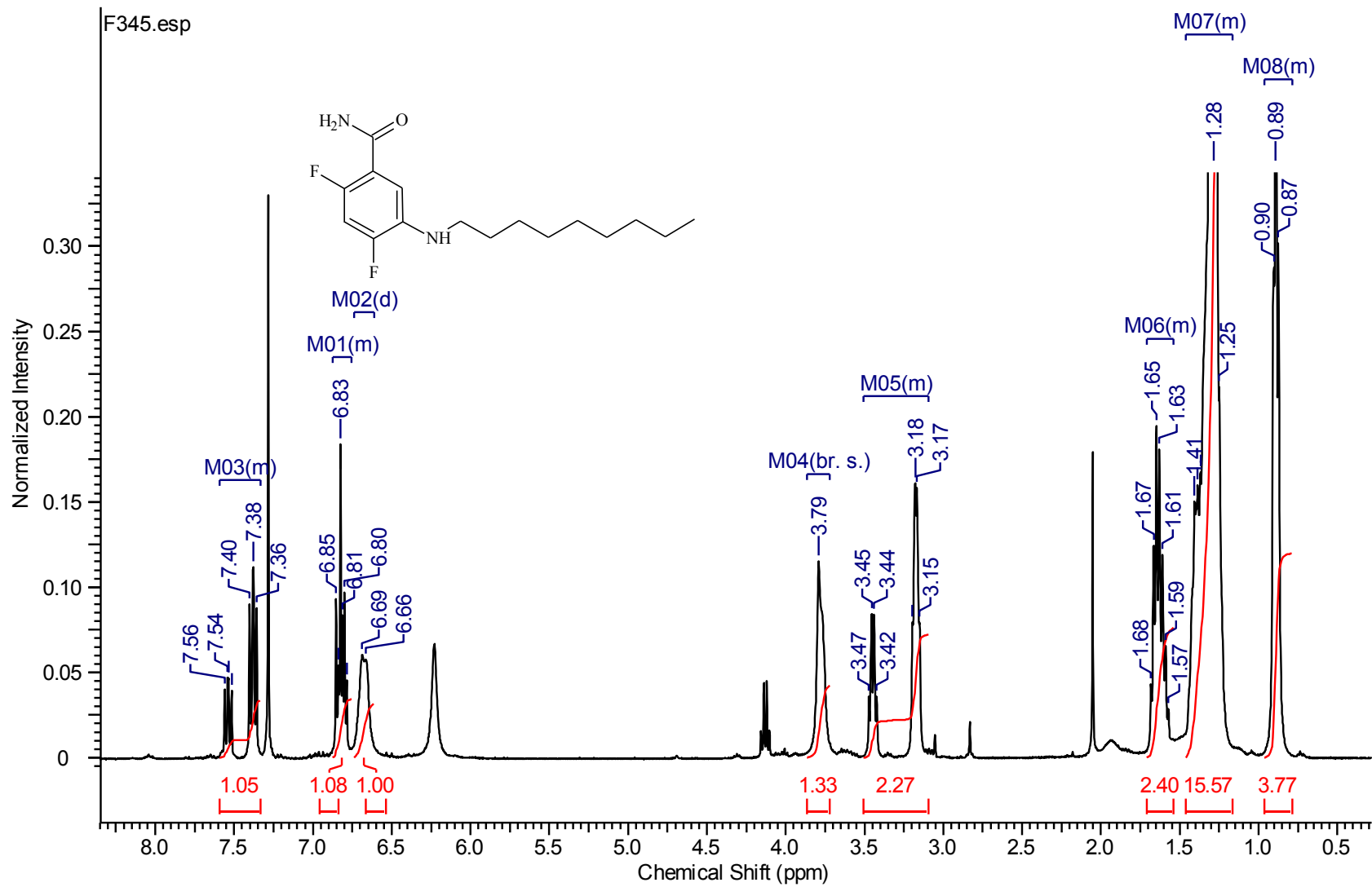




II-25  $^1\text{H}$  NMR spectrum of compound **F327**



II-26  $^1\text{H}$  NMR spectrum of compound F342



II-27  $^1\text{H}$  NMR spectrum of compound **F345**

## References

1. Overbye K. M. & Barrett J. F. (2005) *Antibiotics: Where did we go wrong*, Amsterdam: Elsevier.
2. <http://www.who.int/mediacentre/factsheets/fs194/en/>, Antimicrobial resistance, World Health Organization, 2013
3. <http://www.chp.gov.hk/en/data/1/10/26/43/590.html>, Number of notifications for notifiable infectious disease in 2012, Department of Health of Hong Kong, 2012
4. Walsh C. (2000) Molecular mechanisms that confer antibacterial drug resistance, *Nature*, 406(6797):775-781.
5. Walsh C. (2003) *Antibiotic: Actions, Origins, Resistance*, Washington, DC: ASM Press.
6. Erickson H. P. (1997) FtsZ, a tubulin homologue in prokaryote cell division, *Trends in Cell Biology*, 7(9):362-367.
7. Adams D. W. & Errington J. (2009) Bacterial cell division: assembly, maintenance and disassembly of the Z ring, *Nature Reviews Microbiology*, 7(9):642-653.
8. Mukherjee A. & Lutkenhaus J. (1994) Guanine nucleotide-dependent assembly of FtsZ into filaments, *Journal of Bacteriology*, 176(9):2754-2758.
9. Lutkenhaus J. & Addinall S. G. (1997) Bacterial cell division and the Z ring, *Annual Review of Biochemistry*, 66(1):93-116.
10. Lowe J. & Amos L. A. (1998) Crystal structure of the bacterial cell-division protein FtsZ, *Nature*, 391(6663):203-206.

11. Lu C., Stricker J., & Erickson H. P. (1998) FtsZ from *Escherichia coli*, *Azotobacter vinelandii*, and *Thermotoga maritima*—quantitation, GTP hydrolysis, and assembly, *Cell Motility and the Cytoskeleton* 40(1):71-86.
12. Anderson D. E., Gueiros-Filho F. J., & Erickson H. P. (2004) Assembly dynamics of FtsZ rings in *Bacillus subtilis* and *Escherichia coli* and effects of FtsZ-regulating proteins, *Journal of Bacteriology*, 186(17):5775-5781.
13. Raskin D. M. & de Boer P. A. J. (1999) MinDE-dependent pole-to-pole oscillation of division inhibitor MinC in *Escherichia coli*, *Journal of Bacteriology*, 181(20):6419-6424.
14. Lutkenhaus J. (2007) Assembly Dynamics of the Bacterial MinCDE System and Spatial Regulation of the Z Ring, *Annual Review of Biochemistry*, 76(1):539-562.
15. Wu L. J. & Errington J. (2012) Nucleoid occlusion and bacterial cell division, *Nature Reviews Microbiology*, 10(1):8-12.
16. Cho H., McManus H. R., Dove S. L., & Bernhardt T. G. (2011) Nucleoid occlusion factor SlmA is a DNA-activated FtsZ polymerization antagonist, *Proceedings of the National Academy of Sciences*, 108(9):3773-3778.
17. Lock R. L. & Harry E. J. (2008) Cell-division inhibitors: new insights for future antibiotics, *Nature Reviews Drug Discovery*, 7(4):324-338.
18. Huang K. C., Meir Y., & Wingreen N. S. (2003) Dynamic structures in *Escherichia coli*: Spontaneous formation of MinE rings and MinD polar zones, *Proceedings of the National Academy of Sciences*, 100(22):12724-12728.
19. [http://www.idsociety.org/2013\\_Antibiotic\\_Development/](http://www.idsociety.org/2013_Antibiotic_Development/), Despite superbug crisis, progress in antibiotic development 'alarmingly elusive', The infectious Diseases Society of America, 2013

20. Bramhill D. & Thompson C. M. (1994) GTP-dependent polymerization of Escherichia coli FtsZ protein to form tubules, *Proceedings of the National Academy of Sciences*, 91(13):5813-5817.
21. Ma S. & Ma S. (2012) The Development of FtsZ Inhibitors as Potential Antibacterial Agents, *ChemMedChem*, 7(7):1161-1172.
22. Mukherjee A., Dai K., & Lutkenhaus J. (1993) Escherichia coli cell division protein FtsZ is a guanine nucleotide binding protein, *Proceedings of the National Academy of Sciences*, 90(3):1053-1057.
23. Mahendran R., Jenifer F. J., Palanimuthu M., & Subasri S. (2011) Sequence and structural analysis of FtsZ homologs and comparison of bacterial FtsZ with eukaryotic tubulins, *Indian Journal of Science and Technology*, 4(2):141-146.
24. Spiegelman B. M., Penningroth S. M., & Kirschner M. W. (1977) Turnover of tubulin and the N site GTP in Chinese hamster ovary cells, *Cell*, 12(3):587-600.
25. Wang X., Huang J., Mukherjee A., Cao C., & Lutkenhaus J. (1997) Analysis of the interaction of FtsZ with itself, GTP, and FtsA, *Journal of Bacteriology*, 179(17):5551-5559.
26. Domadia P. N., Bhunia A., Sivaraman J., Swarup S., & Dasgupta D. (2008) Berberine targets assembly of Escherichia coli cell division protein FtsZ, *Biochemistry*, 47(10):3225-3234.
27. Lämpchen T., Hartog A. F., Pinas V. A., Koomen G.-J., & den Blaauwen T. (2005) GTP analogue inhibits polymerization and GTPase activity of the bacterial protein FtsZ without affecting its eukaryotic homologue tubulin, *Biochemistry*, 44(21):7879-7884.

28. Stokes N. R., Sievers J., Barker S., Bennett J. M., Brown D. R., Collins I., Errington V. M., Foulger D., Hall M., Halsey R., Johnson H., Rose V., Thomaides H. B., Haydon D. J., Czaplowski L. G., & Errington J. (2005) Novel inhibitors of bacterial cytokinesis identified by a cell-based antibiotic screening assay, *Journal of Biological Chemistry*, 280(48):39709-39715.
29. Wang J., Galgoci A., Kodali S., Herath K. B., Jayasuriya H., Dorso K., Vicente F., González A., Cully D., Bramhill D., & Singh S. (2003) Discovery of a small molecule that inhibits cell division by blocking FtsZ, a novel therapeutic target of antibiotics, *Journal of Biological Chemistry*, 278(45):44424-44428.
30. Schaffner-Barbero C., Martín-Fontecha M., Chacón P., & Andreu J. M. (2011) Targeting the assembly of bacterial cell division protein FtsZ with small molecules, *ACS Chemical Biology*, 7(2):269-277.
31. Anderson D. E., Kim M. B., Moore J. T., O'Brien T. E., Sorto N. A., Grove C. I., Lackner L. L., Ames J. B., & Shaw J. T. (2012) Comparison of small molecule inhibitors of the bacterial cell division protein FtsZ and identification of a reliable cross-species inhibitor, *ACS Chemical Biology*, 7(11):1918-1928.
32. Fabiano R. J. & Tu A. T. (1981) Purification and biochemical study of viriditoxin, tissue damaging toxin, from prairie rattlesnake venom, *Biochemistry*, 20(1):21-27.
33. Rai D., Singh J. K., Roy N., & Panda D. (2008) Curcumin inhibits FtsZ assembly: an attractive mechanism for its antibacterial activity, *Biochemical Journal*, 410:147-155.
34. Kaur S., Modi N. H., Panda D., & Roy N. (2010) Probing the binding site of curcumin in *Escherichia coli* and *Bacillus subtilis* FtsZ – A structural insight to unveil antibacterial activity of curcumin, *European Journal of Medicinal Chemistry*, 45(9):4209-4214.

35. Kunwar A., Barik A., Mishra B., Rathinasamy K., Pandey R., & Priyadarsini K. I. (2008) Quantitative cellular uptake, localization and cytotoxicity of curcumin in normal and tumor cells, *Biochimica et Biophysica Acta (BBA) - General Subjects*, 1780(4):673-679.
36. Possoz C., Newmark J., Sorto N., Sherratt D. J., & Tolmasky M. E. (2007) Sublethal concentrations of the aminoglycoside amikacin interfere with cell division without affecting chromosome dynamics, *Antimicrobial Agents and Chemotherapy*, 51(1):252-256.
37. Wang H. Z., Chang C. H., Lin C. P., & Tsai M. C. (1996) Using MTT viability assay to test the cytotoxicity of antibiotics and steroid to cultured porcine corneal Endothelial cells, *Journal of Ocular Pharmacology and Therapeutics*, 12(1):35-43.
38. Ruiz-Avila L. B., Huecas S., Artola M., Vergoñós A., Ramírez-Aportela E., Cercenado E., Barasoain I., Vazquez-Villa H., Martin-Fontecha M., Chacon P., Lopez-Rodriguez M. L., & Andreu J. M. (2013) Synthetic inhibitors of bacterial cell division targeting the GTP binding site of FtsZ, *ACS Chemical Biology*, 8(9):2072-2083.
39. Ohashi Y., Chijiwa Y., Suzuki K., Takahashi K., Nanamiya H., Sato T., Hosoya Y., Ochi K., & Kawamura F. (1999) The lethal effect of a benzamide derivative, 3-methoxybenzamide, can be suppressed by mutations within a cell division gene, *ftsZ*, in *Bacillus subtilis*, *Journal of Bacteriology*, 181(4):1348-1351.
40. Haydon D. J., Stokes N. R., Ure R., Galbraith G., Bennett J. M., Brown D. R., Baker P. J., Barynin V. V., Rice D. W., Sedelnikova S. E., Heal J. R., Sheridan J. M., Aiwale S. T., Chauhan P. K., Srivastava A., Taneja A., Collins I., Errington J., & Czaplewski L. G. (2008) An Inhibitor of FtsZ with Potent and Selective Anti-Staphylococcal Activity, *Science*, 321(5896):1673-1675.



41. Matsui T., Yamane J., Mogi N., Yamaguchi H., Takemoto H., Yao M., & Tanaka I. (2012) Structural reorganization of the bacterial cell-division protein FtsZ from *Staphylococcus aureus*, *Acta Crystallographica Section D*, 68(9):1175-1188.
42. Domadia P., Swarup S., Bhunia A., Sivaraman J., & Dasgupta D. (2007) Inhibition of bacterial cell division protein FtsZ by cinnamaldehyde, *Biochemical Pharmacology*, 74(6):831-840.
43. Thorén L. M., Tuomi J., Kämäräinen T., & Laine K. (2003) Resource availability affects investment in carnivory in *Drosera rotundifolia*, *New Phytologist*, 159(2):507-511.
44. Bhattacharya A., Jindal B., Singh P., Datta A., & Panda D. (2013) Plumbagin inhibits cytokinesis in *Bacillus subtilis* by inhibiting FtsZ assembly: A mechanistic study of its antibacterial activity, *The FEBS Journal*, 280(18):4585-4599.
45. Farr S. B., Natvig D. O., & Kogoma T. (1985) Toxicity and mutagenicity of plumbagin and the induction of a possible new DNA repair pathway in *Escherichia coli*, *Journal of Bacteriology*, 164(3):1309-1316.
46. Drews J. (2000) Drug discovery: A historical perspective, *Science*, 287(5460):1960-1964.
47. Bleicher K. H., Bohm H. J., Muller K., & Alanine A. I. (2003) Hit and lead generation: beyond high-throughput screening, *Nature Reviews Drug Discovery*, 2(5):369-378.
48. Harvey A. L. (2008) Natural products in drug discovery, *Drug Discovery Today*, 13(19–20):894-901.
49. Blondelle S. E., Pérez-Payá E., & Houghten R. A. (1996) Synthetic combinatorial libraries: novel discovery strategy for identification of antimicrobial agents, *Antimicrobial Agents and Chemotherapy*, 40(5):1067-1071.

50. McInnes C. (2007) Virtual screening strategies in drug discovery, *Current Opinion in Chemical Biology*, 11(5):494-502.
51. Kellenberger E., Rodrigo J., Muller P., & Rognan D. (2004) Comparative evaluation of eight docking tools for docking and virtual screening accuracy, *Proteins: Structure, Function, and Bioinformatics*, 57(2):225-242.
52. Zhang J. H., Chung T. D. Y., & Oldenburg K. R. (1999) Simple statistical parameter for use in evaluation and validation of high throughput screening assays, *Journal of Biomolecular Screening*, 4(2):67-73.
53. Lipinski C. A., Lombardo F., Dominy B. W., & Feeney P. J. (1997) Experimental and computational approaches to estimate solubility and permeability in drug discovery and development settings, *Advanced Drug Delivery Reviews*, 23(1-3):3-25.
54. Erlanson D. A., McDowell R. S., & O'Brien T. (2004) Fragment-Based drug discovery, *Journal of Medicinal Chemistry*, 47(14):3463-3482.
55. Spangler B. D. (1992) Structure and function of cholera toxin and the related *Escherichia coli* heat-labile enterotoxin, *Microbiological Reviews*, 56(4):622-647.
56. Ochi K., Penyige A., & Barabas G. (1992) The possible role of ADP-ribosylation in sporulation and streptomycin production by *Streptomyces griseus*, *Journal of General Microbiology*, 138(8):1745-1750.
57. Penyige A., Saido Sakanaka H., & Kozo O. (1996) Endogenous ADP-ribosylation of proteins during development of *Streptomyces griseus*, *The Society for Actinomycetes Japan*, 10(2):98-103.
58. Czaplewski L. G., Collins I., Boyd E. A., Brown D., East S. P., Gardiner M., Fletcher R., Haydon D. J., Henstock V., Ingram P., Jones C., Noula C., Kennison L., Rockley C.,

- Rose V., Thomaides-Brears H. B., Ure R., Whittaker M., & Stokes N. R. (2009) Antibacterial alkoxybenzamide inhibitors of the essential bacterial cell division protein FtsZ, *Bioorganic & Medicinal Chemistry Letters*, 19(2):524-527.
59. Hopkins A. L., Groom C. R., & Alex A. (2004) Ligand efficiency: a useful metric for lead selection, *Drug Discovery Today*, 9(10):430-431.
60. Ma S., Cong C., Meng X., Cao S., Yang H., Guo Y., Lu X., & Ma S. (2013) Synthesis and on-target antibacterial activity of novel 3-elongated arylalkoxybenzamide derivatives as inhibitors of the bacterial cell division protein FtsZ, *Bioorganic & Medicinal Chemistry Letters*, 23(14):4076-4079.
61. Gujadhur R., Venkataraman D., & Kintigh J. T. (2001) Formation of aryl-nitrogen bonds using a soluble copper(I) catalyst, *Tetrahedron Letters*, 42(29):4791-4793.
62. Sorto N. A., Olmstead M. M., & Shaw J. T. (2010) Practical synthesis of PC190723, an inhibitor of the bacterial cell division protein FtsZ, *The Journal of Organic Chemistry*, 75(22):7946-7949.
63. Matthew A. Wikler F. R. C., William A. Craig, Michael N. Dudley, George M. Eliopoulos, David F. Hindler, Donald E. Low, Daniel J. Sheehan, Fre C. Ternover, John D. Turnidge, Melvin P. Weinstein, Barara L. Zimmer (2006) Methods for Dilution Antimicrobial Susceptibility Tests for Bacteria That Grow Aerobically, *Clinical And Labortory Standards Institute*, 26(2).
64. Cozzini P. & Spyrakis F. (2006) Hydrophobicity in drug design, *The International Union of Pure and Applied Chemistry*.
65. <http://www.cytoskeleton.com/pdf-storage/datasheets/bk054.pdf>, Cytophos Phosphate Assay Biochem Kit (BK054), Cytoskeleton incorporation, 2006

66. Chan F. Y., Sun N., Neves M. A. C., Lam P. C. H., Chung W. H., Wong L. K., Chow H. Y., Ma D. L., Chan P. H., Leung Y. C., Chan T. H., Abagyan R., & Wong K. Y. (2013) Identification of a new class of FtsZ inhibitors by structure-based design and in vitro screening, *Journal of Chemical Information and Modeling*, 53(8):2131-2140.
67. Mukherjee A. & Lutkenhaus J. (1999) Analysis of FtsZ Assembly by Light Scattering and Determination of the Role of Divalent Metal Cations, *Journal of Bacteriology*, 181(3):823-832.
68. Andreu J. M., Schaffner-Barbero C., Huecas S., Alonso D., Lopez-Rodriguez M. L., Ruiz-Avila L. B., Núñez-Ramírez R., Llorca O., & Martín-Galiano A. J. (2010) The antibacterial cell division inhibitor PC190723 is an FtsZ polymer-stabilizing agent that induces filament assembly and condensation, *Journal of Biological Chemistry*, 285(19):14239-14246.